Scuola Internazionale Superiore di Studi Avanzati - Trieste

New issues in phototransduction

Thesis submitted for the degree of Doctor Philosophiae

Neuroscience area

PhD in Neurobiology

November 2018

Candidate
Ulisse Bocchero

Supervisor
Vincent Torre

SISSA-Via Bonomea 265 – 34136 Trieste, Italy

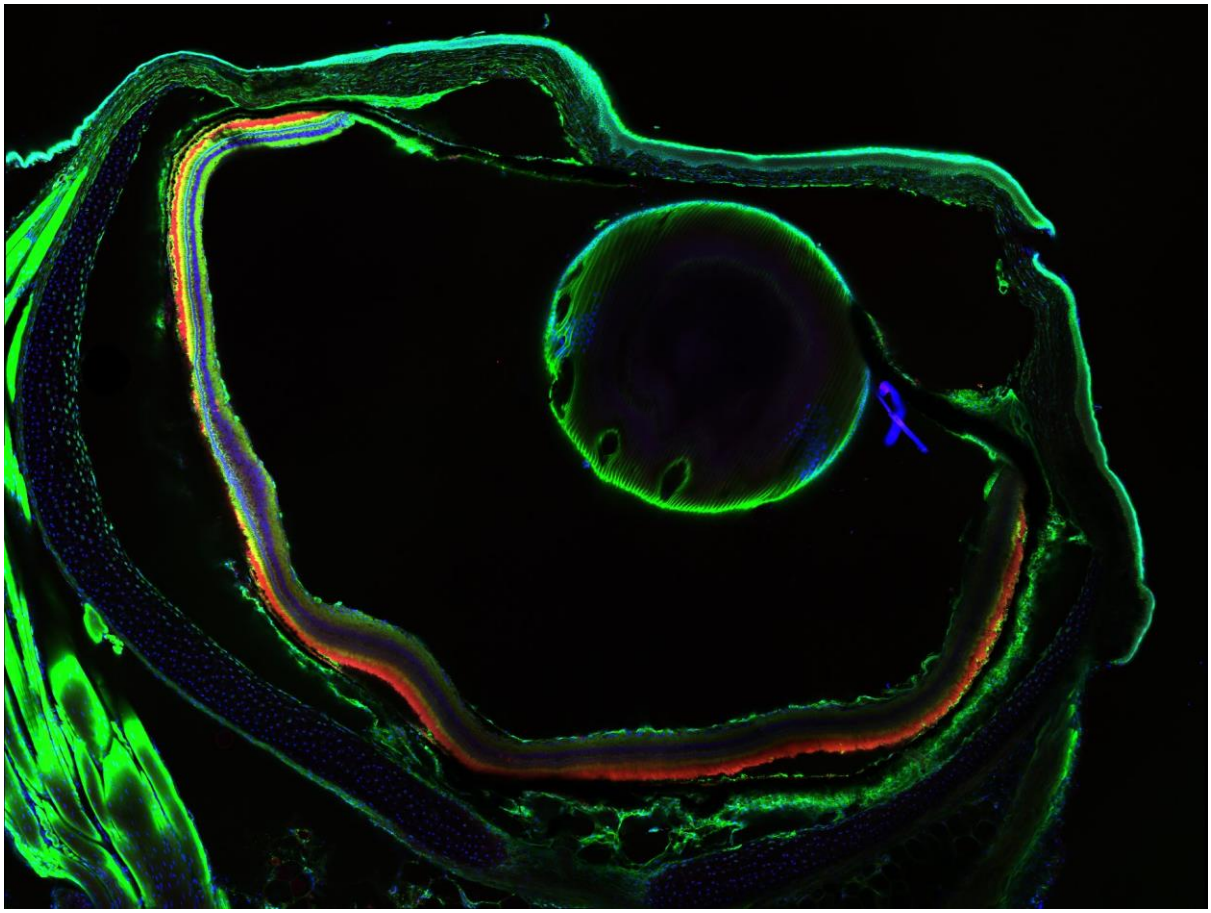

Un istinto ben comprensibile, lo stesso che ci ha spinti sulla luna, induce i girini ad allontanarsi dallo specchio d'acqua dove hanno compiuto la muta; non importa verso dove, in qualunque luogo salvo quello.
(Primo Levi)

An understandable instinct, the same that led us to the moon, guides tadpoles to move away from the body of water where they have completed the molting; it does not matter where, everywhere, except there.
(Primo Levi)

To my grandparents

Table of Contents

Abstract

Light and dark cycles are one of the principal driving forces for the metabolism of both eukaryotic and prokaryotic organisms, which are the evolutionary closest one to the first living beings. Therefore, is reasonable to think that the alternation between light and dark has influenced the evolution of all the organisms on Earth. Cyanobacteria as well as yeasts have evolved oscillating rhythms of gene expression, also known as circadian rhythms, in order to synchronize their physiological processes with Earth's day/night cycles. Light cues can also drive unicellular organisms' motility and growth. However, the light perception of these organisms is limited, and the vast majority of them can express a small number of molecules that can detect a limited range of the light spectrum.

On the other hand, metazoan and in particular vertebrates have evolved very specialized and sensitive neurons, rods and cones, which enable visual perception in almost all the lightning conditions that occur during the 24 hours of the day. It has been hypothesized that vertebrates have evolved firstly cone photoreceptors, to perceive light changes during the day (photopic vision). However, cones' sensitivity is very limited at night and in low illumination conditions their functions as photons detectors are drastically reduced. Rods instead can perceive very dim light signals at night (scotopic vision), even single photons, ensuring an approximate visual stimulus also in poor lighting conditions. It has been proposed that rods are the latest evolved photoreceptors, which have conferred to vertebrates an extraordinary sensitive visual system.

The cellular and molecular mechanisms of light and dark adaptation in vertebrates' photoreceptors have been widely studied and accurately described since the early seventies of the last century. Nonetheless, the study of these fascinating and complex dynamics has left some open questions, regarding both physiological and pathological aspects of photoreceptors metabolism as well as the influence of these alternating mechanisms on phototransduction, the set of enzymatic reactions that transform light stimuli into electrical signals.

During the course of my PhD, I have focused my attention on rod's physiology, in particular on the mechanisms that govern light induced degeneration of photoreceptors, in a Xenopus laevis model of retinitis pigmentosa. Frogs carrying a specific genetic mutation displayed an altered turnover of their cellular body as well as some deficits of phototransduction signaling cascade. In our work, we attempted to estimate how many light induced photoisomerization were necessary to see these alterations.

Moreover, I have partially continued the assessment of the response of rods photoreceptors to very localized light stimuli, elicited by mean of a special type of metal coated, tapered optical fibers. Through this technique, we have studied light adaptation of Xenopus laevis' rods to very confined light stimuli, in order to understand if variations of this process may occur along the rod cells bodies.

Furthermore, I have assessed the possible contribution of the circadian rhythms on the phototransduction machinery, by altering the light and dark adaptation cycles of Xenopus frogs. Finally, I have initiated the study of the possible coupling between mechano and phototransduction in rod photoreceptors. This last part is the most fascinating one and made me embrace the idea that sensory neurons are surely specialized cells for one sensory stimulus such as light, sound or chemicals molecules, but others sensory stimuli like temperature variations and small mechanical forces could modulate significantly the perception of the principal stimulus.

Declaration

All the single cell results described in sections 2.1, 2.2 and 4 of my thesis derived exclusively from my experimental work. Prof. Moritz and his group performed the ERG experiments and the immunohistochemical analysis described in section 4. Together with Fabio Falleroni we did all the experiments of section 2.3 and 6. Simone Mortal has done the immunohistochemical analysis of section 2.3.

1. Introduction

1.1 Vertebrates and invertebrates photoreceptors

The vast majority of metazoan are responsive to light. The ability of perceiving luminous variations during the day/night cycle, the detection of food, the evasion from predators and the recognition of a suitable partner for mating have been determinant and compelling factors for the development of a visual system [1]. All the metazoan have evolved this complex sensory system, with ocular and/or extraocular photoreceptors cells that can be divided in rhabdomeric or ciliary photoreceptors. The general distinction between these two main categories of photoreceptors can be done accordingly to their morphological features and to the molecular mechanism that they adopt to transduce light signals [2]. Protostomes organisms (invertebrates) mostly display rhabdomeric photoreceptors, which have photosensitive cellular membranes composed of modified microvillar projections. The strategy to transduce light signals in rhabdomeric photoreceptors involves the phospholipase-C signal pathway [3]. When a light stimulus activates this signal pathway, the rhabdomer depolarizes and transmits the electrical signal through the release of histamine, which hyperpolarizes the downstream neurons [4,5].

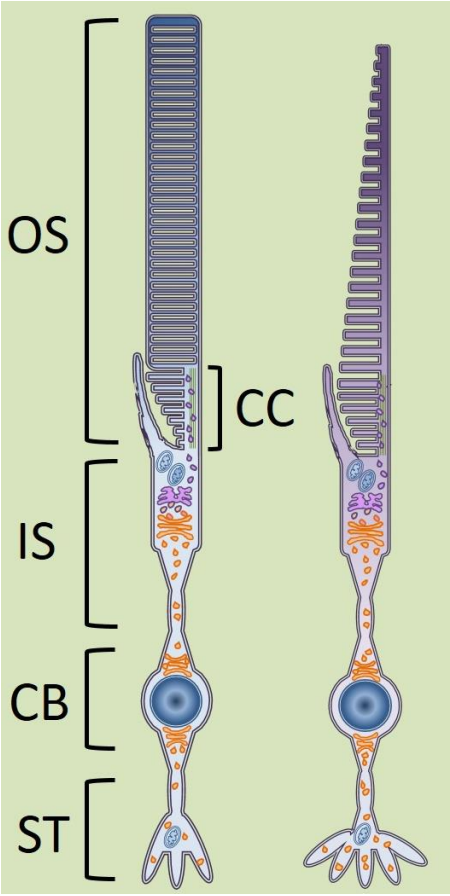

Figure 1.1. Representation of vertebrates' photoreceptors. Schematic representation of a rod (on the left) and a cone (on the right). All the compartments of the cells are evidenced by abbreviations: **ST**, synaptic terminal; **CB**, cellular body; **IS**, internal segment; **CC**, connecting cilium; **OS**, outer segment.

On the other hand, deuterostomes organisms (comprising vertebrates) mostly exhibit ciliary photoreceptors. In particular, the two major categories of photoreceptors of vertebrates organisms, rods and cones, provide a reliable precise and fast sensory input for the visual system [2]. They transform the gradual changes of light during the day, the perception of colors, as well as the shape of objects in electrical impulses, which are elaborated by the central nervous system in a complex visual perception [2].

Rods and cones are very specialized neurons, with an elongated and polarized cellular body subdivided in different morphological and functional regions (**Figure 1.1**). The synaptic terminal (**ST**) connects them with the others cells of the retina [6]. The cell body (**CB**) contains the nucleus; the inner segment (**IS**) contains the endoplasmic reticulum (**ER**), the Golgi apparatus and the mitochondria. The IS is in continuity with the outer segment (**OS**) through a tiny

portion of cytoplasm called connecting cilium (**CC**). The OS is the most characteristic feature of rods and cones. It is a modified cilium that contains a densely packed stack of membranous disks, in which are embedded all the protein of the phototransduction [2]. This signaling cascade is very similar in both rods and cones [7], but for the purpose of my thesis I will focus mostly on rods' physiology.

1.2 Phototransduction activation and termination mechanisms in vertebrates

1.2.1 Photoreceptors in resting dark conditions

In dark conditions, excluding the spontaneous activations that are mostly due to the thermal activation of the signaling machinery (dark noise components) [8], phototransduction is turned off. The opening of non-selective cationic channels activated by cGMP (**CNG** channels) expressed on the OS membrane, as well as the activity of the electrogenic Na^+/Ca^{2+}, K^+ exchanger (**NCKX**), maintain a net inward current of positive charges from the extracellular space to the OS cytoplasm, which

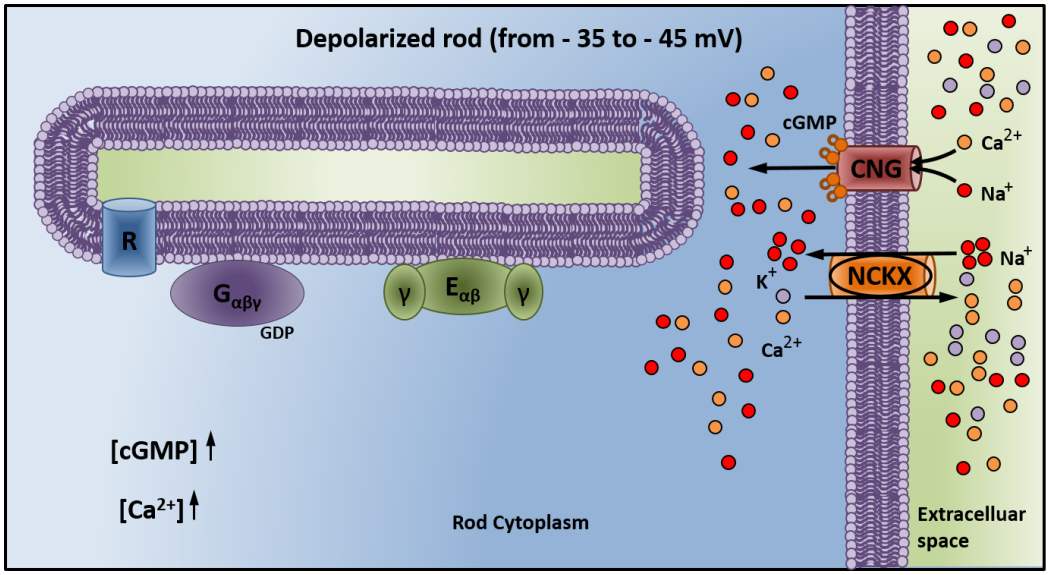

Figure 1.2.1. Phototransduction in resting conditions. Representation of the resting state of the phototransduction machinery, in dark conditions. Rhodopsin (**R**), transducing (**G**) and phosphodiesterase (**E**) are all inactive and the CNGs are opened, allowing the influx of positive ions inside the OS. Calcium as well as cGMP concentration are elevated and the rod is depolarized at around -35/-45 mV.

depolarize the photoreceptor (**Figure 1.2.1**) [9]. On the IS membrane are expressed two main types of K^+ channels, the hyperpolarization-activated, cyclic nucleotide–gated channels (**HCN**)[10] and the K_x channels that do not inactivate and are important for the light responsiveness of rods [11]. Together with the activity of the Na^+/K^+-ATPase, these channels maintain a net outward current of positive charges from the IS cytoplasm to the extracellular space [12]. These two ionic fluxes generate a loop of positive charges called "dark current" that keeps the photoreceptor resting membrane potential at around -35/-45 mV [7]. Therefore, in dark conditions, rods are depolarized and release the excitatory neurotransmitter glutamate from their synaptic terminal [13].

1.2.2 Phototransduction activation

Phototransduction begin when light encounters a rod and rhodopsin (**R**) absorbs a photon. R is a member of the G-protein-coupled receptor (**GPCR**) family, expressed on the disks membranes of the OS. Like all the other GPCR, is composed of seven transmembrane helices linked by six extra-membrane loops and it accommodates the chromophore molecule 11-cis retinal on the seventh helix [14]. Retinal is the actual photons sensor and consequently to the absorption of a photon, it changes conformation from 11-cis to all-trans retinal, becoming a stronger agonist of the enzymatic activity of R [7]. Activated R (**R***) became metarhodopsin and contacts hundreds of molecules of the G-protein transducin (**G**), amplifying the signal [12]. This trimeric G protein is a complex of three subunits, G_α, G_β, and G_γ anchored to the disks membrane. The successful activation of G promotes the substitution of the guanosine di-phosphate (**GDP**) molecule on its G_α-subunit with a guanosine tri-phosphate (**GTP**) molecule [2]. This substitution is energetically expensive for photoreceptors and in terms of adenosin triphosphate molecules (**ATP**) consumption, it has been estimated that it requires around $3*10^6$ ATP s^{-1} [15]. Two G_αGTP complexes leave the respective $G_{\beta\text{-}\gamma}$ complexes and bind to two inhibitory γ subunits of another protein anchored to the disk membrane, the phosphodiesterase (**E**). Consequently, the catalytic $E_{\alpha\text{-}\beta}$ subunits are activated and catalyze the hydrolyses of thousands of cyclic guanosine monophosphate (**cGMP**) molecules [7].

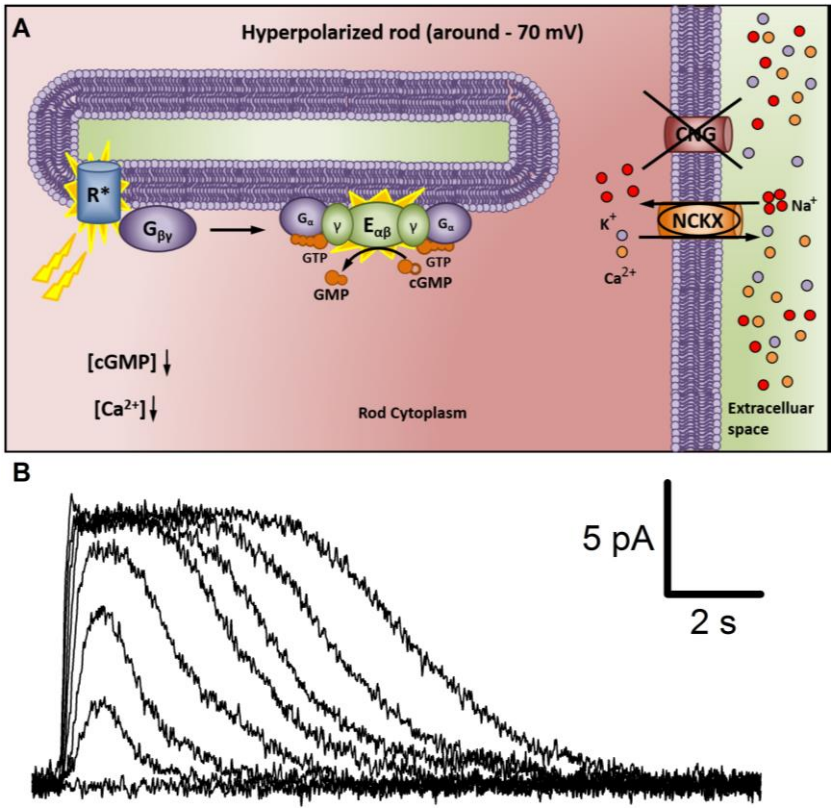

Figure 1.2.2. Phototransduction activation. (A) Schematic representation of the phototransduction activation (see the main text for the details). **(B)** Representatives traces of the progressive decrease of circulating dark current, which is proportional to the light intensities.

Therefore, the cytoplasmic concentration of cGMP decrease and this reduction leads to the closure of CNG channels on the OS membrane. The major effects of this closure are the progressive shutdown of the depolarizing inward current throughout the OS, the dropping of the Ca^{2+} concentration in the

OS, mostly due to the still functioning Na^+/Ca^{2+}, K^+ exchanger, and the progressive hyperpolarization of the cell (**Figure 1.2.2 A**) [16]. The hyperpolarization is proportional to the intensity of the light stimulus and reaches a saturation level at which all the CNG channels are closed (**Figure 1.2.2 B**) [17].

Unlike others sensory neurons, the activating stimulus of phototransduction signaling cascade inhibits the release of glutamate from the synaptic terminal, therefore inhibiting the synaptic transmission [18,19]. Hence, metabolic energy consumption drops during a light stimulus and rods require less energy to maintain their hyperpolarized state [15].

1.2.3 Phototransduction termination and modulation of dark adaptation

The mechanisms involved in the recovery of the phototransduction machinery after the light onset and partially in the termination of the photoresponse, are calcium-mediated by negative feedback mechanisms (**Figure 1.2.3**)[20], for instance, the termination of the enzymatic activity of R*. This process is mediated by recoverin (**Rec**), a soluble modulatory calcium binding protein, not anchored to the plasma membrane. In dark condition Rec binds two calcium ions and is linked to rhodopsin kinase (**RK**) at the disk membrane, preventing its phosphorylation activity on R [18]. After phototransduction, calcium concentration drops in the OS. Therefore, Rec releases the two calcium ions and dissociates from RK, which is able to interact with the activated R* and to phosphorylate its serine residues near the C-terminus [7]. Phosphorylated R* is then recognized by arrestin (**Arr**) that reduces its catalytic activity (**Figure 1.2.3A**). In the deactivated R*, the retinal is in its all-trans conformation, it has lost the ability to absorb photons (is 'bleached') and detaches from R* [2]. The all-trans retinal is reduced to all-trans retinol and leaves photoreceptors, translocates to the retinal-pigmented epithelium (**RPE**) cells, which restore its 11-cis conformation. Therefore, a supply of 11-cis isomer is necessary to maintain the responsiveness of the photoreceptors [7].

On the other hand, the mechanism of inactivation of the $G_\alpha GTP\text{-}E_\gamma$ complex is not calcium mediated and involves the regulator of G-protein signaling (**RGS9**) as well as the type 5 G-protein β subunit (**Gβ5**). These two modulatory proteins bind the complex $G_\alpha GTP\text{-}E_\gamma$, forming an intermediate quaternary complex that accelerates the intrinsic GTPase activity of the G_α subunit. Moreover, this transitory complex may favor the access of water molecules to the GTP binding site on the G_α subunit, supporting the hydrolysis of the GTP molecule and the inactivation of the G_α [12], therefore inhibiting the activity of E* (**Figure 1.2.3B**).

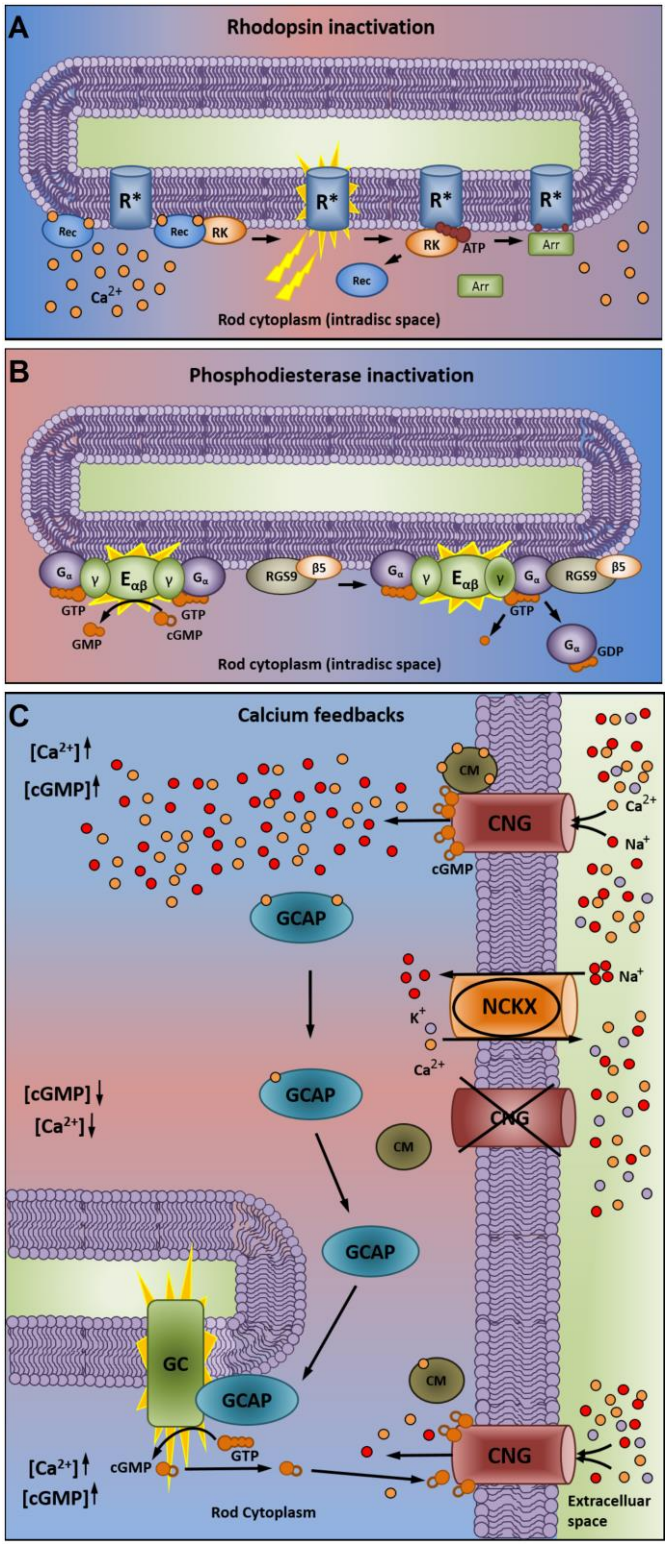

Figure 1.2.3. Inactivation mechanisms of the photoransduction. General mechanisms of inactivation of the principal proteins, involved in the phototransduction signaling pathway. All the mechanisms are described in details in the text. The shading between blue and red backgrounds represents the transition between light and dark.

A third mechanism, which directly modulates the restoration of the cytoplasmic concentration of cGMP in the OS, is calcium dependent. In dark conditions, the high calcium concentration inhibits the activity of two calcium-binding proteins, the guanylate cyclase-activating protein 1 and 2 (**GCAPs**). During a light stimulus, the drop in calcium concentration inside the OS activates the GCAPs, which in turn activate the enzyme guanylyl cyclase (**GC**). The enzymatic activity of GC increase the cGMP concentration in the OS, counteracting the activity of E* and leading to the re-opening of the CNG channels, which restore the depolarizing dark current across the OS [2].

Moreover, the modulation of the reopening of the CNG channels is also calcium mediated. In dark conditions, high calcium concentrations in the OS saturate the calcium binding sites of the protein Calmodulin (**CM**), which in turn is bound to the CNG channels. The complex calcium-CM-CNGs increase the $K_{1/2}$ of CNG channels for cGMP [21]. When calcium concentration drops during the light onset, CM dissociates from the CNGs. This mechanism leads to the decrease of their $K_{1/2}$ for cGMP and promotes the repolarization of the rod (**Figure 1.2.3C**).

Therefore, while luminous stimulus ends, rods rapidly regain their dark-adapted state. This process is extremely costly for the cell [15]. Photoreceptors have to shutdown the activated R* and to restore the concentration of cGMP, reactivating the dark current through CNG channels. It has been

estimated that the phosphorylation of R* and the termination of its active state, costs $6*10^5$ ATP s^{-1}, whereas the restoration of the cGMP concentration in the OS and consequently the reopening of CNG channels, needs around $5.7*10^7$ ATP s^{-1} [15]. Therefore, in dark conditions photoreceptors have to maintain their depolarized state trough the opening of CNG channels; they also release glutamate from the synaptic terminal and as a consequence metabolic energy consumption rises [15]. Considering these aspects, darkness might be seen as the excitatory stimulus for rods [7].

1.3 Molecular bases of light adaptation

1.3.1 General principles of light adaptation

The changes of light during the day/night cycle vary over 10 orders of magnitude [22]. Besides, the diurnal switch between rod and cone sensory pathways allows vertebrate to adjust their visual perception and respond properly to these changes [23]. The different sensitivity of rod and cone photoreceptors to the light spectrum is the origin of this elevated plasticity.

In general, the sensitivity (S) can be described as the response amplitude (∂r) in relation to the intensity of the stimulus (∂I).

$$S = \frac{\partial r}{\partial I}$$

For photoreceptors, this relation can be indicated in quantal terms, namely from a very dim flash it can be estimated the number of activated R* [18]. Rods are more sensitive to dim light stimuli than cones and they can even respond to single photons [24]. In other terms, rods that have been dark adapted to be fully responsive, can transduce a signal over their intrinsic noise range, by even the photoisomerization of a single R molecule [25]. This extraordinary sensitivity allows the visual system to function also with very low levels of illumination. However, rods responses saturate to moderate light intensities, so that the release of glutamate from their synaptic terminal during the day is almost completely abolished [26,7].

Cones instead are less sensitive to dim light. They detect a signal only if at least 4-10 molecules of visual pigment are isomerized. Even so, their responses to steady stimuli do not saturate and their spectral sensitivity to light is wider in respect to rods [27,28]. Therefore, it has been hypothesized that vertebrates have evolved firstly cone-like photoreceptors, to perceive the changes of light during the day and secondly rods and their sensory pathway [1].

Despite the differences in spectral sensitivity, exposing both types of photoreceptors to a long lasting stimulus, such as an impulse of steady light, results in a decrease of the circulating dark current, which

partially recovers after some seconds (**Figure 1.3.1 A**). This adjustment is called light adaptation and is generally characterized by a reduction in photoreceptor sensitivity (desensitization) and by the acceleration of the response kinetics [23].

The process of desensitization of a photoreceptor follows Weber's Law, which is generally used to describe the relation between the actual physical nature of a stimulus and its perception:

$$S_{steady} = \frac{S_0}{\left(1 + I_{steady}/I_{1/2}\right)}$$

This simple equation highlights the inverse proportionality between photoreceptors' sensitivity (S_{steady}) that declines from its initial value (S_0), and the amplitude of a steady stimulus (I_{steady}); $I_{1/2}$ is the steady intensity that half-desensitizes the response. The value of $I_{1/2}$ is strictly dependent on the degree of light/dark adaptation of the cells and is calculated from rods' responses [18]. In general, all light adapted photoresponses reach the peak amplitude faster, and have also a faster falling phase [29]. Light adapted rods display this peculiar acceleration of the response kinetics that are related to changes in the underlying molecular machinery of phototransduction (**Figure 1.3.1 B**).

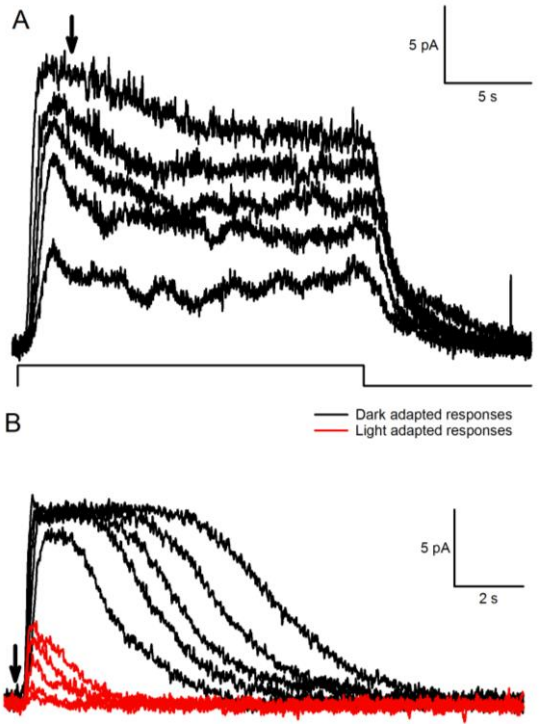

Figure 1.3.1. Photoresponses' light adaptation and light adapted photoresponses. (A) Representative recording of the photoresponses of a dark-adapted rod, to long lasting stimuli of progressively higher intensities of light. The arrow indicates the beginning of the delayed decrease of amplitude associated with light adaptation. The black squared line represent the "step" of light that triggered the photoresponse. **(B)** Response of a light adapted (red traces) and a dark-adapted (black traces) rod to similar light intensities. The first three red traces represent the responses of a light adapted rod to the same light intensities that elicited the last three responses of a dark-adapted rod. The arrow indicates the timing of the light pulse.

1.3.2 Molecular mechanisms of light adaptation

The ensemble of the mechanisms that govern light adaptation is a combination of phototransduction activation, modulation and termination [7]. Besides, it has been shown that calcium play a fundamental role in light adaptation of photoreceptors [30,31]. When calcium concentration is maintained around its resting dark level in the OS, with specific Ringer solutions, photoreceptors fail to adapt to light stimuli. Namely the range of their responses is severely restricted and they saturate at very low light intensities [23]. Therefore, the physiological decline of calcium concentration in the OS prevents rods' responses from saturation at low light intensities, contributing in both extending their operating range (the range of light intensities at which they can respond with distinguishable events) and in modulating flash sensitivity (i.e., the minimum

amount of light that rods can perceive) [23]. Nine main mechanisms have been described as key aspects of light adaptation. They can be classified considering their role in increasing or decreasing photoreceptor sensitivity, operating range and the involvement of calcium [7,23].

Two main mechanisms are involved in the extension of the operating range and in the increase of sensitivity of photoreceptors, and both are calcium mediated (see also section *1.4*):

1) *GC steady increase in synthesis activity*. In dark, the resting calcium concentration in the OS is around 400-600 nM and drops to 30-50 nM during a light stimulus. This decline triggers the activity of GCAP proteins that in turn activates the GC. The activity of GC can increase almost 10 times when calcium concentration declines in the OS, during a steady light stimulus [32,33]. Therefore, this mechanism modulates indirectly the re-opening of CNG channels by restoring the cytoplasmic concentrations of cGMP. Hence, more dark current could be available and modulated by a second flash of light.

2) *Effect of CM modulation on CNG channels*. Another mechanism that modulates the reopening of CNG channels is carried out directly by CM. This calcium protein has two binding sites on the β subunit of the CNG channels. In darkness, CM is bound to calcium and is associated to the CNG channels, increasing their $K_{1/2}$ for cGMP, thus lowering their opening probability [23]. When calcium concentration drops after a light stimulus, CM dissociates from CNG channels, decreasing their $K_{1/2}$ for cGMP and increasing their opening probability.

By favoring the reopening of the CNG channels after and during a light stimulus, these two calcium-mediated processes not only extend the operating range of the rods, but they also increase their sensitivity, partially rescuing phototransduction machinery from saturation [7]. The remaining seven mechanisms, influence mostly photoreceptors desensitization and not all of them are calcium dependent:

3) *Compression of the range of rods' responses*. In a rod exposed to a not-saturating steady light stimulus, dark current is partially shut down and the amount of residual currents that could be modulated with a second flash of light is reduced. In fact, steady light closes a fraction of CNG channels and the phototransduction activated by a second flash has a limited operating range, until reaching saturation. Therefore, in this conditions, photoreceptor sensitivity and the range of its responses are reduced [34]. This compression effect can derive not only from different background illumination, but also from different recording conditions, for example clamping calcium concentrations around its dark levels in the OS [35].

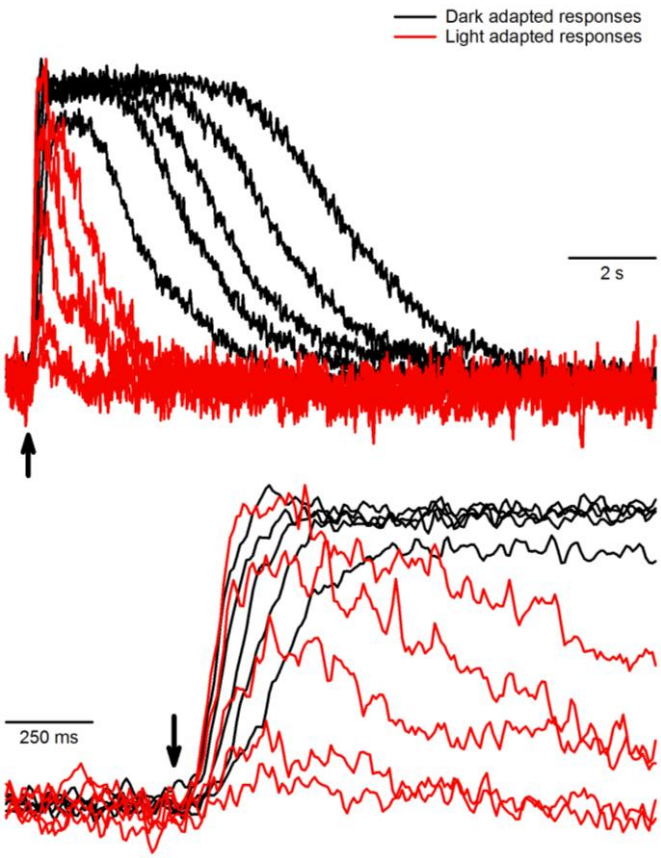

Figure 1.3.2. Normalized dark adapted and light adapted photoresponses. The responses' kinetics of the light adapted rod and the dark-adapted rod are very different when observed with their original scale (**Figure 1.3.1 B**). On the other hand, the normalized traces evidence similar time course of the rising phase, indicating that light adaptation affects mostly the falling phase of the photoresponses. Indeed the amplification of the phototransduction cascade is unaltered by the light adaptation and the only major change is in the amplitude of the responses, which is proportional to the available signaling machinery.

In order to analyze and compare the variations of photoresponses kinetics and to account for the compression of the operating range and the changes in sensitivity, it is sufficient to normalize the responses by dividing them for the value of the peak amplitude of the circulating dark current (**Figure 1.3.2**) [36]. This normalization is based on the assumption that if the reduction of rods sensitivity was caused only by the compression of the responses, the number of additional E* catalytic subunits activated by a second flash would be independent from the background intensity [23,35]. Consequently, the activity of the additional E* catalytic subunits would produce a constant change in cGMP concentration, which would be independent from its initial concentration [35]. Furthermore, it has been demonstrated analytically that a constant portion of the opened CNG channels would be closed by a given flash, independently from the background intensity [37]. Thus, all these mechanisms involved in the initial phase of phototransduction should be considered as independent from background light.

4) *Intrinsic gain of R* activity*. The decrease in sensitivity of photoreceptors, due to a background light stimulus, was related to a reduced increment of the activation and amplification reactions of phototransduction (from the activation of R* to the activation of E*) as an effect of the decrease of calcium concentration in the OS [38,39]. This hypothesis was rejected on the bases of experimental evidences that showed that independently from the

background light and from calcium concentration, the rising phase of the responses to the same stimulus followed the same initial amplification pathway [37]. However, a progressively higher intensity of background light decreased the time of the recovery phase of these responses, indicating that the lifetime of one or more of the amplification intermediates was also shortened [35].

Experimental evidences showed that the reactions governing the life time of the activated R* and of cGMP, are mostly influenced by calcium drop and are the main responsible for the acceleration of the recovery phase during light adaptation [23,35]. This conclusion were drawn from the step-flash paradigm experiments: in these experiments, Fain et al. demonstrated that clamping calcium concentration inside the OS near the dark level resulted in a complete failure of the shortening of the recovery phase, when a flash was presented after steps of increasing background light.

5) *Reduction of R* lifetime induced by the decrease in calcium concentration*. The mean lifetime of catalytically active R*, during light adaptation to a steady stimulus, is reduced by its phosphorylation mediated by RK and its modulator Rec and the subsequent binding with Arr. This reaction is quite fast (0.5 s)[7] and governed by the negative feedback calcium mechanism that involves Rec. Strong experimental evidence demonstrated that in knockout mice for RK, Rec or Arr, responses to flashes of light were prolonged, indicating an increase in the lifetime of activated R* and the absence of the calcium negative feedback loop [7,40,41]. These responses resemble those obtained when calcium was clamped at a certain concentration and prevented to change.

The contribution of calcium can be taken into consideration also for the life time of the catalytically active R*, triggered by a simple flash of light. Consequently to this transient activation of R, calcium concentration in the OS is transiently reduced. This reduction can trigger a transitory decline in the activated R*, similar to the one described for the steady light stimulus[42]. However, this feedback process can be mostly appreciated when rods are maximally dark adapted, because the majority of the Rec molecules are bound to RK and therefore R* has the largest initial lifetime. This mechanism is less evident when rods are subjected to higher background illuminations that lead to the complete activation of the RK molecules.

6) *Reduction of cGMP lifetime in relation to the steady activity of E**. During a steady background stimulus, the number of catalytically active E* subunits increase, increasing the rate of cGMP hydrolysis while decreasing the sensitivity. A second flash of light activates additional E* catalytic subunits resulting in: a reduction of the time to peak of the response, a decrease of the cGMP concentration in the OS and finally to a drop of rods' sensitivity. This mechanism accelerates the recovery of the response, activating indirectly the calcium feedbacks by closing the CNG channels [37]. On the other hand, the inactivation of the $G_{\alpha}GTP$-E_{γ} complex is not calcium mediated. Therefore, the inactivation of this complex is independent from any other mechanism. Indeed this step is the limiting temporal factor or dominant time constant that govern the overall sensitivity of the response [43].

To have a global view of the mechanisms that describe the variations of cGMP concentration during light adaptation, Prof. Lamb and Prof. Pugh formulated the 'bathtub analogy' [7]. Imagine a rod as a bathtub, with a steady influx of water from a tap (cGMP produced by the GC) and a steady efflux of water from a plughole (hydrolysis of cGMP by E*), at a rate proportional to the water levels (concentration of cGMP). If a second small hole is opened and immediately closed in the tab (brief light pulse), this would cause a transient increment of the efflux rate (transient increment of the hydrolysis of cGMP by E*), which would be re-equilibrated immediately by the influx of water from the tap (cGMP produced by the GC). If the size of the plughole would be enlarged (steady light stimulus), the water level would be maintained only if from the tap, the influx rate would be increased and equilibrate the efflux (increased cGMP synthesis by GC). If in this condition, a second small hole is opened and immediately closed in the tab (brief light pulse), the transient increment of the efflux rate would be smaller than previously, and the recovery of the steady state would be faster (more cGMP synthetized by GC). This analogy may help understand why, in the light adapted rod, the additional E* catalytic subunits activated by a second flash, the variations of cGMP concentration and the opening of CNG channels are considered independent from the background light.

7) *Transient increase in synthesis activity of GC*. The response of a rod to a brief flash stimulus is accompanied by a transient decrease of the OS calcium concentration, mediated by the activity of the Na^{+}/Ca^{2+}, K^{+} exchanger [16]. Consequently, the activity of the GC temporary

rises, leading to a transitory increase of the cGMP synthesis and ensuring a rapid recovery from the stimulus [30]. The overall effect on sensitivity is the opposite if compared to that of the steady activation of GC: the peak amplitude is reduced as well as the flash sensitivity [23]. However, the relation between the sensitivity and the background light illumination is not affected much by the transient calcium-mediated increase of GC activity [30]. Hence, the normalized sensitivity obtained when calcium concentration is free to change closely resembles the one obtained when calcium concentration is clamped to the levels of steady stimuli [30].

8) *Increased calcium buffering*. Calcium buffering in the rod OS is necessary to slow the transient decrease in calcium concentration. This mechanism retards the increase of GC activity, the recovery of the response and increases its peak amplitude, increasing also the flash sensitivity [23]. The primary buffer protein for calcium is Rec, but also CM and GCAPS are involved in this process. It has been estimated that the concentration of Rec in the OS is around 30 μM [23]. When calcium concentration decreases in the OS, in relation to an increase of steady illumination, the free concentration of Rec increase and in an intermediate range of calcium concentration (not saturating light stimuli) its buffering power also increase [7].

9) *Light adaptation in cone photoreceptors*. Light adaptation in cones seams to work basically with the same molecular mechanism as rods, except that cones adapt to higher intensities of light, by bleaching their pigment [7]. Overall, cones can still respond to a wide range of stimuli, even if 90% of their total pigment is bleached. In comparison, rods responses saturate if 1% of their total pigment is bleached. This is due to the mechanism of amplification of the phototransduction, which in rods induce a great desensitization with moderate light intensities.

Light adaptation in rod photoreceptor is a very complex system of biochemical reactions, which has been modeled in great detail and in a very comprehensive manner, through the years [7, 23].

1.4 Rhodopsin mutations causing retinitis pigmentosa

1.4.1 Non-syndromic retinitis pigmentosa

Retinitis pigmentosa (**RP**) is the most common form of neurodegenerative disease of the retina. It causes visual disability and blindness in more than 1.5 million patients all over the world [44]. RP cases have two major origins. The genetic or non-syndromic forms of RP are caused by mutations of more

than 80 genes, which have been characterized and proposed to be responsible for this group of disorders. These mutations are expressed mostly in retina photoreceptors or in the RPE cells [44,45]. On the other hand, the syndromic forms of RP are associated with extra-ocular pathologies [44]. Generally, patient affected by RP initially experience deficit of dark adaptation and of peripheral vision, in the early phase of the adolescence or of the young adulthood. The early onset of these deficits can remain unnoticed because many patients, in particular children, can compensate for them. However, the most severe cases lose normal vision in the early childhood and therefore progress more rapidly [44]. The initial symptoms that characterize RP derive from rods degeneration, the most common are night blindness and the progressive loss of peripheral vision, which leads to an alteration of the visual field called tunnel vision. Anatomical abnormalities can appear early in the central retina, but most of the RP patients retain central vision until the late and most severe stage of the pathology, where also central vision is lost, indicating the degeneration of cones photoreceptors [46].

The severity of the non-syndromic form is also related to the inherited genetic traits. RP mutations can be inherited as X-linked, which account for the 5-15% of all patients and have a more severe prognosis compared to autosomal recessive (**arRP**) mutations, which account for the 50-60% of RP patients. The autosomal dominant (**adRP**) mutations affect the 30-40% of the totality of the RP cases and these patients display the best long-term outcome for retaining central vision. Many mutations of at least 14 gene have been identified as responsible for the adRP subtype and the 26% of them are mutations on the R gene [47].

1.4.2 Rhodopsin mutations in autosomal dominant Retinitis Pigmentosa

More than 150 missense and nonsense mutations of R have been characterized and associated with adRP phenotype. These mutations are the most common cause of adRP, accounting for 20-30% of all cases [47]. They can be classified accordingly to their clinical outcome in two major categories: class A, which present an early onset of rod degeneration, a fast progression and a more severe clinical outcome; class B is associated with a slower progression and a later onset of rod dysfunctions.

A recent and meticulous classification of adRP mutations accounted for in vivo and in vitro experimental results, obtained using cell lines as well as more physiological models such as transgenic animal model. These results have contributed to define additional criteria of classification such as thermal stability, the constitutive activation R, the activation of transducin, the R trafficking [46]:

- Class 1 refers to the mutations that induce a normal folding of R, but are subjected to anomalous post Golgi trafficking and OS targeting.

- Class 2 mutations induce the misfolding of R, which can be retained in the ER, cannot reconstitute its binding with the 11-cis retinal after bleaching and can be structurally unstable.
- Class 3 mutations affect vesicular trafficking and endocytosis.

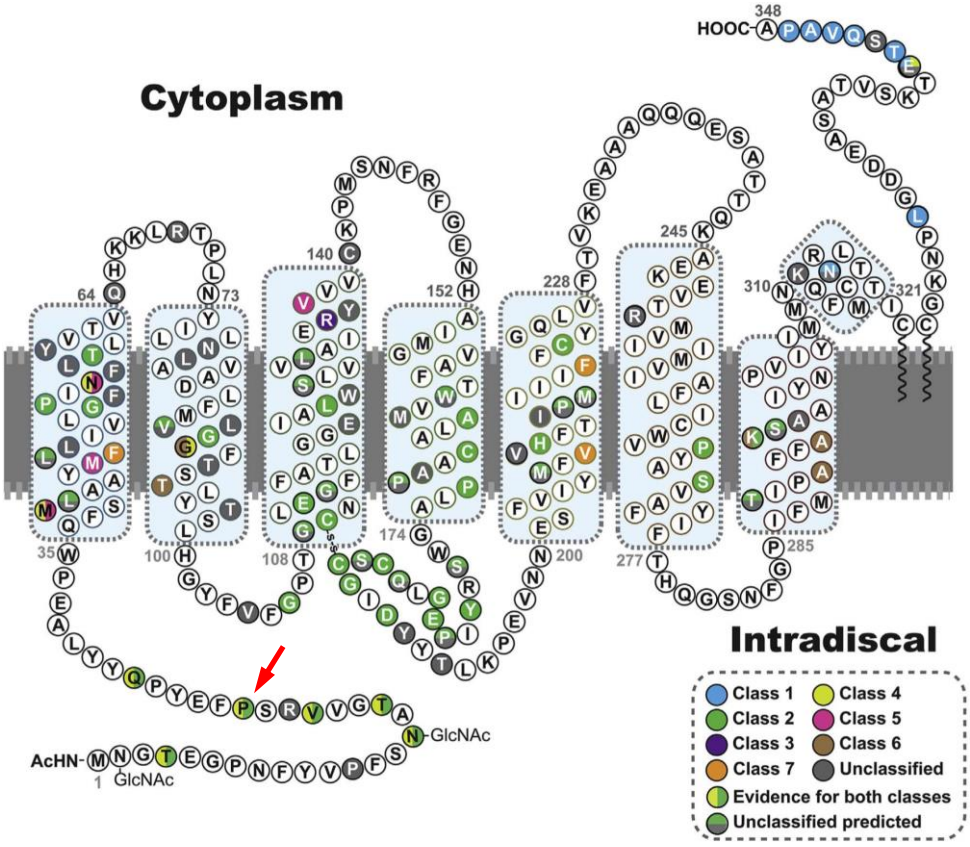

Figure 1.4.2. Rhodopsin mutations causing adRP. Schematic representation of all the known rhodopsin mutations that cause adRP. The citoplasmatic and the intradiscal domains are indicated, as well as the major classes of mutations (modified from Verbakel, S. K. et al. 2018). The red arrow indicate the position of the P23H mutation, which is taken in exam in section 2.1.

- Class 4 refers to those mutations that display altered post-translational modification and structural stability.
- Cass 5 mutations are characterized by an amplification of the activation rate of G.
- Class 6 encloses all those mutations that fold correctly, but are constitutively active.
- Class 7 mutations display dimerization defects.

A large number of mutations do not display biochemical or cellular defect, or have not been studied in detail, therefore remain unclassified (**Figure 1.4.2**).

1.4.3 The P23H mutation

adRP mutations are localized throughout the amino acid sequence of R. The mutations located in the N-terminus often correlate with less severe cases of RP, with low progressing symptoms and better prognosis [48]. The substitution of the proline in position 23 with an histidine (**P23H**) on the N-terminus

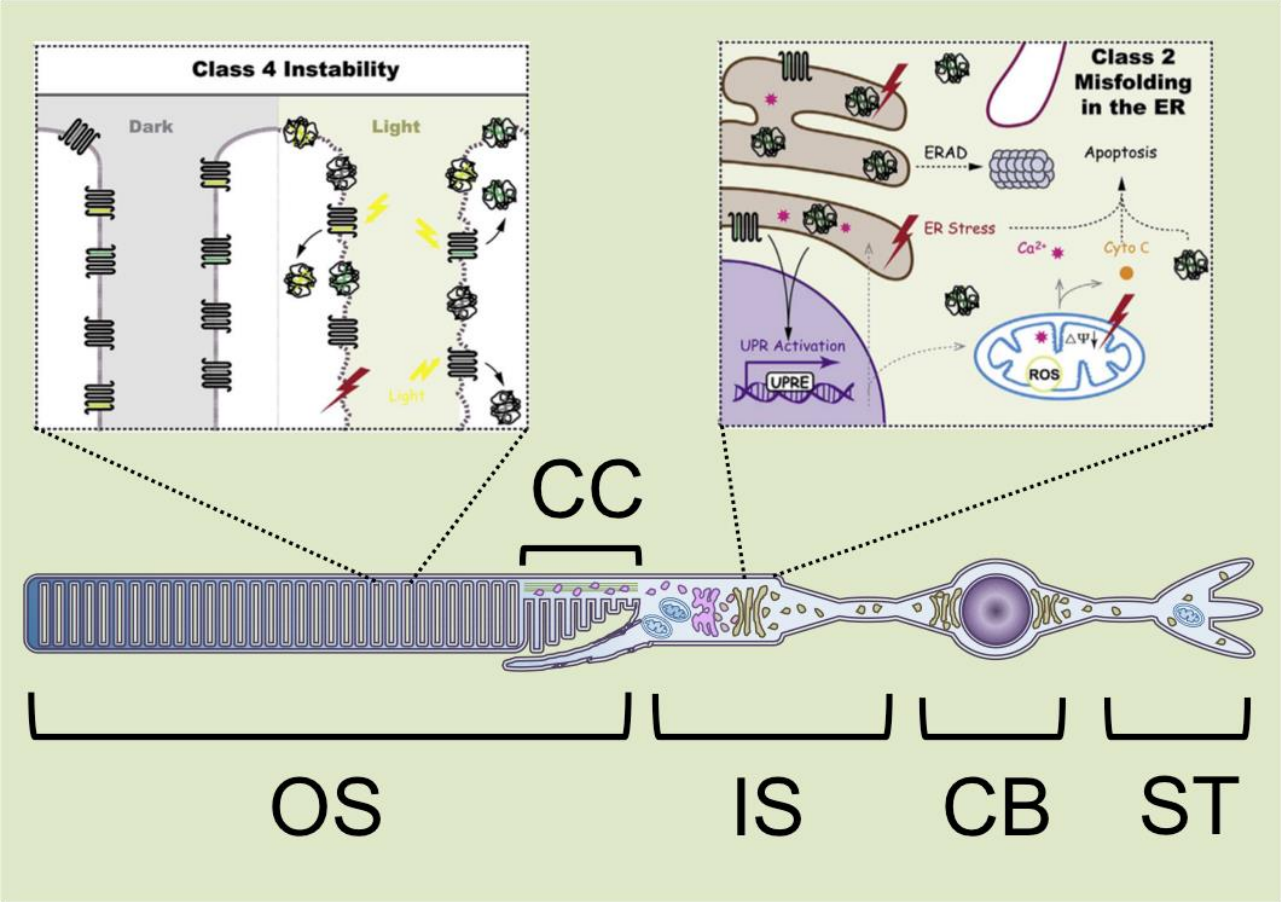

Figure 1.4.3 General pathophysiological mechanisms proposed for P23H mutant photoreceptors. P23H mutation has been classified as a class two mutation (top right panel). Class 2 mutants in the ER may induce ER stress, can be degraded by ERAD complex and can potentially aggregate, leading to the activation of pro-apoptotic pathways. On the other hand, light stimuli may lead to mutated rhodopsin instability, which could aggregate in the disk of the OS, causing structural damage to the plasma membrane and to the disc membrane (modified from Verbakel, S. K. et al. 2018).

of R (R_{P23H}) is the most common cause of adRP in North American patient, accounting for almost 10% of all cases [48]. This mutation is one of the most widely studied and an early attempt of classification partially identified the biochemical and cellular dysfunctions associated to it [49,50]. R_{P23H} mutants were unable to form a functional and correctly folded R that was either fully or partially retained in the ER [49,50]. Interestingly, these and more recent studies have highlighted that the altered absorption spectra derived from the misfolded R_{P23H} could be rescued administrating the 11-cis retinal [51,52,53]. However, the interpretation of these important results was limited because R_{P23H} abnormalities were assessed in heterologous systems, which did not fully account the complexity of photoreceptors' cellular and biochemical features. Others studies carried on transgenic animals confirmed that P23H

mutants receptors were retained in the ER of photoreceptors [54,55,56,57]. The accumulation of mutated R in the ER has been associated with cell stress and the activation of the unfolded protein response (**UPR**). This signaling network is necessary to restore the protein-folding homeostasis in the ER, but can lead to cell death if the stress is too severe and prolonged [48,54,58]. Importantly, glycosylations on the N-terminus may play a fundamental role for the translocation of mutated R_{P23H} in the OS. The molecular chaperones of the ER system normally recognize glycosylations on mutated protein and induce their ubiquitination and ER-associated degradation (**ERAD**) [58,59,60].

However, non- glycosylated or mono glycosylated R_{P23H} might escape the ERAD system and be expressed on the OS causing structural instability of the disk membrane after light exposure, photoreceptor degeneration and ultimately their death [54,55,56,57]. The destabilization of the mutated R_{P23H} in the rod OS has been associated also with the truncation of the N-terminus [61] and with an abnormal disulfide bond between cysteines in the intradiscal domain [62]. Some experimental evidences have also shown that in Xenopus laevis model expressing R_{P23H} in the OS, light could exacerbate rod cell death and that dark rearing preserved mutated rod from degeneration[63,64,61]. Interestingly, P23H and others N-terminus mutations were identified in patients in which degeneration interested mostly the light exposed sector of the retina [65,66]. Moreover, in some of these patients was observed an altered and prolonged dark adaptation phase after the light stimuli, which suggested an altered recovery phase of rod responses [65,67]. This mechanism was reported also in electroretinogram (ERG) measurements, obtained from VPP mice [68]. Thus, mutated R_{P23H} can be classified as a mixed of class 2 and class 4 mutation for its retention in the ER and the translocation in the OS respectively (**Figure 1.4.3**).

1.5 Rods physiology in relation to circadian rhythms

1.5.1 The role of the retina in the day/night cycle

Circadian rhythms are the ensemble of the biochemical, physiological and behavioral processes that oscillate within the 24 hours daily period, regulating the metabolism of most of the organisms [69]. All these rhythms are synchronized with day/night cycle by light induced settings, thus they can be adjusted accordingly to luminous environmental changes [70]. This mechanism is called photoentrainment. The master pacemaker that controls the mammalian circadian system is the suprachiasmatic nucleus (**SCN**) of the hypothalamus. This region of the brain is responsible for fundamental physiological functions, such as the regulation of sleep, the food consumption, regulation of the body temperature, the release of hormones and the heart rate [71].

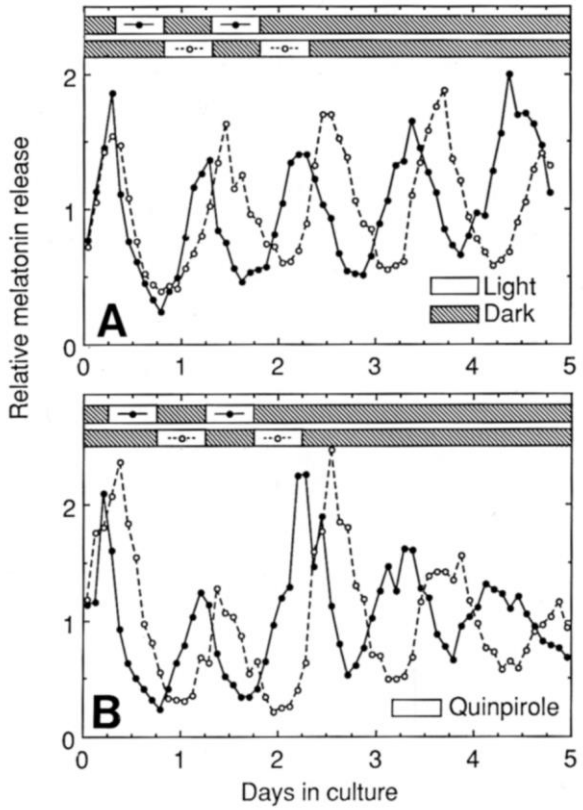

Figure 1.5.1. Shift of melatonin release in cultured photoreceptor layers of Xenopus laevis. The effects of the shifted light/dark cycle on melatonin release are very similar to those determined by the administration of quinpirole (an agonist of the D2 dopamine receptors). The graphs displayed the melatonin release as a function of the day in culture of the isolated photoreceptor cells layers. Both light stimuli and the treatment with 50 nM quinpirole displayed similar effects on the melatonin release (modified from Gregory M. Cahill and Joseph C. Besharse, 1993)

However, the SCN receives a significant bilateral projection from the retina and it was shown that even blind mole rats are subjected to photoentrainment and express cone opsin in their highly degenerate eyes [72]. Moreover, it has been shown that the complete enucleation of the eyes results in the total failure of the photoentrainment process induced by light shifts [73,74]. Therefore, the retina contributes significantly to the day/night photoentrainment, with an intrinsic circadian clock system and a specific biochemical machinery [74,75]. The first evidences of the role of the retina in the circadian regulation of vertebrates were obtained in Xenopus laevis cultured eyecups, in which was described the circadian activity of the serotonin N-acetyltransferase, a key enzyme for the production of melatonin [76]. Further experiments showed that melatonin acts in the eye with a neuromodulatory feedback, suggesting a possible role in the regulation of cellular metabolism of photoreceptors, RPE cells and other inner layer neurons [75,77]. Moreover, it was shown that Xenopus retinas alone, in which photoreceptor layers were isolated, were capable of generating circadian melatonin rhythms. Exposing the photoreceptors to alternated periods of light

and darkness or to an agonist of the D2 dopamine receptors, resulted in the phase shift of the release of melatonin, suggesting that rod and/or cone photoreceptors were the primary clock cells for melatonin rhythms in these animals (**Figure 1.5.1**) [78].

Interestingly, further experiments in mouse evidenced another type of cell responsible for light entrainment. Mice lacking both rods and cones were still able to maintain the phase shifting responses to light, meaning that they were still photoentrainable [73]. Moreover, light stimuli induced a strong depolarization in the retina ganglion cells that innervate the SCN, even when all the synaptic inputs from rod and cones were blocked. Retinal ganglion cells were able to respond to light stimuli, with a peak wavelength of 484 nm and further experiments identified that the photopigment molecule expressed in these cells was melanopsin, another member of the light-sensitive retinal receptors [79,80,81].

Overall, circadian clocks are found in many ocular structures such as the RPE and the cornea [71], but the photic entrainment of the all eye it seams to be under control of the neural retina, via melatoin, dopamine and eventually others humoral signals, since these additional structures are not able to sense light [82].

1.5.2 Circadian control of rod physiology

Beside the already mentioned circadian control of the melatonin/dopamine cycle, others aspects of rods physiology, metabolism and gene expression are influenced by circadian rhythms. Early experiments carried on rat and frogs demonstrated that the renewal of the OS, which consists in the progressive detachment of the tip of the OS, was light driven [83,84,85]. This process is called disc shedding and it was shown to occur independently from the light regime in which the rats and frogs were kept [83,84]. On the other hand, in Xenopus laevis different mechanism for normal disc shedding was proposed. In this type of frog different light/dark exposure could induce significant variation in the amount of new disc added or shed, with suggested independent mechanisms [85]. Interestingly, it has been proposed that the variations of rods OS length and of the amount of expressed rhodopsin per OS were a consequence of the adaptation to different luminous conditions [86,87]. This mechanisms could contribute in both light and dark adaptation processes in this type of phototreceptors [86].

Recently, it has been shown that rods photoreceptors are able to escape saturation during light adaptation and this mechanism could partially extend the response range and the sensitivity of rods, in day light conditions [88,89]. Since it has been shown that dopamine mediates light adapted vision [90], there could be a possible relation between this neurotransmitter and rod responses in light adapted conditions. On the other hand, melatonin could contribute in regulating rod responses in dark-adapted

state. It has been shown that rod dark adaptation is slower in day light condition or when mice retinas are subjected to stimuli that bleach 90% of the available R. Whereas, the dark adaptation in mice lacking melatonin production is not affected by circadian oscillation of light [91].

Moreover, several experimental evidences have demonstrated that the light/dark cycle controls the electrical coupling of rods and cones [92,93]. The dependence of rods coupling on dopamine cycle was firstly proposed in an important study that showed that in both goldfish and mouse retinas, rods-cones coupling is stronger at night. In this part of the day, cones sensitivity is very low and experimental evidences suggest that rods can 'share' with cones their responses to very dim light signals, and this mechanism could be dependent on D1-D2 dopamine receptors [92]. Recently, it has been shown that the electrical coupling between rods depends on the mice strains and on the time of the day. In one strain of mice the conductance measured between two rods was similar during the subjective day and the subjective night, whereas another strain displayed higher conductances at night. However, in both strain, the conductance was reduce to 0 pS during bright light adaptation [93]. On the other hand, it has been proposed that the rods-cones coupling is dependent on the activation of the D2-dopamine receptors, which is stronger during the day and diminishes the extent of this coupling. Thus, in general, dopamine and melatonin cycles can be light entrained in both mammals and other vertebrates. The mechanisms proposed for this circadian control have similarities, but also significant differences, depending on the species and on the genetic control exerted by specific clock genes [94].

1.5.3 Light regulation of gene expression

The expression of a great number of genes of vertebrates organisms is subjected to fluctuation during the day [69]. Besides the circadian regulated expression of both melatonin and dopamine, also the principal master regulator clock genes CLOCK, BMAL1, Per1,2 and Cry1,2 are rhythmically expressed in photoreceptors or in others cells of the retina [95,94]. Interestingly, it has been shown that the deletion of BMAL1 in mice retina resulted in altered pattern of expression of circadian regulated genes. Moreover, the responses of these mice in both scotopic and photopic conditions were altered, in particular the ERG b-wave, which indicated that the deletion of BMAL1 influenced mostly the inner retina electrical activity in response to light [96]. Furthermore, it has been demonstrated that in zebrafish retina, CLOCK expression is necessary to maintain the circadian expression of cone opsin mRNA [97]. It has also been shown that Cry plays an important role in stabilizing the signalplex of phototransduction interacting with actin, and enhances photereceptors sensitivity in drosophila rhabdomeres [98].

Early experimental results obtained in both fish and frog, demonstrated that the expression of R is light dependent and follows the circadian rhythms in both fish and frogs [99]. Moreover, in a study conducted in our laboratory, it has been evidenced that the expression levels of both Arr and GCAP proteins are upregulated with a prolonged exposition to light [88]. In a more recent study, AFM experiments have displayed variations of the structural properties of rod disc membranes and of rhodopsin domain, in response to different housing light conditions [100]. Mice were subjected to constant darkness or constant light conditions from 10 to 30 days. The experimental results displayed differences in both size of rhodopsin nanodomains and in the density of rhodopsin molecule, which were larger in animals kept in constant darkness. Moreover, ERG recordings of these animals confirmed that to structural changes corresponded significant variation of photoreceptors responses. Indeed, animals kept in constant darkness had larger a-b waves compared with animal kept in constant and in cyclic light. These authors have proposed that the adaptive structural changes of the OS required output from the phototransduction cascade, initiated by rhodopsin. Indeed, transgenic mice lacking the G_{α} subunit or born and raised in constant darkness do not display these variations. However, the packing density of rhodopsin in the membrane seams to be independent from rhodopsin expression. Overall these results support the concept of photostasis, which is a proposed mechanism for the adaptation and the optimal functioning of photoreceptors subjected to long term changes in lightening environment.

Overall, these results suggested that there might be a relation between the circadian control of the genes involved in the phototransduction and the responses of photoreceptors to light stimuli.

1.6 Light activated mechanoresponses in rod photoreceptors

Mechanotransduction is a nascent field of study and only very recently, the physiological and structural characterizations of Piezo channels have widened the knowledge on this fascinating field. Both the structure and the gating mechanism of Piezo channels have been recently described in great details [101,102]. In particular, mechanotransduction can influence the response of sensory neurons, such as olfactory neurons. For instance, in a paper of 2017 it has been shown that the temporal pattern of responses to odorant in mitral and tufted cells of the olfactory bulb is partially influenced by mechanical signals, generated by mouse sniffing [103]. Iwata and colleagues suggest that the phase coding of odors, i.e. the temporal resolution of odorant perception, is part of a novel mechanism of chemicals signals identification and that the airflow-induced mechanosensation is fundamental for this process, in these sensory neurons.

Interestingly, it has also been shown that Drosophila melanogaster rhabdomers contract in response

to light. This mechanical event has been suggested to be triggered by the PLC signal pathway activated by light, and in particular by the cleavage of phosphatidylinositol 4,5-bisphosphate (PIP2). In particular, the depletion of this substrate and the proton release accompanied to its hydrolysis could be a second messengers for the mechanotransduction pathway, which may influence the transduction of light signals [104]. Moreover, the expression TRP channels have been assed in mouse retina and many member have been identified, throughout all the retina layers [105]. These channels are associated with the ability of cells to perceive multiple sensory inputs, from variations of temperatures, chemosensation and mechanosensation [106]. These channels may play an important role in vertebrates as well.

The most fascinating results regarding a possible coupling between mechano and phototransduction have been obtained in mouse and humans. Recently it has been demonstrated that light regulates R and peripherin2 transport and inclusion in the OS disks membrane. Peripherin2 is a very important protein for the OS formation and it is expressed on the disks' rim. The results obtained by Hsu et al. suggest a light regulated mechanism for R and peripherin2 inclusion in the nascent disks membranes, which is preferentially activated by dark adaptation and inhibited by light stimuli. Furthermore, these authors suggest that the OS could be subdivided into ten sub-compartments, with alternatively enriched R or peripherin disks regions. Others results obtained in Xenopus laevis display a similar inhomogeneity, which also determine variations of the rigidity of the rods OS [107]. Overall, these results validate the findings that the OS is not an homogeneous compartment, from both a morphological and a physiological point of view [9,108].

Interestingly, it has been reported that the optical path length of humans' photoreceptors increases of ~ 50 nm after a light stimulus, by mean of the optical coherence tomography (**OCT**) [109]. This non-invasive technique offers a great spatiotemporal resolution of optical signals. It is based on the 3D infrared imaging of backscattered light from the retina and allows precise signal localization, minimizing the light stimulation. The optical path length (l) is the phase of the light scattered from the retina. It is determined by multiplying the refractive index of the crossed mean (n) and the geometric distance (d) that the light has traversed $l = nd$. In photoreceptor outer segment this measure is proportional to the time that light requires to pass photoreceptors and gives information about their morphology and their refractive index, which could both vary when phototransduction is activated [109].

Moreover, using the same technique, it has been demonstrated that mouse photoreceptors OS elongates of ~ 2 μm after a light stimulus that bleaches 10% of the total available R molecules. This

elongation mechanism has been proposed to be governed by the osmotic swelling of photoreceptors OS, suggesting a possible variation of volume that accompany phototransduction and light adaptation [110]. Surprisingly, in 2016 it has been visualized for the first time the OS disc shedding of human photoreceptors, in a living retina, using OCT. The results published in the paper by Kocaoglu et al. evidenced a transient loss of the scattering signals emitted by the photoreceptors OS tip, with an average duration ~ 9 minutes and an average loss of OS length of ~ 2 μm. This proposed shedding is maximal in the morning and diminishes during the rest of the day.

Overall, these results suggest that light not only activate phototransduction, but it may also activate a mechanical response, that could be related to disc shedding of photoreceptors OS. The OS elongation by osmotic swelling and the loss of the photoreceptors OS tip are surprisingly of similar length. Therefore, it is fascinating to speculate that the volume variation induced by light in the rods OS could be associated with photoreceptors disc shedding.

1.7 Aim of the thesis

The main aim of my experimental work was to get new insight on the mechanisms that govern phototransduction in rod photoreceptors. In order to study light adaptation efficacy along rods' OS, I used an innovative type of metal-coated optical fibers as light source, which allowed precise stimulations of small portions of the OS (**Section 2.1**). Moreover, to investigate the possible effect of circadian rhythms on phototransduction, I have recorded rods responses during the day and at night, after different periods of light and dark adaptation (**Section 2.2**). Furthermore, I have analyzed the possible relation between mechano and phototransduction (**Section 2.3**). Finally, I have studied the effects of a rhodopsin mutation that lead to retinitis pigmentosa, the most common neurodegenerative disease of the retina (**Section 4**).

2. Results

2.1 Efficacy of light adaptation along the rods' OS

Early work on phototransduction machinery analyzed the spatial spread of its activation along the rods' OS and their desensitization to steady light stimuli [108]. Further experimental evidences obtained in our laboratory have contributed to describe and characterize this strong, functional gradient of phototransduction along the OS of rod photoreceptors, obtained from Xenopus laevis adult males. In the recent work by Mazzolini et al. 2015, it has been reported that the duration of the responses to brief flashes of confined light, applied by mean of metal coated tapered optical fibers (**TOF**) at the base, center and tip of rods OS, do not increase linearly with the increase of light intensity. These results suggest a variable concentration and an inhomogeneous diffusivity, between the OS compartments, of the proteins involved in the phototransduction signaling cascade.

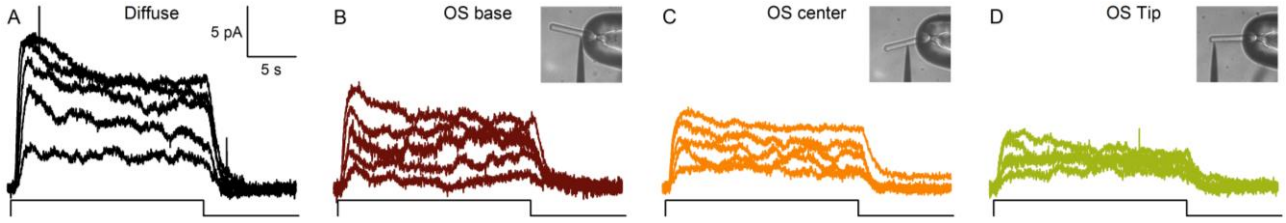

Figure 2.1.1. Light adaptation decline along the rods OS. (A) Photoresponses to diffuse laser light stimuli. The light intensities elicited respectively 120-200, 300-500, 600-1k, 1.2k-2k and 3k-5k Rh* and they were presented as described in the paper by Mazzolini et al., 2015; **(B-D)** Photoresponses to TOF stimuli at the base (dark red traces), at the center (orange traces) and at the tip (green traces) of the OS respectively. The insets represent the rod trapped inside the glass capillary and the position of the optical fiber. The laser light intensities used in these cases elicited respectively 3k-5k, 6k-10k, 12k-20k, 30k-50k, 60k-100k Rh*. In all the panels, the squared line represents the onset and the duration of the light step.

To assess and characterize light adaptation along the OS of Xenopus rods, we have used the previously described TOF system to stimulate photoreceptors with long pulses of light of increasing intensity, lasting 20 seconds (**Figure 2.1.1 A-D**) [9]. Xenopus laevis adult males were dark adapted overnight and sacrificed in the morning, to achieve the maximal photoreceptors sensitivity. The recorded photoresponses started to display light adaptation when diffuse stimuli, triggering form 300 to 500 photoisomerization (**Rh***), were presented to the rods (Second trace of **Figure 3.1.1 A**). The delayed decline of the amplitude of the responses, associated with the onset of light adaptation was still evident when rods were stimulated with stronger intensities, eliciting from 3k to 5k Rh* (**Figure 2.1.1 A**). Besides, also the photoresponses at the base of the OS displayed this characteristic, but the minimum amount of confined light that was necessary to clearly trigger adaptation was between 6k and 10k Rh* (**Figure 2.1.1 B**). Moreover, light adaptation was visible also when cells were stimulated with stronger steps of confined light, eliciting from 60k to 100k Rh*. The decline of photoresponses' amplitude associated with light adaptation was less evident at the OS center, with all the tested intensities (**Figure 2.1.1 C**), whereas at the OS tip was almost completely abolished (**Figure 2.1.1**

D). These preliminary results suggested that light adaptation efficiency might decrease along the rods OS.

In order to better characterize this decrease, we evaluated the responses to the maximum amount of

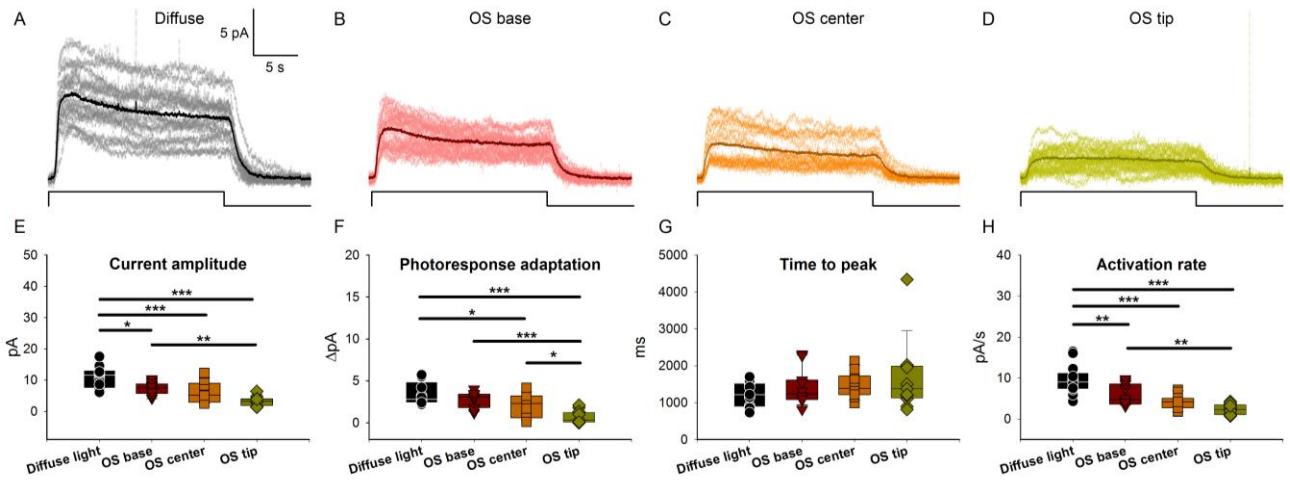

Figure 2.1.2. The tip of rods' OS displays light adaptation deficits. (A) Photoresponses to diffuse light stimuli, eliciting 3k-5k Rh*. The bold black trace is an average of 15 responses, obtained from 12 rods of four Xenopus males. **(B-D)** Photoresponses to TOF light stimuli, eliciting from 60k to 100k Rh*. The bold dark red, dark orange and dark green traces are averages of 20 responses, obtained from 10 rods of 4 Xenopus males. **(E-H)** Variation of the current amplitude, phototresponses light adaptation, time to peak and activation rate, between the diffuse light and the TOF photoresponses. The current amplitude decreases progressively along the OS, as well as the adaptation and the activation rate. On the other hand, the time to peak increases. The multiple comparison of these measurements was performed with the statistical method One Way ANOVA (values for P: * <0.05; ** <0.01; ***<0.001). In all the panels, the squared line represents the onset and the duration of the light step

light that elicited maximal adaptation, in both the totality of the OS and in the various compartments of 10 to 12 rods, obtained from 4 different frogs (**Figure 2.1.2 A-E**). The adapted responses to diffuse steps of light, evoking between 3k to 5k Rh*, were compared with the ones obtained along the OS, with confined steps of light that evoked from 60k to 100k Rh*. These stimuli maximally activated light adaptation at the base and at the center of the OS, whereas at the tip of the OS the light adapted photoresponses were small and difficult to distinguish, with most of the stimuli tested in our preliminary experiments (**Figure 2.1.1 D**). Therefore, in order to assess clearly light adaptation along the OS, we used only the maximum confined light intensities that triggered adaptation at both the OS base and center (**Figure 2.1.1 B-C**). The photoresponses to diffuse stimuli showed on average higher amplitude, compared to confined light responses of all the compartments of the OS. Furthermore, photoresponses at the base of the OS had larger currents compared with the ones at the tip (**Figure 2.1.2 E**). We have also noticed significant differences in the adaptation of the photoresponses to our test step, along the OS. To estimate these differences we calculated the delta of the current amplitude, between the peak of the response and the end of the stimulus (**ΔpA**), and compared the values obtained with diffuse light steps with those obtained with restricted light. The adaptation observed

with diffuse light stimuli was significantly larger in respect to the adaptation at the center and the tip of the OS. Interestingly, also the adaptation at the base and at the center of the OS was larger if compared with the tip (**Figure 2.1.2 F**). Moreover, we have analyzed the time to peak of the responses in the various positions of the OS, but we didn't find any significant differences (**Figure 2.1.2 G**). Considering the activation rate of the responses, i.e. the peak amplitude of the responses divided by the time to reach this peak, we were able to account for the differences in the activation steps of the phototransduction, along the OS (**Figure 2.1.2 F-G**) [9]. Diffuse light stimuli activated phototransduction faster than restricted light stimuli. Moreover, confined light at the base elicited faster activation of the responses, if compared with the activation at the tip. Overall, these results suggested a decreased ability to adapt to light stimuli of the tip of the rods OS, whereas at the base and the center, photoresponses to prolonged steps of light still displayed the characteristic delayed decrease of amplitude associated with light adaptation.

2.2 Circadian rhythms influence on phototransduction

As I have discussed in section 1.5.2, circadian rhythms strongly influence the physiology and the metabolism of photoreceptors. The expression of many key proteins involved in phototransduction, oscillates during the 24 hours daily period. To evaluate if and how phototransduction was affected by these daily rhythms of expression, we performed electrical recordings with suction electrodes technique on rods obtained from Xenopus laevis adult males, sacrificed at different moments of the day and adapted to different periods of dark and light.

1 PM	day1	7	8	9	10	11	12	13	14	15	16	17	18	19	20	21	22	23	24	1	2	3	4	5	6
	day2	7	8	9	10	11	12	13 †	14	15	16	17	18	19	20	21	22	23	24	1	2	3	4	5	6
		5h30min light adaptation (circadian rhythm)																					
1 AM	day1	7	8	9	10	11	12	13	14	15	16	17	18	19	20	21	22	23	24	1	2	3	4	5	6
	day2	7	8	9	10	11	12	13	14	15	16	17	18	19	20	21	22	23	24	1 †	2	3	4	5	6
		18h30min light adaptation (extended light period)																					

Table 2.2.1. Light adaptation experimental conditions. Schematic representation of the light adaptation conditions adopted for our experiments. The number of hours of light exposure are indicated below the 1PM and 1AM tables, as well as the time of the sacrifice of the animal.

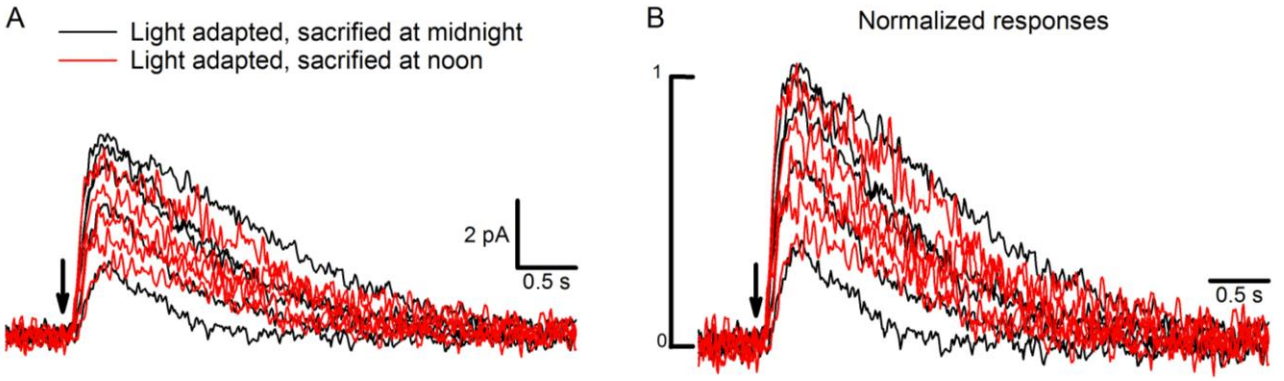

Figure 2.2.1. Light adapted rods responses make difficult to account for any influence of the circadian rhythms. (A) Averaged light adapted photoresponses of 3 (red traces) and 4 (black traces) rods of a Xenopus sacrificed at 1PM and a Xenopus sacrificed at 1 AM, respectively (see the experimental scheme in **Table 3.2.1**). The diffuse laser stimuli used in these experiments induced 60-100, 150-250, 300-500, 600-1k and 1.5k-2.5k Rh*. The arrow indicates the onset of the stimuli. **(B)** Normalized photoresponses in **(A)** for the maximum amplitude reached.

The coupling between adaptation and the responsivity of rods is a major variable that drives photoresponses. In order to exclude this variable and to consider only the possible contribution of circadian rhythms, we initially performed experiments on rods obtained from light adapted Xenopus, sacrificed at around 1 PM and at around 1 AM (**Table 2.2.1**). In these conditions, photoresponses displayed the characteristic accelerated kinetics, which were exhaustively described in previous works (**Figure 2.2.1**) [29,35].

The averaged rods' responses to bright light stimuli, lasting 10 ms and eliciting from 60 to 2,500 Rh*, had similar amplitude, time to peak and duration in both 1PM and 1AM light adapted rods (**Figure 2.2.1 A**). Moreover, the normalized responses to the peak amplitude didn't show any major difference (**Figure 2.2.1 B**) indicating that probably in these conditions, it was difficult to distinguish any possible contribution of the circadian rhythms to phototransduction.

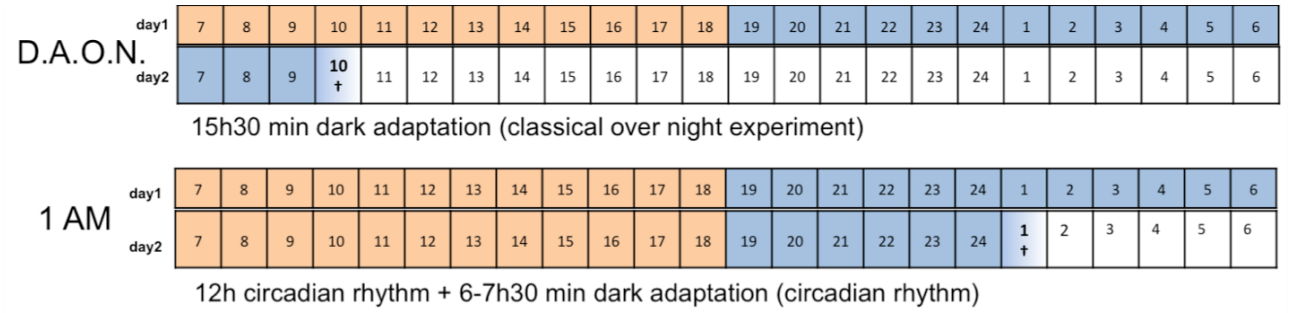

Table 2.2.2. Dark adaptation experimental conditions. Schematic representation of the dark adaptation conditions adopted for our experiments. The number of hours of dark exposure are indicated below the D.A.O.N. and 1AM tables, as well as the time of the sacrifice of the animal.

Therefore, to have a better understanding of the possible variations in phototransduction kinetics determined by intrinsic daily rhythms, we performed experiments on rods obtained from frogs exposed to different periods of dark adaptation (**Table 2.2.2**). Reasearchers that initially described and studied phototransduction adopted the dark-adapted conditions, in order to maximize photoreceptors' responsiveness and to understand the fine details of phototransduction signaling cascade[17]. Thus, we performed electrophysiological experiments on rods obtained from adult Xenopus males that were sacrificed at around 10 AM (dark adapted over night or **D.A.O.N**) in the morning and at around 1 AM at night (**"night"** rods). After the dissection, retinas or eyecups were preserved in the fridge at 4 °C. Keeping these tissues at low temperature allowed us to slow down cells metabolism and to perform experiments for at most one day after dissection. To activate phototransduction in rods obtained from these retinas, we used brief flashes of laser light with a wavelength of 491 nm, of intensities that triggered between 1.5 and 500 Rh*.

In order to identify and visualize differences in the kinetics caused by the circadian rhythm, we averaged photoresponses from 30 and 26 different rods collected from 4 D.A.O.N. (red traces) and 4 "night" (black traces) animals respectively (**Figure 2.2.2 A-D**). These photoresponses displayed increasing amplitudes, which were proportional to the light intensities and reached saturation when we presented stimuli lasting 10 ms and inducing from 30 to 100 Rh* (**Figure 2.2.2 A-B**). Interestingly, the analysis of the responses to dim, not saturating light stimuli eliciting from 6 to 10 Rh*, evidenced a small increase of the amplitude of "night" rods responses compared with the ones obtained from D.A.O.N. rods (**Figure 2.2.2 E**). Moreover, the assessment of the activation kinetics of the phototransduction revealed a small but significant decrease in the time to reach the peak amplitude of the "night" rods responses to saturating or almost saturating stimuli, eliciting from 60 to 250 Rh* (**Figure 2.2.2 F**). Furthermore, the duration of the photoresponses (calculated as the time interval between the current value representing the 25% of the rising phase, and the one representing

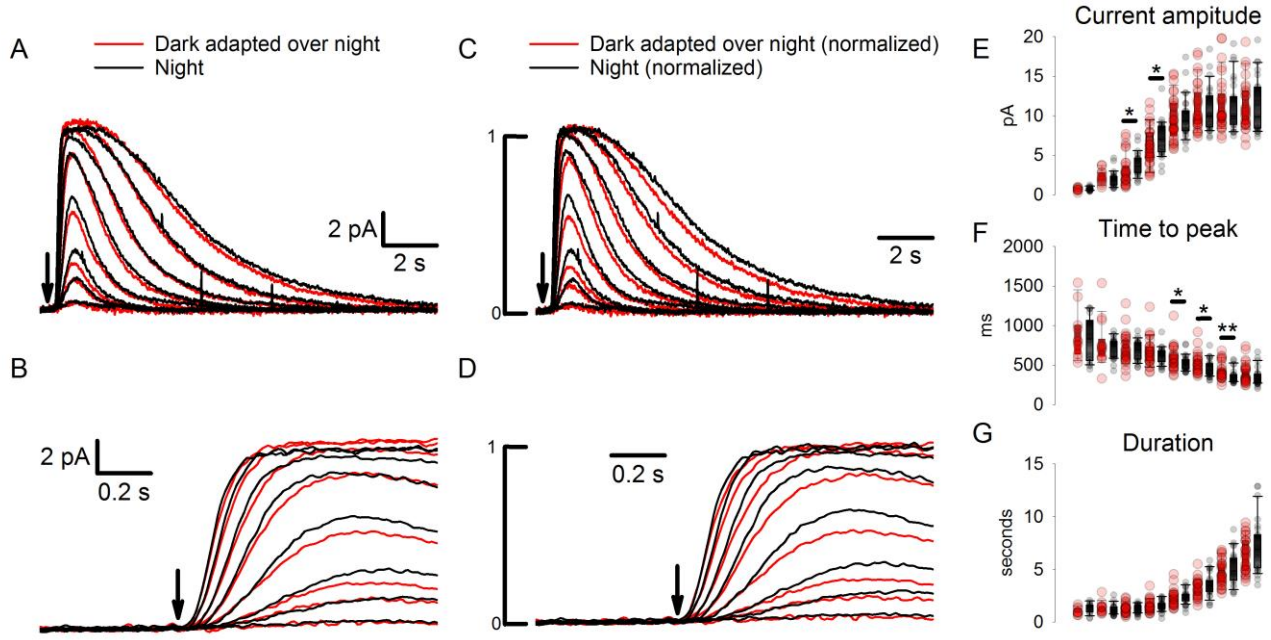

Figure 2.2.2. Dark-adapted rods' response display small differences between "night" rods and D.A.O.N. rods. (A) Averaged responses of 10-30 (red traces) and 17-26 (black traces) rods obtained from 4 D.A.O.N. and 4 1AM frogs respectively, which were kept in dark adaptation and sacrificed as shown in **Table 3.2.2**. The diffuse laser stimuli adopted in these experiments elicited 1.5-2.5, 3-5, 6-10, 15-25, 30-50, 60-100, 150-250 and 300-500 Rh*. **(B)** Enlargement of the rising phase of the responses in **(A)**. Small differences between D.A.O.N. and "night" responses are appreciable. **(C)** Normalized photoresponses in **(A)** for the maximum amplitude. **(D)** Enlargement of the rising phase of the responses in **(C)**. **(E-G)** Analysis of the current amplitude, the time to peak and the duration of all the photoresponses in **(A)**. Statistical significance was assessed with T-test (values for P: * <0.05; ** <0.01; ***<0.001). The arrows indicates the onset of the stimuli.

the 25% of the falling phase of the responses) didn't change significantly between the D.A.O.N. and the "night" rods (**Figure 2.2.2 A-D, G**). Overall, the averaged photoresponses revealed rather similar time courses and amplitudes and this may indicate that the functional properties of phototransduction were very similar in these two conditions, despite the different periods of dark adaptation. Moreover,

these preliminary results may suggest that the small differences that we observed between "night" and D.A.O.N photoresponses could be related only to the different periods of light adaptation. However, since the number of hours of dark adaptation in both conditions should be sufficient to obtain fully dark-adapted rods, the possibility that these differences are genuinely determined by circadian rhythms should not be completely ruled-out.

Moreover, we evaluated rods responses to repetitive, very dim light stimuli of the same intensity, eliciting from 1,5 to 2,5 Rh* and lasting 10 ms (**Figure 2.2.3**). Both D.A.O.N. and "night" rods displayed single photon like responses (**Figure 2.2.3 A, B**). The amplitude distributions of the responses to dim light stimuli were different in both the maximum amplitude reached and in the number of events (counted as 1 to be the totality of the events) per amplitude value (**Figure 2.2.3 C,D**). The averaged single photon responses of two rods, recorded in the two different dark-adapted

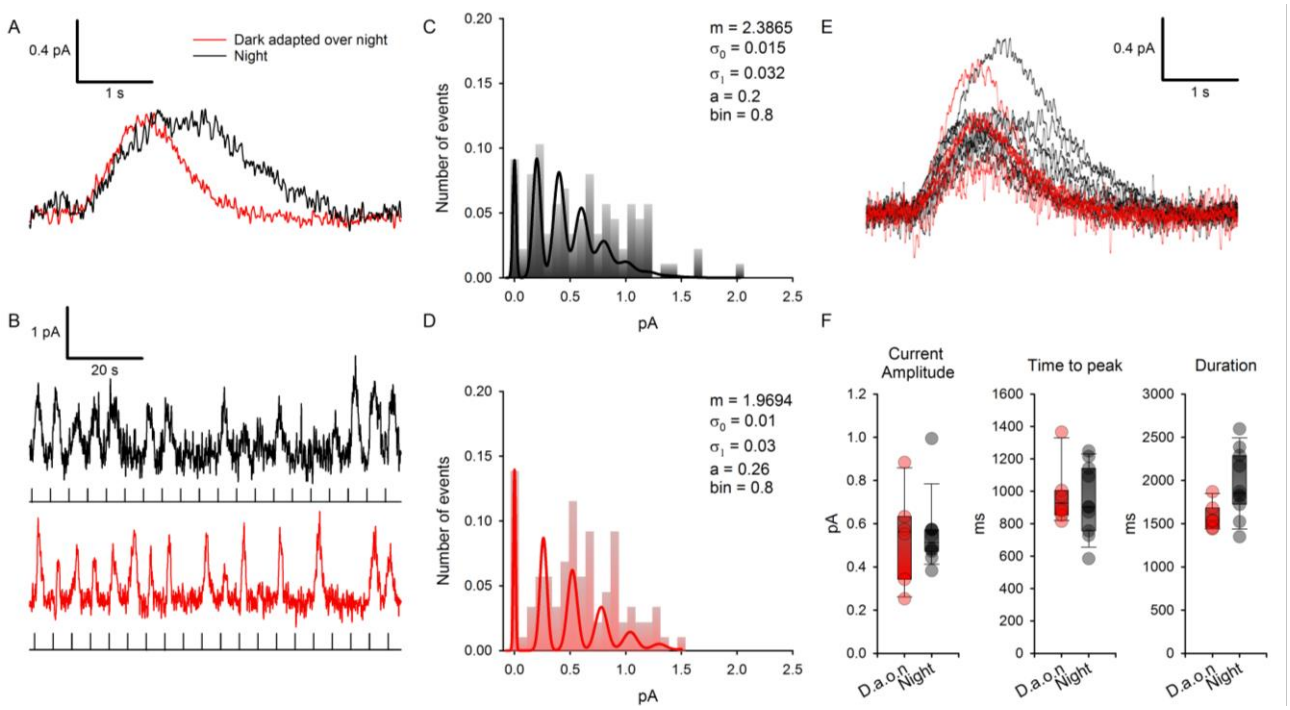

Figure 2.2.3. Single photon analysis of "night" and D.A.O.N rods. (A) Averaged responses of 86 (red traces) and 87 (black traces) single events, obtained from 1 D.A.O.N. and 1 1AM frogs respectively. The diffuse laser stimuli used in these experiments elicited between 1.5 and 2.5 Rh*. **(B)** Portions of the recordings of the two rods in **(A)**. **(C,D)** Histograms of the number of events as function of the amplitudes distributions for the "night" rod (black traces) and the D.A.O.N. rod (red traces), respectively**.** The histograms were fitted with the equation described in the paper by Baylor et al. 1979. Values providing the best fit are reported in the panel; a is the mean response to single photon, σ0 is the noise standard deviation (SD), σ1 is the SD of the mean, and m is the mean number of events per trial. **(E)** Collected averages of 6 D.A.O.N (red traces) and 10 "night" (black traces) rods, obtained from 2 and 4 Xenopus males respectively. **(F)** Analysis of the current amplitude, the time to peak and the duration of the averages in **(E)**.

conditions, displayed very similar amplitudes of 0.56 and 0.55 pA for D.A.O.N and the "night" rod respectively (**Figure 2.2.3 A**). Moreover, the rising phase of this response was remarkably similar, with a time to reach the peak of 977 ms for D.A.O.N. rods and of 913 ms for "night" rods. Interestingly, the average response of the "night" rod lasted roughly 1 second more than the D.A.O.N.

one (**Figure 2.2.3 A, B**). The comparison of the collected data of our single photon experiments confirmed the similarities in both time to peak and amplitude of the averaged responses obtained in the two conditions (**Figure 2.2.3 E, F**). However, the duration of "night" rods' averaged responses had higher variability and these results may suggest that "night" rods sensitivity fluctuates more if compared with D.A.O.N. rods (**Figure 2.2.3 E, F**).

To further analyze rods' sensitivity in the two conditions, we triggered light adaptation in

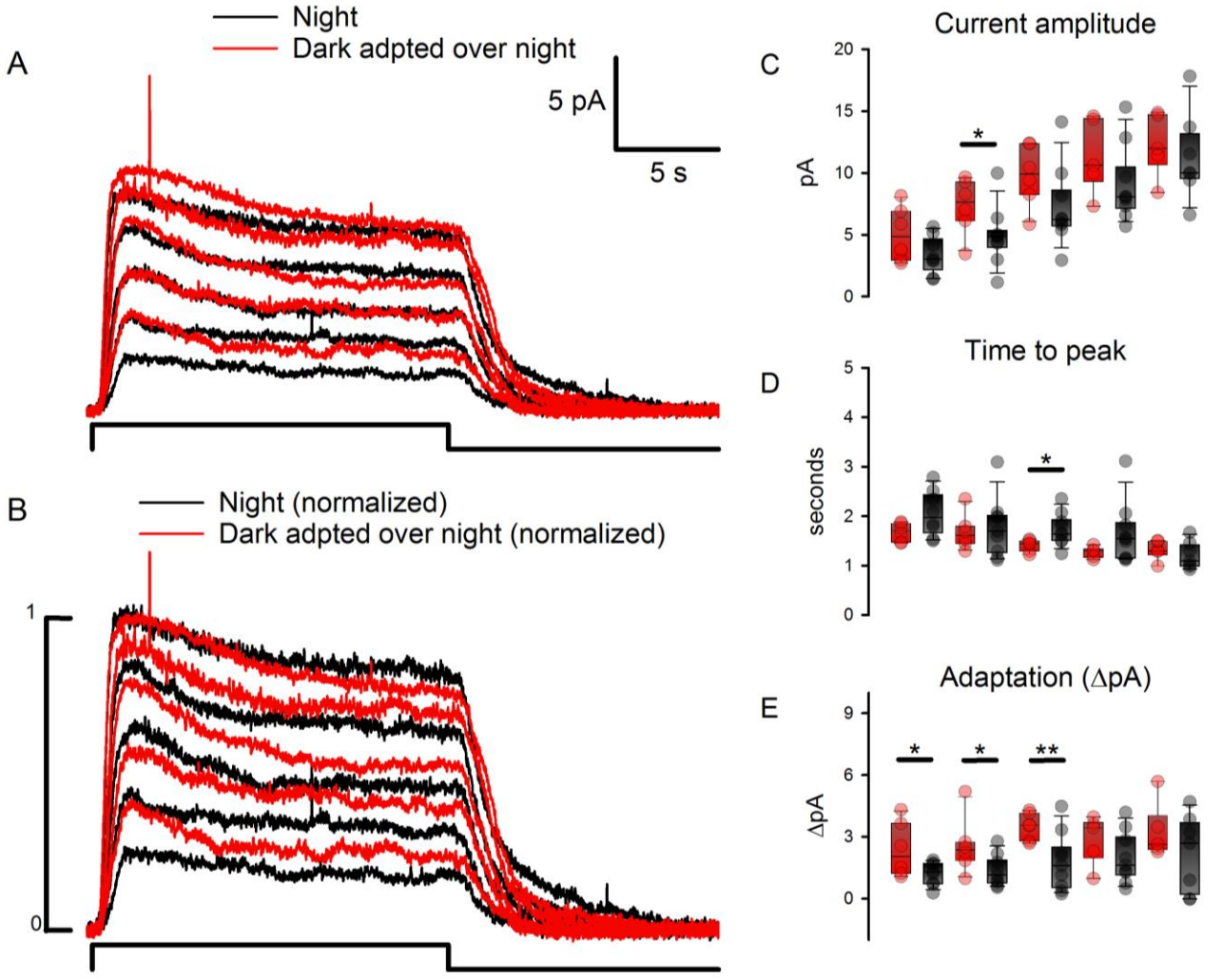

Figure 2.2.4. Light adaptation to dim stimuli is more pronounced in D.A.O.N. rods. (A) Averaged responses of 5-6 (red traces) and 7-9 (black traces) rods obtained from 4 D.A.O.N. and 4 1AM frogs respectively, which were kept in dark adaptation and sacrificed as shown in **Table 3.2.2**. The diffuse laser stimuli adopted in these experiments elicited 120-200, 300-500, 600-1k, 1.2k-2k and 3k-5k Rh* and lasted 20 s. **(B)** Normalized photoresponses in **(A)**. **(C-E)** Analysis of the current amplitude, the time to peak and the duration of the single responses averaged in **(A)**. Statistical significance was assessed with T-test (values for P: * <0.05; ** <0.01; ***<0.001). In all the panels, the squared line represents the onset and the duration of the light step.

photoreceptors by mean of diffuse light stimuli of different dim intensities and lasting 20 seconds (**light steps**). We recorded responses from 6 and 9 rods obtained from 4 D.A.O.N and 4 "night" Xenopus respectively (**Figure 2.2.4 A, B**). The responses of D.A.O.N. rods displayed overall higher current values and faster rising phase if compared with "night" rods but the only significant

differences were observed when stimuli eliciting form 300 to 1k Rh* were presented (**Figure 2.2.4 C, D**). The averaged current values for the responses triggered by stimuli that activated between 300 and 500 Rh* were 7.3 pA and 4.9 pA for D.A.O.N and "night" rods respectively (**Figure 2.2.4 C**). Moreover, the time to peak of the response to stimuli eliciting from 600 to 1k Rh* was significantly smaller in D.A.O.N. rods (1.4 seconds), compared to "night" rods (1.75 seconds) (**Figure 2.2.4 D**). Overall, "night" rods responses were more variable in both amplitude and time to peak, partially confirming the increased fluctuation in sensitivity of these cells. Interestingly, the delayed decrease of amplitude associated with light adaptation was consistently larger in D.A.O.N responses. The delta between the peak amplitude and the amplitude value at end of the currents, elicited by light steps that triggered from 150 to 1000 Rh*, were significantly larger in D.A.O.N than in "night" photoresponses (**Figure 2.2.4 E**). The analysis of our recordings indicates that light adaptation in D.A.O.N. rods is more pronounced, at least when stimuli with very dim light intensities were presented to the cells.

In order to understand what could be the reason for the higher variability of the photoreceptors' sensitivity, especially encountered in rods obtained from frogs sacrificed at night, we subdivided the responses of Figure 2.2.2 accordingly to a temporal criterion. All the recordings performed in the first 12 hours closer to the time of dead of the frog were arbitrary separated from the others, which constituted the second group of recordings. These two main groups were considered and analyzed separately, in both our dark adaptation conditions (**Figure 2.2.5, supplementary figures 1 and 2**).

The D.A.O.N. subgroup of the recordings obtained in the first 12h of experiments was composed of 18 cells (average traces in light red) and the second subgroup of recordings was composed of 12 cells (average traces in dark red/brown) (**Figure 2.2.5 A, B**). The comparison between the photoresponses of these two subgroup revealed a small increase of the amplitude of the responses to very dim flashes of light, eliciting from 1.5 to 2.5 Rh*, of rods recorded closer to the time of sacrifice (**Figure 2.2.5 E**). Moreover, the time to reach the peak amplitude of dim flashes that elicited from 3 to 5 Rh* was faster in cells recorded in the first 12 hours of experiments (**Figure 2.2.5 F**). On the other hand, the duration of the responses was quite similar for all the responses in the two subgroups of cells (**Figure 2.2.5 G**).

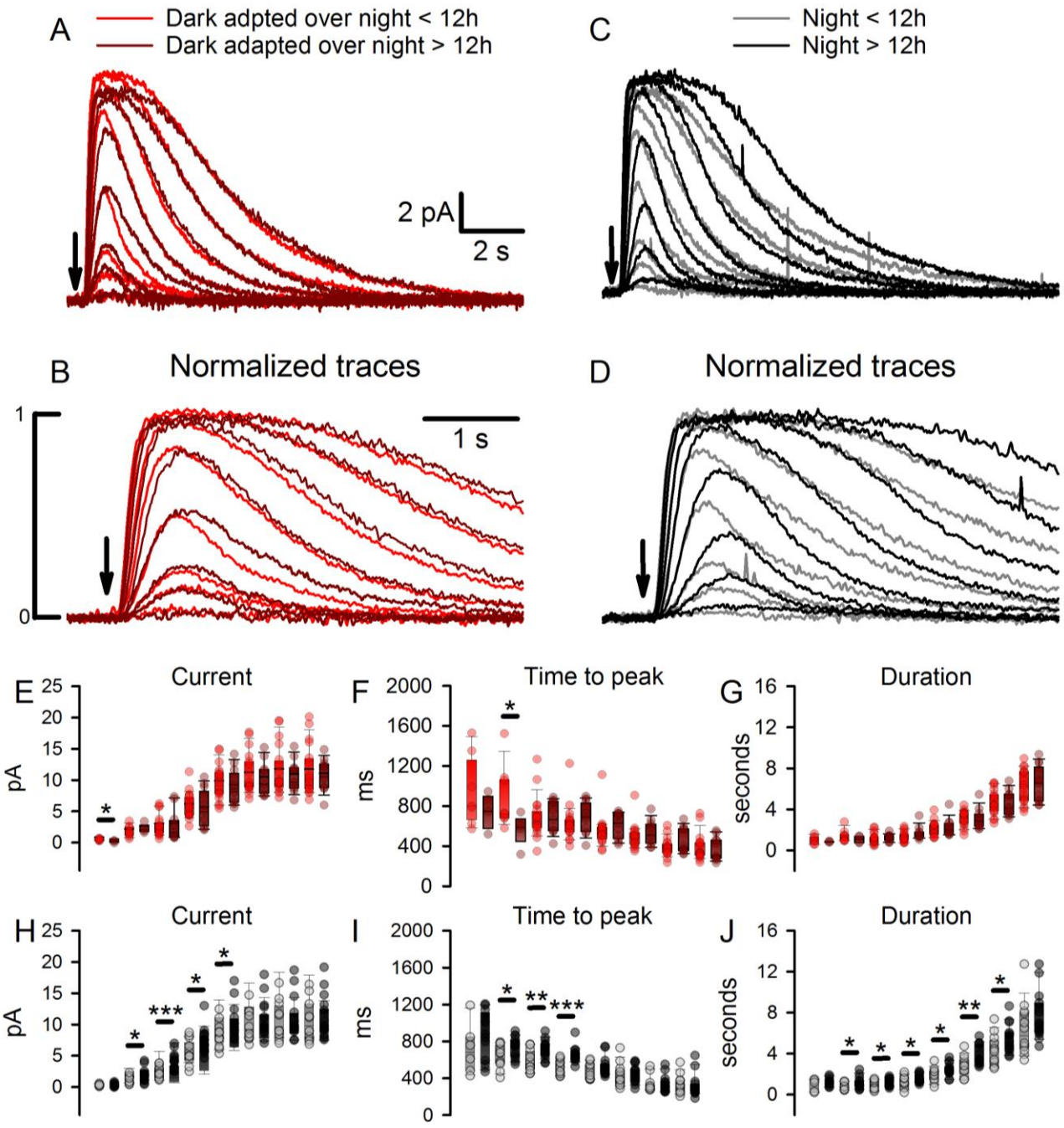

Figure 2.2.5. "Night" rods can further adapt while kept in dark and at low temperature. (A) Averaged responses of 7-18 (red traces) and 3-12 (dark red traces) rods obtained from the same D.A.O.N. frogs as in **Figure 3.2.2** and subdivided in the ones recorded in the first 12 hours close to the dissection (red traces) or afterwards (dark red traces). **(B)** Enlargement of the rising phase of the responses in **(A)**. Small differences between D.A.O.N. subgroups are appreciable. **(C)** Averaged responses of 6-12 (gray traces) and 11-14 (black traces) rods obtained from the same 1AM frogs as in **Figure 3.2.2** and subdivided in the ones recorded in the first 12 hours close to the dissection (gray traces) or afterwards (black traces). **(D)** Enlargement of the rising phase of the responses in **(C)**. An evident shift between 1AM subgroups of responses is appreciable. **(E-G)** Analysis of the current amplitude, the time to peak and the duration of all the photoresponses in **(A)**. **(H-J)** Analysis of the current amplitude, the time to peak and the duration of all the photoresponses in **(C)**. The diffuse laser stimuli adopted in these experiments elicited 1.5-2.5, 3-5, 6-10, 15-25, 30-50, 60-100, 150-250 and 300-500 Rh*. Statistical significance was assessed with T-test (values for P: * <0.05; ** <0.01; ***<0.001). The arrows indicate the onset of the stimuli.

Surprisingly, the analysis of the responses to flashes of light, of intensities that vary between 1.5 and 500 Rh*, revealed interesting and peculiar characteristics of the two subgroups of rods obtained from

frogs sacrificed at night (**Figure 2.2.5 C-J**). The "night" subgroup of the recordings obtained in the first 12h of experiments was composed of 12 cells (average traces in gray) and the second subgroup of recordings was composed of 14 cells (average traces in black). Interestingly, from an immediate inspection of both averaged (**Figure 2.2.5 C**) and normalized traces (**Figure 2.2.5 D**), it was possible to appreciate that the responses of the rods recorded after the first 12 hours from the animal sacrifice, displayed a shift from the responses obtained in the first 12 hours after the dissection. This shift displayed a significant increase of current amplitude of the responses to dim and almost saturating light intensities of the rods' of the second subgroup (**Figure 2.2.5 H**). Furthermore, the time to peak of the responses to dim and mid light intensities was significantly slower in these rods (**Figure 2.2.5 I**). Finally, also the duration of the responses of these two groups changed significantly. The photoresponses of the second subgroup of rods to both dim, mid and saturating flashes displayed a prominent and significant elongation of the duration (**Figure 2.2.5 J**). Overall, these preliminary results may indicate that "night" rods have an higher ability to further adapt to dark conditions, as the recordings obtained after the first 12h from the sacrifice display a marked shift of amplitude, time to peak and duration. On the other hand, rods obtained from D.A.O.N. Xenopus do not evidenced this shift, suggesting that maybe these rods have less potential to further adapt to dark.

Supplementary figures:

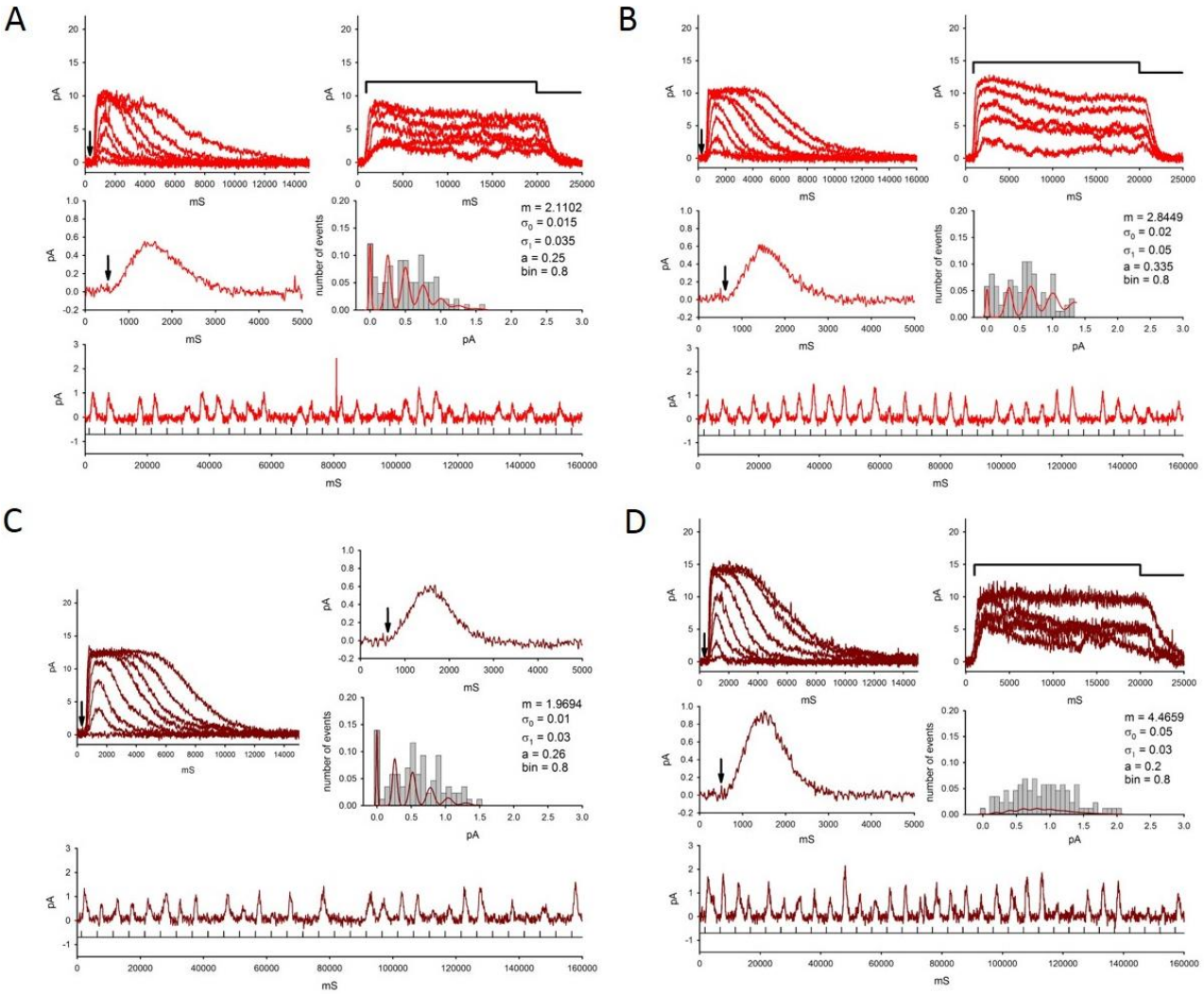

Supplementary figure 1. Recordings of 2 D.A.O.N. rods responses registered in the first 12h close to the animal sacrifice (A,B, red traces) and 2 D.A.O.N. rods responses recorded afterwards (C,D, dark red/brown traces). Cells derived from the same animal.

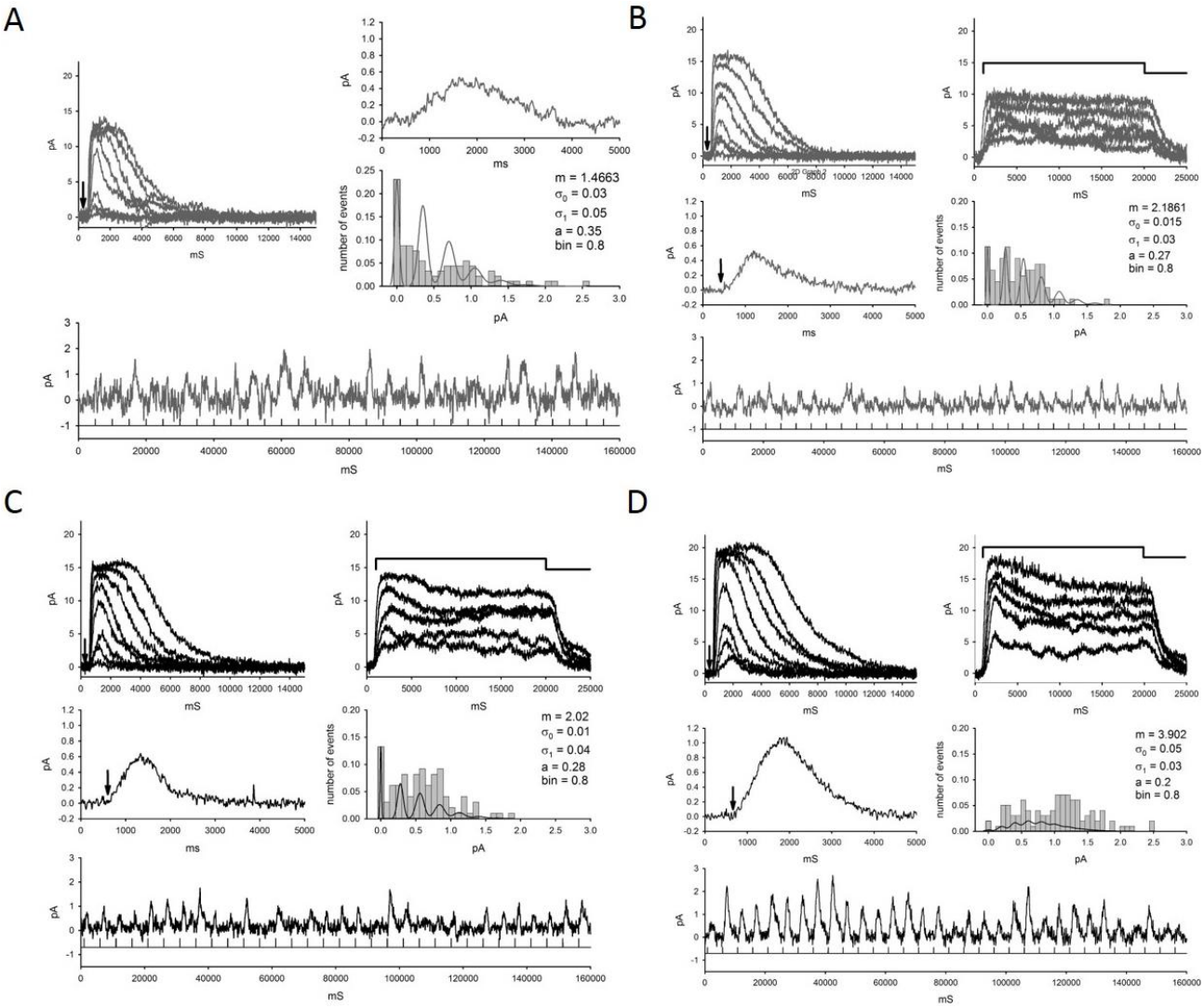

Supplementary figure 2. Recordings of 2 "night" rods responses registered in the first 12h close to the animal sacrifice (A,B gray traces) and 2 "night" rods responses recorded afterwards (C,D black traces). Cells derived from the same animal.

2.3 Mechanotransduction in rods photoreceptors

Photoreceptors are thought to be specialized cells devoted to the transduction of the incoming light stimuli. Nevertheless rod photoreceptors are known to shed from their tip old disks and to synthetize at the base of the OS new disks, indicating the existence of a mechanical machinery inside them. We have recently developed a new method employing an oscillatory optical trap to apply piconewton forces to the cell membrane, for short instants [111]. The experiments described below were designed and performed in order to investigate mechanostraduction in rod photoreceptors with two aims: to establish whether rod photoreceptors sense and transduce mechanical stimulations and whether following the light absorption rod photoreceptors change their volume, as in the drosophila ommatidia

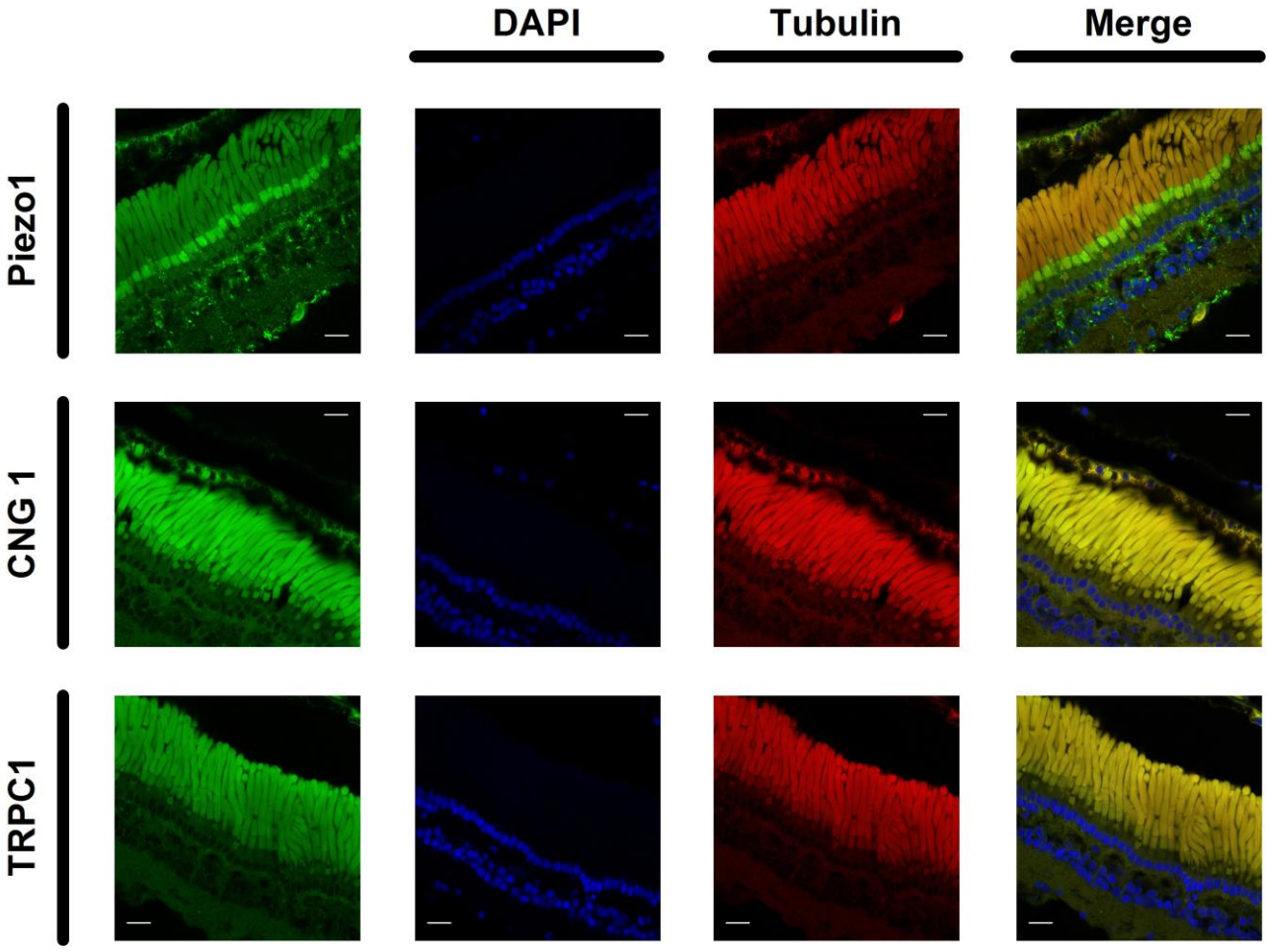

Figure 2.3.1. Localization of TRPC1 and Piezo1 MCS channels on rods photoreceptors. Immunohistochemical images that display the localization of the Piezo 1, the CNG1 and the TRPC1 channels in Xenopus laevis retina. In green are evidenced the channels, in blue the DAPI staining and in red the tubulin (scale bars = 20 µm).

and in mouse photoreceptors [104, 110].

Rod photoreceptors OS host the complicated machinery able to transduce an absorbed photon into an electrical signal [9]. A recent investigation based on mass spectrometry [112] shows that OSs contain a

large population of proteins and it is possible that they host also some of the proteins necessary for mechanotransduction, such as the mechanosensitive channels (MSCs) as Piezo 1 and TRPC1 [101,113,105]. Our preliminar immunohistochemical analysis of Piezo 1 and TRPC1 channels expression showed that Piezo 1 channels are distributed mostly over the membrane of the IS of the rods, in correspondence of the connecting cilium area, whereas TRPC1 channels are more ubiquitously distributed throughout the whole cell membrane (**Figure 2.3.1**). Therefore both rods OS and IS express MCS channels that may allow them to sense mechanical stimuli.

In order to verify if rods were able to respond to weak force stimuli, we mechanically dissociated rods from Xenoups' retinas that were loaded with the calcium sensitive dye Fluo-4 (**Figure 2.3.2**). The morphology of these cells was examined by mean of an IR light and occasionally the green light was switched on for 1 s so to visualize the amount of Fluo-4 loading. Isolated OS were often highly fluorescent, while rods with an IS attached to the OS, had the IS highly fluorescent but with an OS almost completely dark (**Figure 2.3.2**). These observations suggested that rods with a highly fluorescent IS and a dark OS could have maintained their functional integrity. Indeed the absence of calcium loading in the OS suggests that pumps and transporters are operational in these rods.

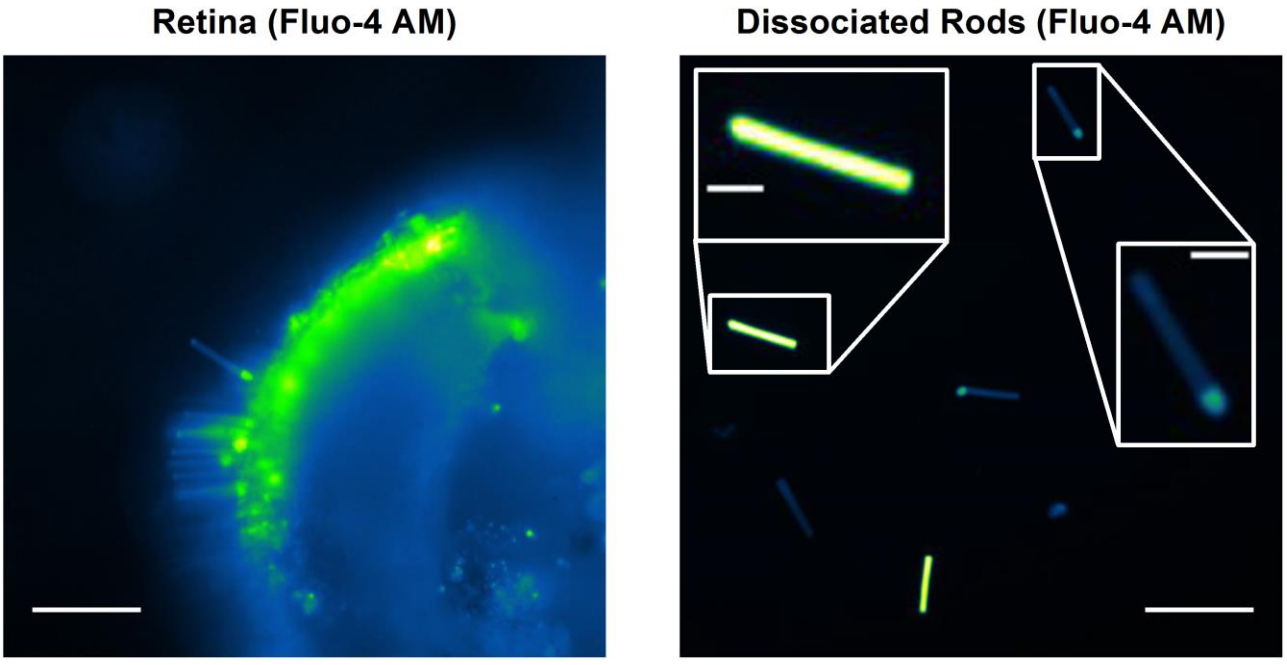

Figure 2.2.2. Differences of Fluo-4 loading between rod OS alone and OS+IS. On the left an image of a portion of a retina loaded with the calcium dye Fluo-4 AM (scale bars = 100 μm); on the right the rods obtained from the mechanical dissociation of the same retina (scale bars of the main picture = 100 μm; scale bars of the insets = 20 μm). Dark-adapted retinas were incubated with Fluo-4 at room temperature for ~ 30 min and the portion that were not used immediately were kept in the fridge for at most 2-3 hours. Recordings of the calcium signals were performed for maximum 2 hours and then the rods were changed.

Therefore, isolated rods loaded with Fluo-4 that had a highly fluorescent IS and a dark OS were expected to be functional and were used to probe mechanotransduction in our experiments.

In order to apply mechanical stimulations to isolated rods under controlled conditions, it is necessary to let them adhere to a rigid substrate such as a glass slide, making difficult to record simultaneously their electrical response by means of either suction or intracellular patch electrodes. In order to stabilize rods and to make them still while applying mechanical stimuli, we coated glass coverslip with polyornitine and incubated the dissociated rods on these coverslips for almost half hour before performing any experiments on them.

After this incubation period, we applied weak and calibrated mechanical forces to the rods by means of a silica bead trapped and manipulated by an optical tweezer set-up, equipped with a Focal Tunable Lens (FTL). By using this recently developed technique [111] it was possible to apply forces in the range of 5-10 pN. A silica bead was positioned by the optical tweezer over the IS of an isolated rod in which the IS was properly loaded with Fluo-4 but not its OS (**Figure 2.3.3**). Mechanical forces of just ~5

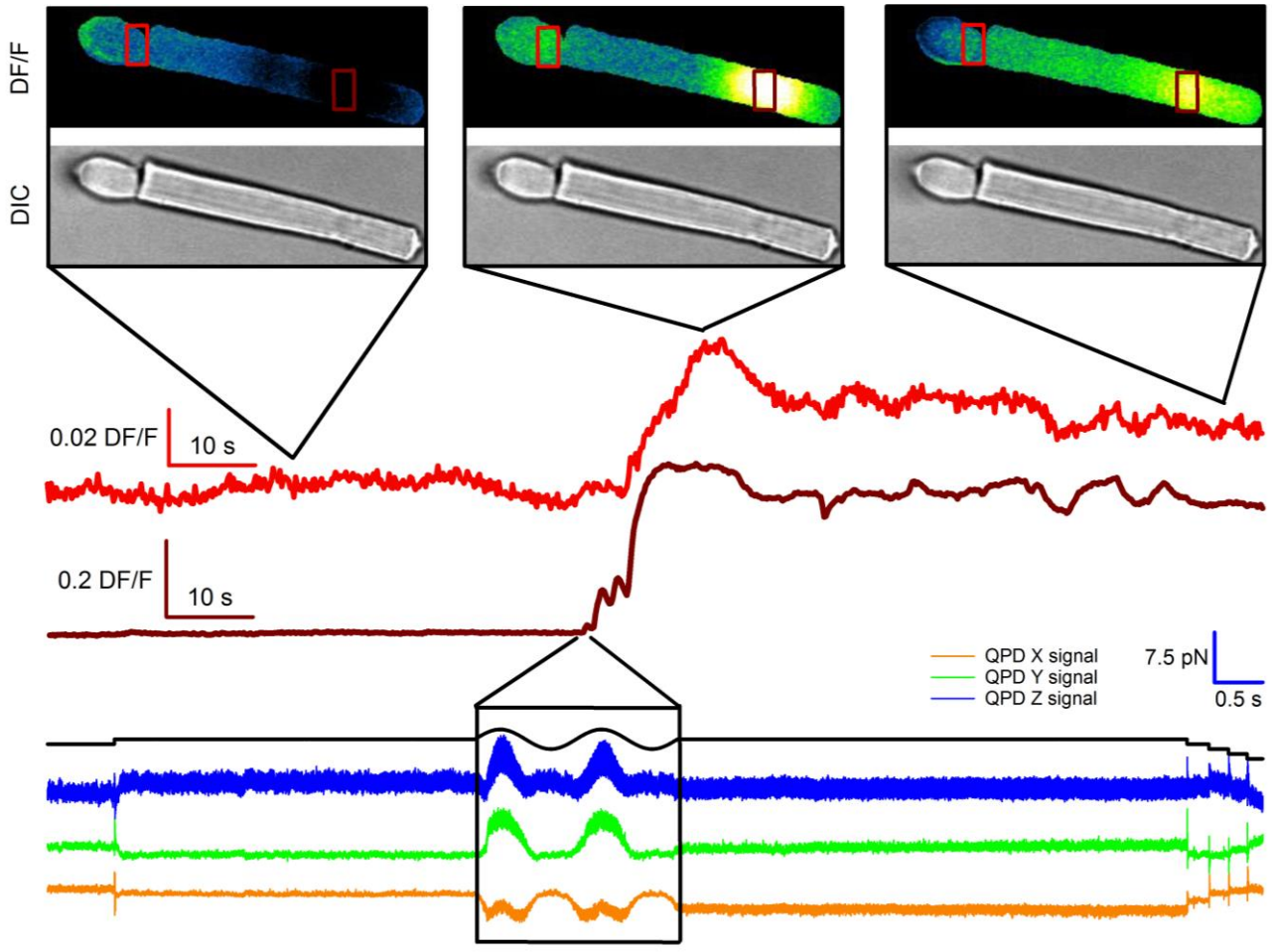

Figure 2.3.3. Rods respond to mechanical stimuli with variations of calcium fluorescence in both the IS and along the OS. The pseudo colors pictures on the top part of the figure indicate three moments of this representative experiment and were obtained with a Fiji (Imagej) plug-in for the estimation of the DF/F. Beneath them are shown the correspondent DIC pictures. The light red trace represents the DF/F of the IS region, evidenced by the red rectangle above. The dark red trace represents the DF/F of the OS region, evidenced by the dark red rectangle above. The three traces on the bottom represent the variations of the QPD signals that were used as an indication of the position of the silica bead (contact with the cell and indentation of the cell membrane), trapped by the infrared laser of the optical tweezer system. From the variance of the Z signal, we were able to estimate the amount of force applied with this system.

pN applied to the IS induced an increase of fluorescence signal, which indicated an increase of calcium inside the IS (**Figure 2.3.3, red trace**). Moreover, in some cases, it was possible to observe also at the base, the middle and the tip of the rod OS an increase of the fluorescence signal (**Figure 2.3.3, orange trace**). In all these experiments, a blue led light, with a wavelength of 489 nm, continuously excited Fluo-4 and therefore the rods were in light adapted conditions. These

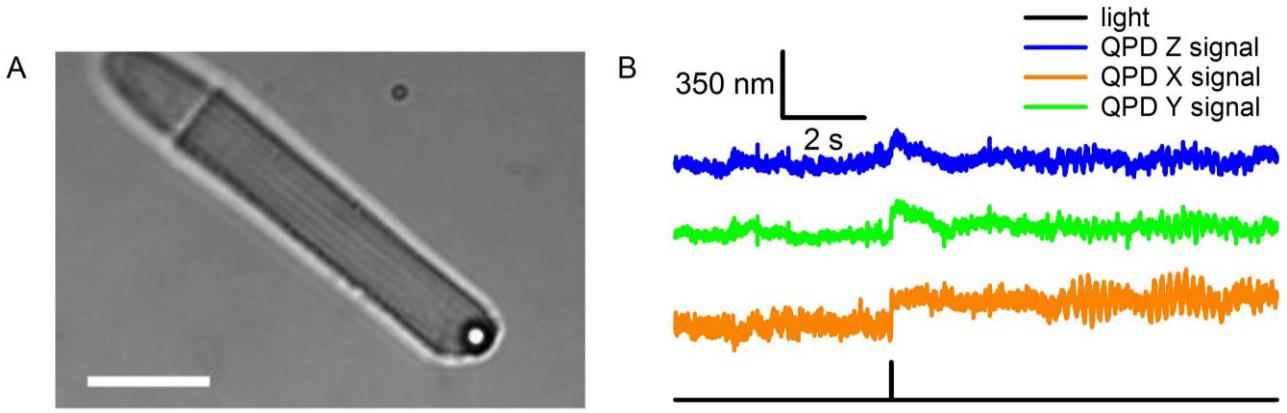

Figure 3.3.4. Rods responses to brief light pulses induced a displacement of the bead trapped by the optical tweezers laser, of around 200 nm. (A) Representative picture of a rod with a bead positioned at the end of the OS (scale bars = 200 µm). **(B)** Representative recording of the displacement of the bead caused by the onset of a brief pulse of sub saturating/saturating led light. The three colored traces represent the QPD signals on the three different axis.

preliminary results may suggest that the IS of the rods is a mechanosensitive compartment of the cell and in some cases the mechanical stimulus can be transmitted along the OS.

In order to further investigate the possible coupling between photo and mechanotransduction, as evidenced in the paper by Prof. Hardie, we performed another series of experiments in which we eliminated from the laser optical path the FTL, so to use the bead to probe possible displacements caused by a rod during phototransduction (**Figure 2.3.4**). In these experiments we positioned a silica bead manipulated by the optical tweezers over the tip of an OS with a IS attached (**Figure 2.3.4 A**). The bead was progressively lowered onto the OS tip so to reach contact, indicated by a change of noise in the recordings from the quadrant photodiode (**QPD**). A bright saturating flash of light displaced the trapped bead by 100-200 nm (**Figure 2.3.4 B**) and no displacement was measured when the bead was above the ROS membrane. Further experiments with longer light stimuli still evidenced a displacement of the bead of about 500 nm, subsequently to the light stimulation (**Figure 2.3.5**). The progressive increase of the displacement and of the noise of the QPD traces in Figure 3.3.5 (from number 1 subsection to number 5 subsection) was probably due to the increasing instability of the bead inside the laser trap and could be coherent with a progressive increment of volume. These preliminary results are in good agreement with the latest results of Prof. Pugh, published in a recent

paper [110] and it may suggest that even isolated rods can go through volume variations, that can be recorded by mean of our optical tweezers set-up.

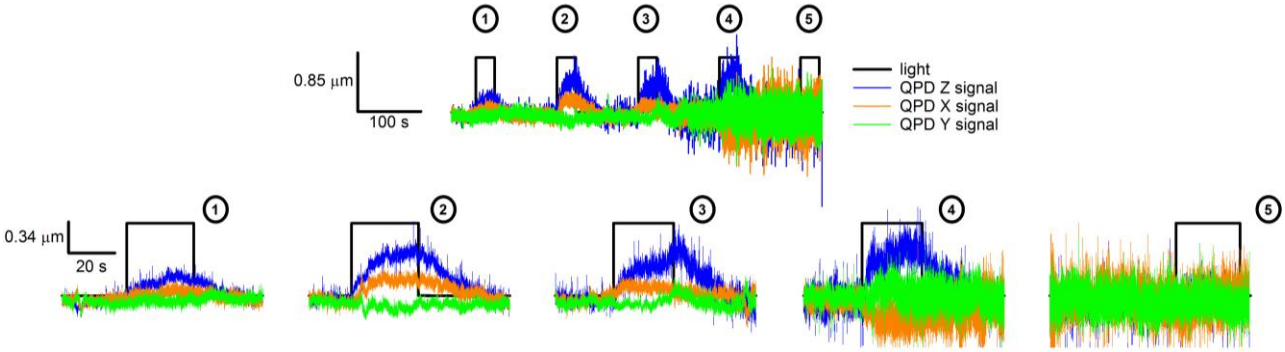

Figure 3.3.5. Rods responses to longer light stimuli induced a displacement of the bead trapped by the optical tweezers laser, of around 500 nm. Representative recording of the displacement of the bead caused by the onset of a 20 seconds step of sub saturating/saturating led light. The three colored traces represent the QPD signals on the three different axis and evidence the variation of the position of the trapped bead in respect to the OS.

3. Conclusions and discussion

3.1 Light adaptation efficacy decrease along the rod outer segment

During my PhD, I have focused my experimental work and my attention on the study of light and dark adaptation mechanisms in rod photoreceptors of the Xenopus laevis frog. These processes have been widely studied in the past, but emerging new technologies such as our optical fibers system, could be of help in further understanding their finer details (**Figure 3.1.1)**. In our preliminary experiments, the currents amplitudes of the diffuse light responses are significantly larger if compared with the confined light responses of all the compartment of the OS. Moreover, the current amplitude of the responses at the base of the OS was larger, if compared to the responses at the tip, obtained with confined light stimuli of the same intensity (**Figure 3.1.2 E**). These results may suggest that the efficacy of phototransduction at the OS tip is reduced.

The decrease of amplitude that characterizes the adaptation to light is larger when diffuse stimuli are presented to the cells (**Figure 3.1.2 F)**. In this condition, a smaller number of photoisomerization triggers light adaptation. However, this may be related to the source of illumination and further experiments will be necessary to better compare and understand the differences between the diffuse light and the restricted light conditions. Moreover, our preliminary results suggest that the ability to adapt to light stimuli might decrease along the OS of the rods. The adaptive responses to confined light obtained at the base of the OS, closely resemble the ones obtained with diffuse light (**Figure 3.1.2 F)**. The analysis of the photoresponses obtained with these stimuli, may suggest that the functionality of the phototransduction machinery in this region is maximal and the reason could be that this compartment of the OS contains all the newly formed disks.

At the center of the OS, the proteins involved in phototransduction signaling cascade are still functional. The adaptive response of this compartment is larger compared to the tip, but smaller than that obtained with diffuse light. More interestingly, the responses obtained at tip of the OS with confined stimuli display smaller amplitude and smaller adaptation if compared with confined light responses at the base. The analysis of the time to peak didn't reveal any significant difference between the conditions tested (**Figure 3.1.2 G)**. However, when we analyzed the activation rate of the photoresponse, i.e. the peak amplitude of the dark current divided by the time to reach the peak, we observed a significantly larger pA/s ratio with diffuse light stimuli in respect to confined light stimuli (**Figure 3.1.2 H**). Moreover, the activation rate at the base was smaller if compared with the tip and this may confirm that phototransduction in this compartment is less effective. The paper by Mazzolini et al. described in details the altered efficacy of the phototransduction along the OS, which is partially

confirmed by our preliminary results. However, further experiments will be necessary to assess the validity of our results and to better understand and characterize light adaptation along the OS of the rods.

3.2 Two steps of photoreceptors degeneration in P23H transgenic Xenopus laevis.

Previous investigations of Prof. Moritz group in Vancouver have shown that when *X. laevis* tadpoles that carry the R_{bP23H} mutation are reared in darkness, mutant rods do not degenerate. Furthermore, our results suggest that they also have functional and almost normal phototransduction machinery (**Figure 3 of section 2.1**). However, when we exposed them to a bright light lasting 1 s, their photoresponses are prolonged (**Figure 5 and 6 of section 2.1**) and when light exposure is maintained for 12 minutes, significant OS shedding occurs and the degeneration of the retina is initiated (**Figure 7 of section 2.1**).

Our results suggest that the initial step of the degeneration could be the impairment of the phototransduction signaling cascade, associated with the Rh* of 5-44 R_{bP23H} per disc. On the other hand, we have estimated that the OS shedding is initiated only by a number of Rh* that is 1-2 orders of magnitude larger. These results may indicate that the mutated rods have an impaired ability to sustain light adaptation for long periods. The morphological alterations observed in the degenerating retinas, resemble the canonical disk shedding, where distal portion of the tip detach from the OS and reach the RPE. The main differences with the normal shedding could be that in this pathological state, rods are unable to recover properly from light stimuli and during dark adaptation, the formation of new disks might be slowed down by the expression of the mutated R_{bP23H}. Therefore the formation of the disks at the base may not counter properly the shedding process at the tip.

The P23H mutation is located in the N-terminus of R, in the intradiscal domain. Structural analysis of this region have evidenced that the P23 residue is important to maintain the structural stability of the protein and for a correct binding with the chromophore. Prof. Moritz and colleagues have shown that a considerable fraction of the bP23H synthesized by the rods can escape the ER quality control checkpoints and be expressed on the OS disks, with a destabilizing amino acid; on the other hand, or the N-terminus region can be cleaved, resulting in the expression of a structural unstable R. In both cases, the expression of these mutated proteins can destabilize the entire structure of the OS disks membranes, resulting in an alteration of the light signaling transduction. Therefore, it is possible that upon light exposure, bP23H rhodopsin adopts an alternate conformation that could alters both the structure of the N-terminus, but also the cytoplasmic domain that interact with signal transduction components.

To our knowledge, our single cell recordings are the first obtained with a P23H mutant and we have also estimated for the first time, the number of Rh* that are necessary to observe an alteration of the phototransduction signaling cascade and of the anomalous disks shedding in an adRP model.

3.3 Circadian rhythms drive the adaptation of rods obtained from animals sacrificed at night.

Circadian rhythms are the ensemble of the cellular and molecular mechanisms that oscillate with a periodicity of 24 hours, and drive both the behavior and the metabolism of most of the organisms on Earth. The periods of light and dark adaptations may influence this rhythmicity, especially in rod photoreceptors, which are the most numerous and sensitive cells of vertebrates' retina.

The adaptation conditions that we have used in our preliminary experiments were designed in order to assess the contribution of the already described oscillatory expression of many proteins involved in the phototransduction signaling cascade and, more in general, in the metabolism of rods. The periods of light and dark adaptation displayed in **Table 3.2.1** and in **Table 3.2.2** were different between the two groups and the comparison of the responses obtained in the two conditions may not be accountable. Another possibility could have been to drastically invert the circadian rhythm of some of our frogs and compare the responses of their rods with the normal ones. However, any combination of light and dark adaptation would have been an alteration of the normal circadian rhythmicity; therefore, it could have been considered as a strong experimental variable.

Interestingly, our preliminary results suggest that the responses of light adapted rods, obtained from animal sacrificed at 1 PM and at 1 AM (**Figure 3.2.1**), display very similar accelerated kinetics and small amplitudes. In this conditions it might be more difficult to take into consideration any relevant contribution of the circadian rhythms, no matter the period of light adaptation. Moreover, it was shown that light drives the expression of R. Therefore, keeping the frogs in light adapted conditions may strongly influence rods responsivity.

The photoresponses to brief light flashes of the dark-adapted rods of the D.A.O.N. and "night" populations, also display very similar kinetics suggesting that overall, different periods of dark adaptation might not change much the photoresponses' kinetics (**Figure 3.2.2**). However, the small differences between the two populations of responses might be attributed to the different dark adaptation periods or to the circadian rhythms. The latter option is the most fascinating one, considering also that the amount of time necessary to fully adapt a frog to dark is in the order of few hours. Moreover, both the single photon (**Figure 3.2.4**) and the light adaptation (**Figure 3.2.5**) analysis have revealed a higher variability of "night" rods responses. The averaged single photon

responses of these cells displayed variable durations, suggesting a variable sensitivity to very dim flashes of light. Furthermore, light adaptation seams to be more pronounced in D.A.O.N. rods, suggesting that in these conditions light adaptation can reach its maximal level.

Surprisingly, dividing the two main populations of dark-adapted responses into two subgroups and comparing the averaged traces, revealed interesting and peculiar characteristics (**Figure 3.2.6**). The comparison between the D.A.O.N. rods' responses, obtained in the first 12 hours of experiments and the responses obtained afterwards revealed very similar kinetics and small differences (**Figure 3.2.6 A, B**). On the other hand, the same comparison between the two subgroups of the "night" rods population displayed a marked shift from the 12 hours averaged traces, of the averaged responses obtained in the following hours (**Figure 3.2.6 C, D**). These results may suggest that even if both populations of rods were kept at 4 °C and in dark conditions, for a long period, only "night" rods express the potential to keep their metabolism going. Possibly their intrinsic circadian rhythms may progress and could be observed as a shift of both current amplitude, time to peak and duration.

However, further single photon and light adaptation experiments may be useful in order to confirm this shift in sensitivity of the "night" rods and may also clarify why our D.A.O.N rod do not display this peculiar behavior.

3.4 Phototransduction in rod photoreceptors may be influenced by mechanotransduction.

The phosphene phenomenon has been described as the perception of light in absence of an actual direct illumination of the eye. This anomalous activation of the phototransduction signaling cascade can be triggered by either electrical, termal or mechanical stimuli. However the physiological reasons why the eye and in particular photoreceptors should sense and transmit any mechanical stimulations remain unknown.

Recent experimental works conducted in both drosophila melanogaster and in mice have shown that both rhabdomeric and ciliated photoreceptors respond to light stimuli, not only by activating phototransduction, but also activating a mechanical response. For the rhabdomeric receptors it was proposed that light induces a contraction of the actomyosin network of the rhabdomer, which is proportional to the intensity of the light stimulus. On the other hand, similar experimental evidences obtained in mice, by mean of the OCT technique, have evidenced a possible volumetric enlargement of the OS of retina photoreceptors. In this case, it has been proposed that the principal reason for this change is an osmotic swelling, which is consequent to the activation of the phototransduction signaling cascade and in particular of the G protein. A very detailed biophysical model has been

proposed, which take into account the increased osmolarity of the OS caused by the activation of the phototransduction.

Our preliminary experimental results not only confirmed that rods responds with a mechanical output to light stimuli, but also that they express some important mechanotransductive channels on both the IS and OS membranes (**Figure 3.3.1**), which might contribute to modulate the influx of ions during this mechanical responses. However, further experiments will be necessary to better understand how and if these channels can influence phototransduction. Moreover, we have evidenced that during light adaptation, rods' IS are mechanosensitive, they respond to mechanical stimuli with variations of intracellular calcium and that mechanical stimuli can be transmitted, in some cases, along the rods' OS, triggering also there some kind of calcium signaling.

A very interesting and fascinating speculation is related to the fact that the fusion between the disks and the plasma membrane, during the disks shedding is calcium mediated. Therefore, the mechanosensation in photoreceptors could be related to the shedding of the tip of the OS. It is also interesting to notice that variation of volume of the OS could generate a small but significant force that could be a trigger for RPE phagocytosis. Moreover, this evolutionary conserved mechanosensation among various species may suggest that this process is an important factor for phototransduction, which has not been widely studied so far. Many other sensory neurons might be influenced by mechanical stimuli and this may suggest that vertebrates sensory neurons are not only specialized machine for the sensation of a specific sensory input, but that they actually perform an integration between many different sensory stimuli.

4. Manuscript under revision

Electrophysiological changes during early steps of retinitis pigmentosa

Authors: Ulisse Bocchero[1], Monica Mazzolini[1], Beatrice M. Tam[2], Colette N. Chiu[2], Vincent Torre[1,#] and Orson L. Moritz[2,#,¥]

1- International School for Advanced Studies (SISSA) via Bonomea 265, 34136 Trieste (Italy)

2- Department of Ophthalmology & Visual Sciences, University of British Columbia, Vancouver, BC, Canada.

[#] Co-corresponding authors To whom correspondence should be addressed: Vincent Torre; e-mail: torre@sissa.it and Orson Moritz: olmoritz@mail.ubc.ca

¥Submitting author

Short title: Early electrophysiological changes in RP

Manuscript length:

Pages: 30

Figures: 5

Tables: 1

Words:

Abstract: 250

Significance: 107

Introduction: 647

Discussion: 1027

Conflict of Interest: The authors have no conflicts of interest to declare

Keywords:

Retinitis pigmentosa, phototransduction, photoresponse, rhodopsin, photoreceptor

Acknowledgements: We thank M. Lough for proofreading. This work was supported by grants from the Foundation fighting blindness (Canada) (OLM) and the Natural Sciences and Engineering Research Council of Canada (OLM). We thank Matteo Caorsi (SISSA Mathematics Area) for the help with the calculations and Marco Gigante for the 3D printed recording chamber (SISSA Mechatronic lab).

Abstract:

Purpose: The rhodopsin mutation P23H is responsible for a significant portion of autosomal dominant retinitis pigmentosa, a disorder characterized by rod photoreceptor death. The mechanisms of toxicity remain unclear; previous studies implicate destabilization of P23H rhodopsin during light exposure, causing decreased endoplasmic reticulum (ER) exit and ER stress responses. Here, we probed phototransduction in *Xenopus laevis* rods expressing bovine P23H rhodopsin, in which retinal degeneration is inducible by light exposure, in order to examine early physiological changes that occur during retinal degeneration.

Methods: We recorded single cell and whole retina responses to light stimuli using electrophysiology. Moreover, we monitored morphological changes in rods after different periods of light exposure.

Results: Initially, P23H rods had almost normal photoresponses, but following a brief light exposure varying from 5 to 44 photoisomerizations per disc, photoresponses became irreversibly prolonged. In intact retinas, rods began to shed OS fragments after a rod-saturating exposure of 12 minutes, corresponding to 10-100 times more photoisomerizations.

Conclusions: Our results indicate that in P23H rods light-induced degeneration occurs in at least two stages, the first involving impairment of phototransduction, and the second involving initiation of morphological changes.

Introduction:

Rod outer segments (OSs) are comprised of thousands of stacked disks containing photon-absorbing rhodopsin molecules packed in an almost crystalline fashion[114–118]. Photo-excited rhodopsins activate G-proteins, each of which activates one phosphodiesterase (PDE) molecule[119–121]. Activated PDEs hydrolyse cyclic guanosine monophosphate, thereby closing cyclic nucleotide-gated channels[122,123] to produce well-characterized photoresponses[115,124,125].

Retinitis pigmentosa (RP), a disease of progressive rod photoreceptor degeneration[126], is caused by mutations in many genes. However, the *rhodopsin* mutation P23H is the most common cause of autosomal dominant RP in North America[127,128]. In *Xenopus laevis* tadpoles expressing the bovine form of P23H rhodopsin (hereafter named bP23H), photoreceptors degenerate rapidly when exposed to cyclic light[61,63,129]. However, when reared in darkness, degeneration is prevented. Therefore these animals have been used as a model for RP[56,61,129,130], particularly the light-exacerbated retinal degeneration (RD) that likely occurs in cases of sector RP[66,131,132]. The exact mechanisms of toxicity remain unclear.

The P23H mutation promotes structural instability[133]. Previous studies suggest a mechanism involving destabilization of bP23H opsin by light, decreasing its exit from the ER[49,134]. In dark-reared *X. laevis*, expression levels of bP23H rhodopsin are low relative to the endogenous (WT) rhodopsin, likely due to ER quality control. However, a significant quantity reaches the OS, resulting in expression levels of 10% relative to endogenous rhodopsin[61,134]. In dark-reared animals subsequently exposed to light, inner segment (IS) and OS membrane abnormalities rapidly develop[63]. Similarly, low basal expression, aggregation and proteolytic degradation of P23H rod opsin expressed in the *C. elegans* neurons can be partially reversed by providing 9-cis retinal[52].

P23H mutant mice have been examined using *electroretinography (ERG)*, and showed abnormal a-waves[55]. At P40 they have abnormal ERGs and reduced rod nuclei numbers[135]. In the present manuscript, we probed phototransduction in intact retina and isolated rods from transgenic *X. laevis* expressing bP23H rhodopsin that were bred and housed in continuous darkness. Under these circumstances, bP23H-expressing rods do not degenerate and have almost normal photoresponses. However, an exposure to light causing just a few photoisomerizations per disc impairs phototransduction, although rods retain their integrity and morphology. *In vivo*, a light exposure of 12 minutes causes rods to shed OS, lose their morphology, and degenerate.

Materials and Methods:

Breeding and rearing of transgenic *X. laevis*: *X. laevis* tadpoles expressing bP23H were generated by mating heterozygous or homozygous transgenic males with wildtype (WT) female[61,129,130]. WT tadpoles were derived from separate matings, or were siblings of transgenic tadpoles. Tadpoles were transferred to an 18-21°C incubator that maintained 24-hour/day constant darkness. All experiments adhered to the ARVO statement for the Use of Animals in Ophthalmic and Vision Research.

Isolation of photoreceptors: Tadpoles and froglets were sacrificed as previously described[136]. The developmental stage of each animal was determined (http://www.xenbase.org/anatomy/alldev.do). Eyes were enucleated and hemisected under infrared 820 nm illumination. Dissociated rods were obtained as reported[9,137]. Isolated intact rods obtained by mechanical dissociation were immersed in Ringer solution containing (in mM): 110 NaCl, 2.5 KCl, 1 $CaCl_2$, 1.6 $MgCl_2$, and 3 HEPES-NaOH, 0.01 EDTA and 10 glucose (pH 7.7-7.8 buffered with NaOH). All chemicals were purchased from Sigma-Aldrich. All experiments were performed at 22-24° C. Images were acquired using HCImage software 4.3.1.33.

Single cell photoresponse recordings: After mechanical isolation, the IS of an isolated intact rod was drawn[138] into a silane-coated[108] borosilicate electrode (Blaubrand, intramark micropipette, Germany) (internal diameter of 4-6 μm) filled with Ringer's solution. Rods were viewed under 900 nm light using two cameras (Hamamatsu ORCA-Flash 4.0 and Jenoptic ProgRes MF) at two magnifications and stimulated with 491 nm diffuse light (Rapp OptoElectronic, Hamburg, Germany) from the 10x objective of an inverted microscope (Olympus IX71). To stimulate the entire OS we used a stable continuous 491 nm laser module (for details see reference[9]). Photoresponses were recorded as previously described[9] using an Axopatch 200A (Molecular Devices) in voltage clamp-mode. The current was low-pass filtered at 20 Hz and digitised at 100 Hz. All recordings were processed, analysed and baselines corrected with Clampfit 10.3 (Molecular Devices). Data are expressed as mean ± SEM; single points represent single experiments.

Single photon response analysis. Single photon responses were evoked by a series of 20-99 dim flashes delivered every 5 s, with duration of 10 ms. The data were fitted with the equations from (6) to (9) described in Baylor et al. 1979[115].

ERG recordings: Dark-reared tadpoles (age 10 weeks, stage 56) (offspring of a heterozygous transgenic and WT animal) or siblings exposed to cyclic light for one week, were anaesthetized in 0.01% Tricaine in 0.1X MMR. ERG recordings to a series of blue light flashes of increasing intensity were obtained as described by Vent-Schmidt et al.[139]. Following ERG analysis tadpoles were genotyped to distinguish bP23H and WT animals as previously described[139].

Confocal microscopy: Eyes were fixed overnight at 4°C in 4% paraformaldehyde in 0.1 M phosphate buffer pH 7.4, and processed, cryosectioned and labelled for confocal microscopy using Alexa488-conjugated wheat germ agglutinin (Invitrogen) and Hoechst 33342 (Sigma) as previously described[136] . Images were obtained using a confocal microscope equipped with a 40X N.A. 1.2 water immersion objective. Phagosomes were identified by morphology by a blinded lab member. Phagosome area was quantified using ImageJ software[140].

Estimation of the number of photoactivated bP23H rhodopsins (Rh*) on a disc: Assuming 25000 Rh/ μm^2 [124] one bP23H disc has an area of 12.6 μm^2 (based on a diameter of 4 µm) giving 25000 Rh/μm^2 x 12.6 μm^2 = $3.15x10^5$ Rh/disc. There are 2100 disks/rod in toad[124] with a length of 60 µm. Our observed bP23H OS length is 33 µm, therefore 1155 disks. The total Rh/rod = $1155x3.15x10^5$ =$3.6x10^8$. In dark-reared animals, bP23H Rh is the 10% of the total[130] giving an estimated number of bP23H Rh per rod of $3.6x10^7$ (bP23H Rh $3.15x10^4$ per disc).

Considering our lower limit of photoisomerization to see an effect on phototransduction of 60000 Rh* in 30-60 minutes, we have: $60000/3.6x10^8$ = 0.00017 Rh*/Rh (2 Rh* every 10000 Rh); considering our upper limit of 500000 Rh* in ~ 6 minutes we have: $500000/3.6x10^8$ = 0.0014 Rh*/Rh (1.4 Rh* every 1000 Rh). Therefore we obtain in the former case 5 bP23H Rh* per disc (0.00017 Rh*/Rh x$3.15x10^4$ bP23H Rh/disc), in the latter 44 bP23H Rh* per disc (0.0014 Rh*/Rh x$3.15x10^4$ bP23H Rh*/disc).

Results:

X. laevis carrying the bP23H mutation have a rapid light-induced RD.

As previously reported[61,63,129,134], *X. laevis* tadpoles expressing bP23H rhodopsin show no detectable RD when reared in complete darkness for up to 10 weeks. However, when exposed to 1700 lux cyclic light for one week, RD occurs rapidly (Fig. 1A). Our transgenic line expresses bP23H rhodopsin at 10% of the level of the endogenous rhodopsin[61]. Therefore, these animals present a unique opportunity to examine the electrophysiology of non-degenerating rods expressing relatively large quantities of a disease-causing rhodopsin mutant, as well as the initial physiological alterations of rods undergoing RD induced by light.

Dark reared *X. laevis* carrying the bP23H mutation have relatively normal ERG responses.

We compared ERG recordings from bP23H and WT tadpoles (Fig. 1B). For animals reared 10 weeks in darkness, bP23H recordings (red traces) were similar to WT (black traces). Although b-wave amplitude appeared slightly lower in bP23H tadpoles, we found no statistically significant effect of genotype. a-wave amplitudes were similar between the two groups, but smaller in bP23H animals at high flash intensities (2-way ANOVA, P = 0.006 for effect of genotype). In contrast, after one week in cyclic light, a- and b-wave amplitudes were markedly different between genotypes (effect of genotype for b-wave, P = 1.2E-12, a-wave, P = 5.6E-8) consistent with significant RD.

Conversion from arbitrary units to photoisomerizations through single photon analysis

For single-cell photoresponse recordings, we calibrated our laser illumination from arbitrary units (a.u.) to induced photoisomerizations (Rh*) per rod. We performed single photon analysis[115] of mutant (Fig.2 A-C) and WT rods (Fig.2 D-F) obtained from tadpoles and froglets kept in constant darkness and WT rods obtained from adults kept in cyclic light (Fig.2 G-I) and estimated the number of rhodopsin molecules activated by a given flash intensity[115]. We established that our dimmest flash of 50 a.u., with a duration of 10 ms, generated 1.5-2.5 photoisomerizations with a mean response amplitude of ~0.5 pA. We use this conversion throughout the manuscript (see Methods). Our *X. laevis* single photon response is slightly lower than previously reported and both estimates are lower than reported for adult *Bufo* rods[115,141,142].

Transgenic *X. laevis* reared in darkness have almost normal phototransduction machinery

We carried out single-cell suction-electrode recordings from isolated rods from WT (Fig. 3A) and bP23H (Fig. 3B) tadpoles reared in darkness. Isolated WT and bP23H rods responded to flashes of increasing intensity with a decrease of the circulating current where the maximal amplitude reflects the size of the dark current (Fig.3C,D) as previously described for adult *X. laevis* rods[9]. The maximal amplitude (I_{dark}) varied between developmental stages (Fig.3C,D and Table 1) as previously observed in WT *X. laevis* rods[141,142] and between WT and bP23H rods. For a given developmental stage, bP23H rods produced 35% lower maximal photoresponses than WT rods. When normalized to their maximal amplitude (Fig.2E), the rising phases of WT and bP23H photoresponses (black vs red traces) were superimposable (red traces) and had a similar time course and time to peak (Fig.3F and Table 1).

An analysis of WT and mutant rod geometry showed that WT OS were 11 μm longer and 0.5 μm wider than bP23H OS (Table 1). Therefore, the ratio of the OS surface area between bP23H and WT rods is about 0.6, in good agreement with the maximal photoresponse ratio. We also compared the relation between the normalized photoresponse amplitude (R/R_{max}) and light intensity (Fig.3K), fitted by a Michaelis-Menten equation (see Table 1). The $I_{1/2}$ value for bP23H was half that of WT, indicating reduced sensitivity. The relation between the maximal amplitude R_{max} and OS length was approximately linear for both bP23H and WT rods (Fig.3H). We also recorded photoresponses from tadpoles maintained in a single 12h light/12h dark cycle. WT rods displayed normal morphology and responses (Fig. 3I,K), whereas the responses and morphology of the (very few) remaining bP23H rods were altered (Fig. 3J,L).

We investigated the rising (Fig.4A) and falling phases (Fig.4B) of photoresponses from WT and bP23H rods (black vs red traces) following normalization to the maximal photoresponse. The photocurrent rapidly decreased (rising phase) after the application of bright flashes, with matching kinetics for WT and bP23H (Fig.4A). In addition, the time course of the falling phase for WT and bP23H was very similar (Fig.4B). We also compared the initial phase of light adaptation during exposure to either repetitive flashes or longer pulses[143]. The time course of photoresponses to 10 consecutive flashes separated by 1 and 2 s was remarkably alike (Fig.4C,D). Complementary results were observed when 20 s pulses were considered (Fig.4E). Additionally, we observed a delayed photoresponse decline associated with the onset of light

adaptation in both WT and bP23H rods, indicating the initial steps of light adaptation were congruent (Fig.4G).

The phototransduction machinery in bP23H rods is impaired following saturating light exposures.

We know that RD occurs if bP23H transgenic animals are reared in light, but how many photons are necessary to trigger degeneration? Is the phototransduction machinery impaired before rod collapse? We exposed WT and bP23H rods to light and estimated the number of Rh* while recording photoresponses. In the majority of WT recordings, photoresponse amplitudes and timecourses were stable over 30-60 minutes. In some cases it was possible to record photoresponses with the same maximal amplitude for 1 hour or longer. Fig.5A shows an initial WT photoresponse to a bright flash (black trace) and responses after 47, 74 and 128 minutes (gray and pale grey traces). The morphology of the rod did not change significantly during recording (see inset of Fig.5A and Fig.6A-D). Fig.5B shows a similar experiment with a bP23H rod: in contrast to WT, the photoresponse was prolonged after approximately 60 minutes of continuous recording (compare red and dark red traces). With time, the photoresponse amplitude declined and the time course was further prolonged (red and pale red traces in Fig.5B). Again, the morphology did not change appreciably (see Fig.5B inset and Fig.6E-H). We compared variation in amplitude (Fig.5C) and duration (Fig.5D) of the maximal response with time for WT (black dots, n=3) and bP23H rods (red triangles, n=3): bP23H photoresponses declined and were prolonged after approximately 60 minutes. We also averaged photoresponses (n=7) from different bP23H rods at the beginning of recording (dark red) and after tens of minutes (red trace in Fig.5E). This averaging confirmed decreased amplitude and prolongation of the photoresponse.

We observed prolongation of bP23H rod photoresponses after tens of minutes and the occurrence of between $6x10^4$ and $1x10^5$ Rh* (Fig. 5B and D- E). To distinguish whether this was due to elapsed time or the number of Rh*, we delivered our standard bright flash and after 2-3 minutes, exposed the rod to a 1 sec step of light with the same intensity, evoking $5x10^5$ Rh* of Rh* (Fig.5F,H). In WT rods, when the standard flash was re-delivered, the photoresponse timecourse was accelerated (compare black and grey trace in Fig.5G). In contrast, in bP23H rods, the photoresponse was prolonged (compare the dark red and red traces in Fig.5I) and its amplitude often declined. The time course and duration of subsequent photoresponses were further prolonged (pale red trace in Fig.5I and Fig.6E-H). Thus, when

bP23H rods are exposed to light of different durations but evoking a total number of Rh* varying from $6x10^4$ to $5x10^5$ Rh*, the phototransduction machinery is altered. In dark-reared rods the fraction of bP23H rhodopsin is about 10%[61,134], therefore the total amount of bP23H rhodopsin per disc is $3.15x10^4$ (see Methods). We estimate that the total number of disks in a bP23H rod is about 1100, based on the total number of disks in a toad rod (2100 disks/rod in toad, length 60 µm; bP23H OS length 33 µm; number of disks = 33x2100/60 = 1155). Therefore, the occurrence of just 5-44 bP23H photoisomerizations/disc is sufficient to impair phototransduction machinery.

Short light exposures trigger OS shedding in mutant rods

Within hours of exposing bP23H animals to light, RD, including OS morphological changes, is initiated[63]. To determine the minimum exposure required, we exposed bP23H animals to varying periods of bright light and returned them to darkness before sacrificing them, for a total period (light + dark) of four hours. We found that exposures of 12 minutes or longer induced massive shedding of bP23H rods into the RPE that was apparent by four hours (Fig. 7). Both the number and area of RPE phagosomes increased dramatically after light exposure (Fig.7A, C) indicating disruption of OS. To verify that we employed a rod-saturating intensity, we examined alpha-transducin migration in light-exposed WT animals (Fig 7B). At rod-saturating intensities, alpha-transducin distribution alters from an exclusively OS localization to a combined OS/IS localization due to saturation of PDE binding[144,145]. As alpha-transducin partially migrated to ISs, our standard illumination was rod-saturating. We estimated the total number of Rh* required to induce disc shedding in bP23H frogs in two different ways and arrived at similar conclusions.

Transducin migration indicates that 1700 lux is sufficient to saturate photoresponses, which in our single rod experiments occurred with flashes of light producing from 100 to 250 Rh*. If the same photon flux is prolonged from 10 ms to 12 minutes the total number of induced Rh* per rod is equivalent to $7.2x10^6$ - $1.8x10^7$. Based on analysis of ERG a-wave data from bP23H tadpoles (Fig 1B), we found that half-maximal retinal stimulation occurred at a value of 126 lux, equating to the value of 16-27 Rh* per bP23H rod shown in Table 1. Thus, 12 minutes of constant 1700 lux light would be predicted to generate 1.55 - $2.6x10^7$ Rh*. Based on these methodologies, we estimate that the number of Rh* leading to disk shedding in bP23H rods is in the range of $7.2x10^6$ - $2.7x10^7$ Rh* (from 630 to 2362 bP23H Rh* per disc).

Discussion:

If *X. laevis* tadpoles carrying the rhodopsin P23H mutation are reared in darkness, mutant rods have functional and almost normal phototransduction machinery. However, when exposed to a bright light lasting 1 s (Fig.4), their photoresponses are irreversibly prolonged. When light exposure is maintained for 12 minutes (Fig.5), significant OS shedding occurs and RD is initiated. Therefore, the first step leading to RD is the prolongation of photoresponses associated with the photoisomerization of $6x10^4$ to $5x10^5$ Rh*, equivalent to 5-44 P23H rhodopsins per disc. However, OS shedding requires 1-2 orders of magnitude greater Rh*. How can we account for this extreme sensitivity? While previous phototransduction models were based on freely diffusing rhodopsin, recent studies indicate that rhodopsins – and presumably bP23H rhodopsin – are organized in disks along parallel tracks of dimers[146–149]. Signal amplification requires multiple diffusion encounters, likely involving rhodopsins anchored in tracks of dimers while other phototransduction components diffuse more freely[146,150]. The photoresponse prolongation observed in bP23H rods is consistent with impaired rhodopsin shutoff. Transducin GTPase, arrestin, rhodopsin kinase and RGS9 are involved in phototransduction shutoff and could have roles in this impairment.

The residue P23 is located on the intradiscal face of rhodopsin in the N-terminal domain of the protein[149,151] . The majority of the bP23H rhodopsin that evades quality control and reaches the OS is proteolytically processed to remove a portion of the N-terminal domain. This portion includes the N-terminal glycosylation sites, (most likely) the P23H residue itself[61], and a hydrophobic cluster which is essential for the structural stability of the entire protein[52]. Therefore, OS bP23H rhodopsin is structurally destabilized, either by insertion of a missense amino acid, or removal of the N-terminus.

Structural destabilization of bP23H rhodopsin could result in aggregation or alterations of track structures that trap activated transducin, or prevent normal interactions of cascade shutoff proteins, effectively impairing not only transduction initiated by bP23H rhodopsin, but also transduction initiated by WT rhodopsins in the same or adjacent tracks. Another possibility is that an alternate bP23H rhodopsin structure is induced by interaction with WT meta-II rhodopsin. Thus, it is possible that upon light exposure, bP23H rhodopsin adopts an alternate conformation that alters not only the structure of the N-terminus, but also the domains that interact with signal transduction components. Under these conditions, a small impairment of

the shutoff of bleached mutant P23H rhodopsins could lead to a noticeable prolongation of the photoresponse as experimentally observed (Fig.4).

A rod-saturating exposure lasting 12 minutes induces OS shedding in mutant bP23H rods but not in WT rods (Fig.5). Based on two different calculations, the number of Rh* leading to OS shedding in bP23H rods ranges from $7.2x10^6$ to $2.7x10^7$ per rod, or 630 to 2362 bleached bP23H rhodopsins per disc, which could aggregate with other rhodopsins, possibly altering local membrane fluidity and slowing local phototransduction shut-off. Indeed, the specific organization of rhodopsins in tracks of dimers[146] is likely to be compromised by the misfolding of very few – and possibly even 5-44 – bleached bP23H rhodopsin, while the presence of some hundreds to thousands of misfolded P23H rhodopsins disrupts OS architecture and could lead to OS shedding.

Single-cell recordings from photoreceptors in animal models of RD are rare because of difficulty in acquiring the data[55,152,153]. In two-week old mutant P23H mice reared in a standard light cycle, it is difficult to identify rod OS even at the retinal margin because of severe RD. However, *X. laevis* models of RP are well suited to this purpose due to the larger size of their rods, and the availability of several RP models in which RD can be dramatically limited by dark rearing[58,61,136,154]. It will be interesting to determine whether the effects we observed are common to multiple animal models, or unique to P23H rhodopsin.

Figure and Table Legends:

Figure 1: Histology and electroretinography of WT and bP23H tadpoles reared in darkness or exposed to one week of cyclic light. (A) Confocal micrographs stained with wheat germ agglutinin (green) and Hoechst 33342 nuclear stain (blue). There is no evidence of retinal degeneration in dark reared bP23H animals relative to WT, while bP23H animals transferred to cyclic light for 1 week have few remaining rods. (B) Electroretinography of WT and bP23H animals housed under the same conditions as in (A) showing averaged traces (top) and a- and b- wave analysis (below). bP23H results are shown in red, and WT results are shown in black. Error bars are +/- SEM For dark-reared conditions (left) bP23H n = 8 and WT n =8. For light-exposed animals (right) bP23H n = 7 and WT n=5). P-values shown on charts represent the statistical significance of the effect of genotype in a 2-way ANOVA analysis (intensity vs. genotype). The effect of intensity was highly significant in all cases ($P < 10E^{-12}$).

Figure 2: Single photon analysis of a bP23H and WT rod, obtained from tadpoles kept in constant darkness, and a WT rod obtained from an adult kept in cyclic light. (A)(D) Photoresponses elicited by diffuse dim flashes of light, evoking 1.5-2.5 Rh* for a mutant (red), a WT (black) rod respectively. Insets represent the rods, with the IS inside the electrode (scale bar 10 μm). (G) The same as (A) and (D) but for a WT adult kept in cyclic light. (B)(E) Histograms of the amplitudes of evoked photoresponses (n = 20). (H) The same as (B), (E) but for a WT adult kept in cyclic light (n = 99). The histograms were fitted with the equation described in Materials and Methods. Values providing the best fit are reported in the panel; a is the mean response to single photon, σ0 is the noise standard deviation (SD), σ1 is the SD of the mean, and m is the mean number of events per trial. (C)(F) Averages of the evoked photoresponse to diffuse dim flashes of light in (A) and (D) respectively. (I) The same as (C), (F) but for a WT adult kept in cyclic light.

Figure 3: Comparison of photoresponses of WT and bP23H rods. (A, B) Isolated rods from a WT and a bP23H *Xenopus laevis* tadpole respectively. (C) A family of photoresponses to diffuse light of increasing intensity for the WT rod in (A). The maximal amplitude of current is 8.7 pA for a flash inducing 150-250 Rh*. The flashes were applied at the time indicated by the black bar and had a duration of 10 ms. The light intensity produced by the laser was equivalent to 6-10, 15-25, 30-50, 60-100 and 150-250 Rh* respectively. The photoresponses of WTs'rod had a maximal amplitude of 6.5 ± 0.5 pA (n = 2) at stage 49-54,

7.0 ± 0.7 pA (n = 7) at stage 55-59 and 13.4 ± 1.1 pA (n = 6) starting from the stage 66 (froglets-adult stage) of development. (D) Example of a family of photoresponses as in (C) but for the bP23H rod in (B). The maximal amplitude of current is 6.0 pA for a flash inducing 150-250 Rh*. This response also display a spike derived from an artifact. The photoresponses of bP23H rods increased with development and was approximately 3.6 ± 0.2 pA (n = 3) at stage 49-54, 4.9 ± 0.5 pA (n=4) at stage 55-59 and increased to 7.2 ± 1.2 pA (n = 7) pA starting from the stage 66 (froglets-adult stage) of development. (E) Superimposition of normalized photocurrent in (C) (black) and in (D) (red). (F) Superimposition of normalized dim flashes, eliciting 6-10 Rh*, from 10 WT and 8 bP23H rods (developmental stage 49-60). (G) Comparison of the relation between the normalized amplitude of photoresponses (R/R_{max}) and light intensity (I) for WT (black circle; n = 3-10) and bP23H (red triangles; n = 3-8). The data were fitted with the equation $R/R_{max} = I/ (I + I_{1/2})$ where $I_{1/2}$ is equivalent to 10-16 Rh* ± 1 for WT (black line) and to 16-27 Rh* ± 2 for mutants (red line). (H) Relation between OS length and saturating current for WT (black circles; n=10) and bP23H (red triangles; n=8). The data were fitted with a linear regression $R_{ma\ x} = c*l$, with a value of 0.13 and 0.11 of c for WT and bP23H rods respectively. (I, J) Isolated rods from a WT and a bP23H *Xenopus laevis* tadpoles that were exposed to a single 12h light/12h dark cycle. (K) Family of photoresponses from the rod in (I) elicited by 6-10, 15-25, 30-50, 60-100 and 150-250 Rh* respectively. The maximal amplitude of current is 6.9 pA for a flash inducing 150-250 Rh*. (L) Family of photoresponses of the rod in (J) elicited by 15-25, 30-50, 60-100 and 150-250 Rh* respectively. The maximal amplitude of current is 3.6 pA for a flash inducing 150-250 Rh*. In (A), (B), (I) and (J) the scale bars represent 10 μm.

Figure 4: Comparison of rising/falling phases of bP23H and WT photoresponses. Analysis of light adaptation response to repetitive flashes and step of light, WT and bP23H rods. (***A***) Expanded scale for families of selected photoresponses to normalized diffuse light (Fig.1E) of increasing intensity of a WT (black traces) and bP23H rods (red traces) showing the rising phase. The histograms represents the collective data for the activation rate of the saturating responses of tadpoles at stage 55-59. (*B*) The same as in (***A)*** but for the falling phase. Black and red lines are exponential decay fittings with the equation $y = ae^{-bx}$. (C) Averaged photoresponses evoked from ten identical non-saturating light flashes with a duration of 10 ms, equivalent to 150-250 Rh* applied with a time interval (Δt) of 1 s for the WT (black traces n=7) and for the bP23H (red traces n=3). (D) As in (C) but for photoresponses evoked with a Δt of 2 s (black traces n=6 and red traces n=7). (E) Example of photoresponse to a step of light

with a duration of 20 s in non-saturating light conditions for WT (black traces) and bP23H (red traces) equivalent to 15-25 Rh*/sec and 30-50 Rh*/sec respectively.

Figure 5: Comparison of the photoresponses of WT and bP23H rods to prolonged or acute exposure of saturating light (developmental stage 60 to 66). (A) Examples of photoresponses evoked by identical saturating flashes (100k a.u., equivalent to $3x10^3$-$5x10^3$ Rh*) with a duration of 10 ms applied at the beginning of the experiments (black traces) and at specific time interval (*gray traces*) for a WT rod. In the inset, the correspondent isolated rod from WT *X. laevis* froglet at the beginning (0 min) and at the end (128 min) of the experiment. (B) Examples of photoresponses evoked by identical saturating flashes as in (A), applied at the beginning of the experiments (*dark red traces*) and at specific time interval *(red traces*) for a bP23H rod. In the inset, the correspondent isolated rod from bP23H rod *X. laevis* froglet at the beginning (0 min) and at the end (96 min) of the experiment. (C) Plot representing the variation of maximal current amplitude (in pA) in relation to different time along the experiment (WT and bP23H rods n = 3; values represent mean ± SEM). (D) Plot representing the elongation of saturation time (in pA) in relation to different time along the experiment (WT and bP23H rods n = 3; values represent mean ± SEM). (E) Averaged photoresponses for the bP23H at the beginning (dark red trace n=7) and at the end (light red trace n=7) of the experiment. (F) Example of photoresponses of WT rods evoked by identical saturating flashes (equivalent to $3x10^3$-$5x10^3$ Rh*) with a duration of 10 ms applied before (Pre) and after (Post) a step (in the middle) with a duration of 1 s (equivalent to $3x10^5$-$5x10^5$ Rh*). (G) Superimposition of photoresponses of WT rods evoked by identical saturating flashes (equivalent to $3x10^3$-$5x10^3$ Rh*) with a duration flash of 10 ms applied at the beginning (Pre), in the middle (Post) and at the end of the experiment (Last). (H) The same as in (F) but for bP23H rod. (I) The same as in (G) but for bP23H rod. In all insets scale bar=10 μm.

Figure 6: bP23H rods display the same morphology during multiple saturating light stimulations. (A-D) Monitoring of a WT rod morphology through time (same rod as in Fig. 5A). The traces represent examples of photoresponses to saturating flashes of light equivalent to $3x10^3$-$5x10^3$ Rh*, shortly before/after the associated pictures. (E-H) Monitoring of a bP23H rod morphology through time (same rod as in Fig. 5B). The traces represent examples of photoresponses to saturating flashes of light equivalent to $3x10^3$-$5x10^3$ Rh*, shortly before/after the associated pictures.

Figure 7: Titration of light exposures sufficient to induce retinal degeneration in bP23H tadpoles. bP23H and WT tadpoles were reared in complete darkness and exposed to bright light (1700 lux) for the indicated periods, and then returned to darkness, for a total time of four hours. (A) Plots representing quantitative data of phagosome structures expressed in terms of phagosome area. P values shown on the plots were obtained using Dunnet's test for multiple comparisons following ANOVA. (B) High magnification panels showing that transducin localization changes on light exposure, indicating that 1700 lux is a rod-saturating light intensity. (C) Confocal micrographs of cryosectioned retinas corresponding to plot (A). A 12 minute light exposure is sufficient to induce significant retinal degeneration including abundant shedding of photoreceptor outer segments into the RPE (arrowheads). In contrast, exposures of 4 minutes or less did not induce significant retinal degeneration, and WT retinas were unaffected. Green: Wheat germ agglutinin, Blue: Hoechst 33342 nuclear stain. Scale bar=10 µm (B) or 40 µm (C)

Table 1: Idark: is the light-saturated responses dark current; I1/2 : is the light intensity that is necessary to obtain a response that is half of the saturating response. Sf(n) is the fractional sensitivity of the normalized dim flash, calculated as the amplitude of the dim flash response divided by its strength and then normalized for the amplitude of the saturating response. Tpeak: is the time to peak of a dim flash response with an amplitude of approximately 0.2 of the Idark. Tintegr: is the integration time and it is estimated as the integral of dim flash responses (with amplitudes of approximately 0.2 Idark) normalized to its peak amplitude. Values shown are mean ± SEM. * < 0.05, ** < 0.01, *** < 0.001, compared with WT values.

Figures:

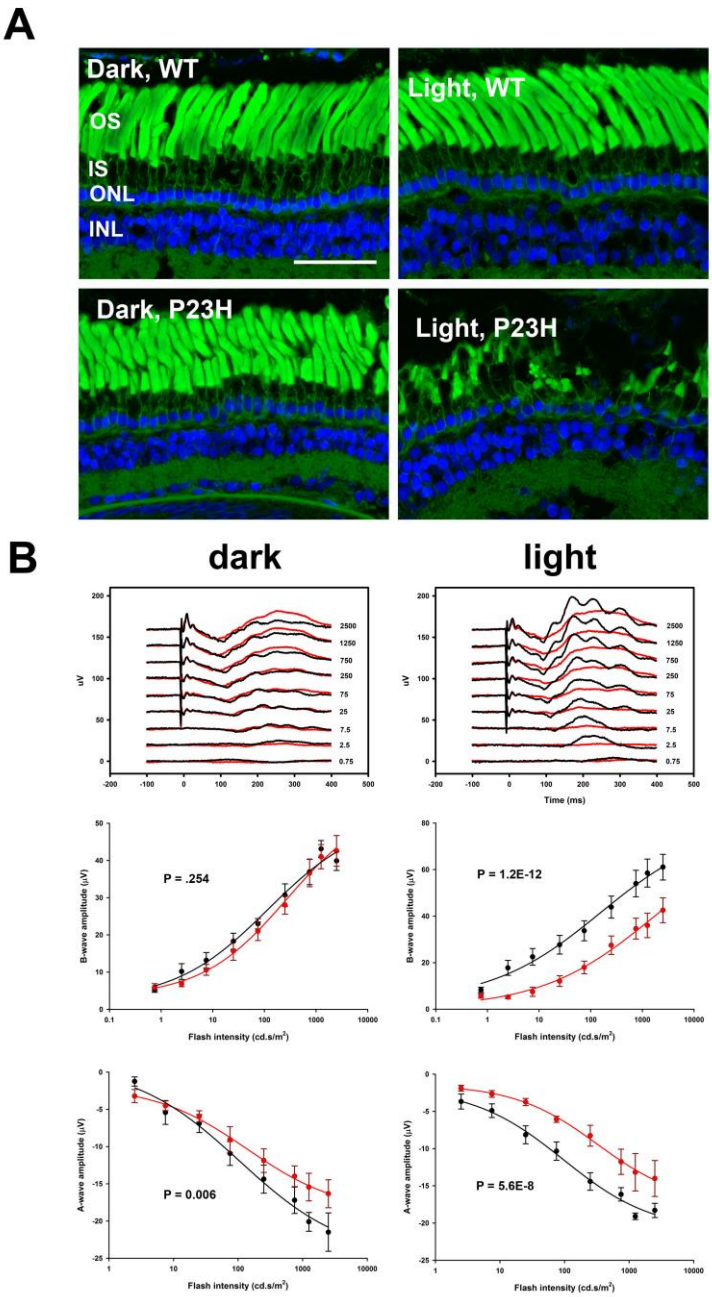

Figure 1

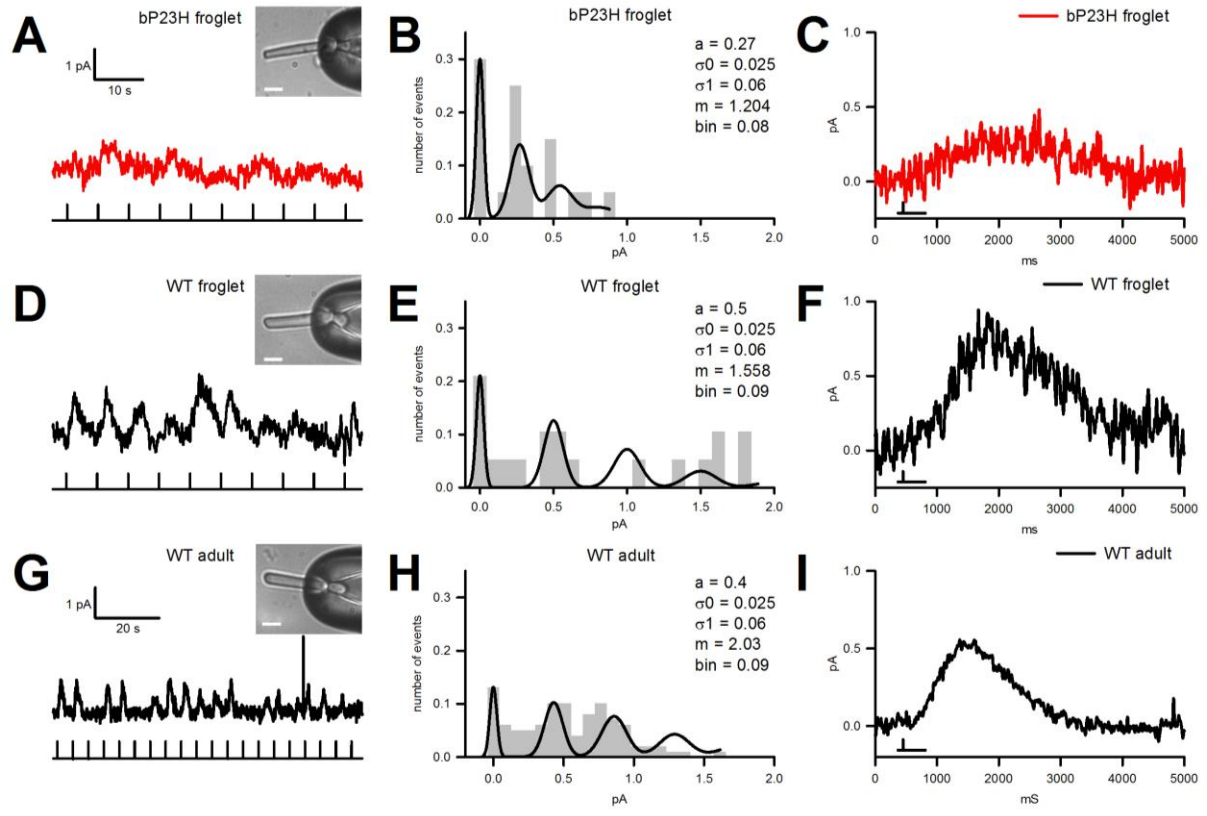
A
bP23H froglet
1 pA
10 s
B
bP23H froglet
a = 0.27
σ0 = 0.025
σ1 = 0.06
m = 1.204
bin = 0.08
number of events
pA
C
bP23H froglet
pA
ms
D
WT froglet
E
WT froglet
a = 0.5
σ0 = 0.025
σ1 = 0.06
m = 1.558
bin = 0.09
number of events
pA
F
WT froglet
pA
ms
G
WT adult
1 pA
20 s
H
WT adult
a = 0.4
σ0 = 0.025
σ1 = 0.06
m = 2.03
bin = 0.09
number of events
pA
I
WT adult
pA
mS

Figure 2

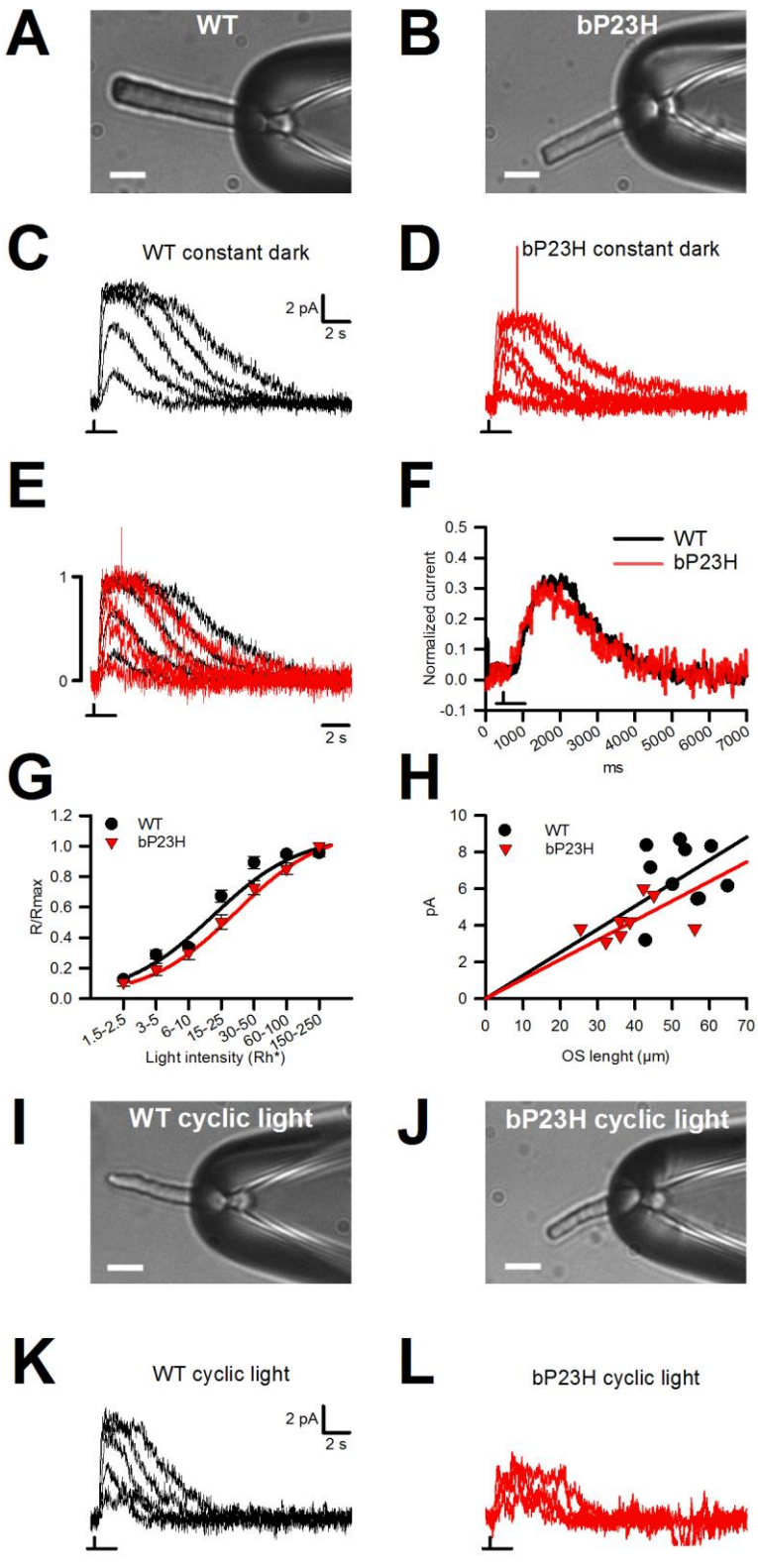
A
WT
B
bP23H
C
WT constant dark
2 pA
2 s
D
bP23H constant dark
E
1
0
2 s
F
WT
bP23H
Normalized current
0.5
0.4
0.3
0.2
0.1
0.0
-0.1
0
1000
2000
3000
4000
5000
6000
7000
ms
G
WT
bP23H
R/Rmax
1.2
1.0
0.8
0.6
0.4
0.2
0.0
1.5-2.5
3-5
6-10
15-25
30-50
60-100
150-250
Light intensity (Rh*)
H
WT
bP23H
pA
10
8
6
4
2
0
0
10
20
30
40
50
60
70
OS lenght (µm)
I
WT cyclic light
J
bP23H cyclic light
K
WT cyclic light
2 pA
2 s
L
bP23H cyclic light

Figure 3

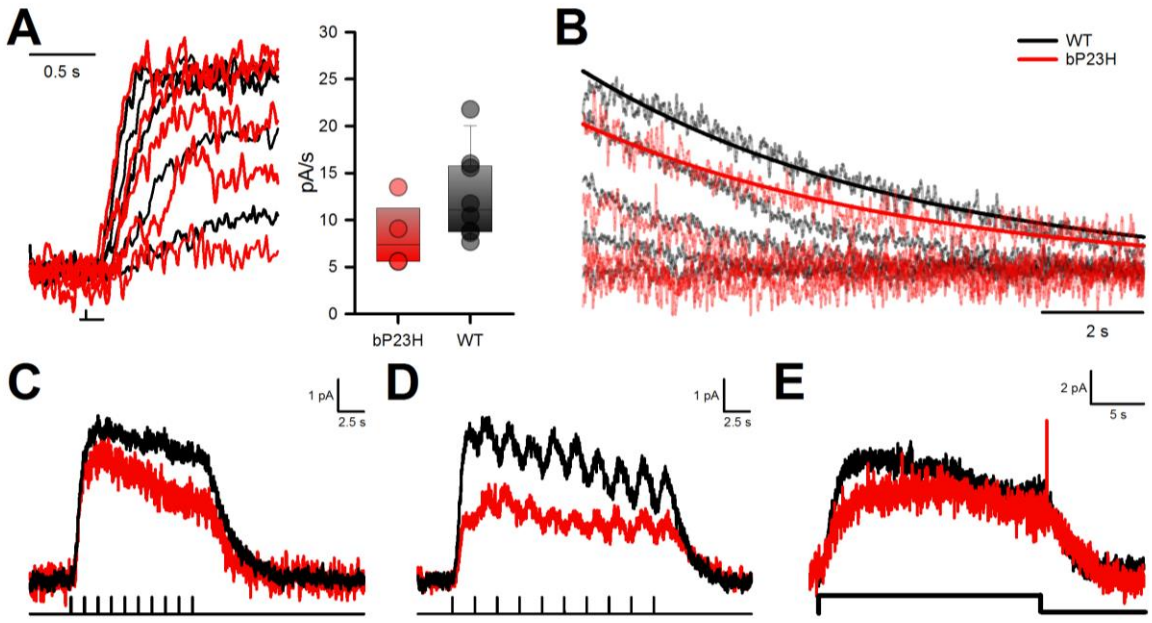
A
0.5 s
30
25
20
15
10
5
0
pA/s
bP23H
WT
B
WT
bP23H
2 s
C
1 pA
2.5 s
D
1 pA
2.5 s
E
2 pA
5 s

Figure 4

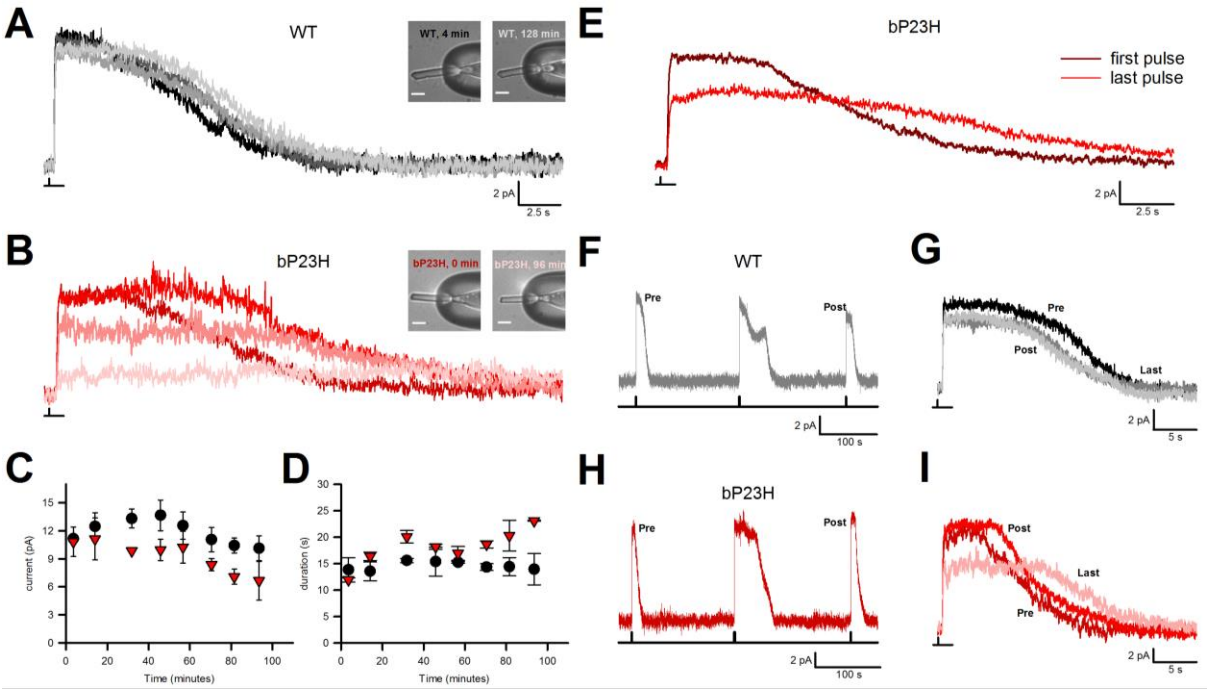

Figure 5

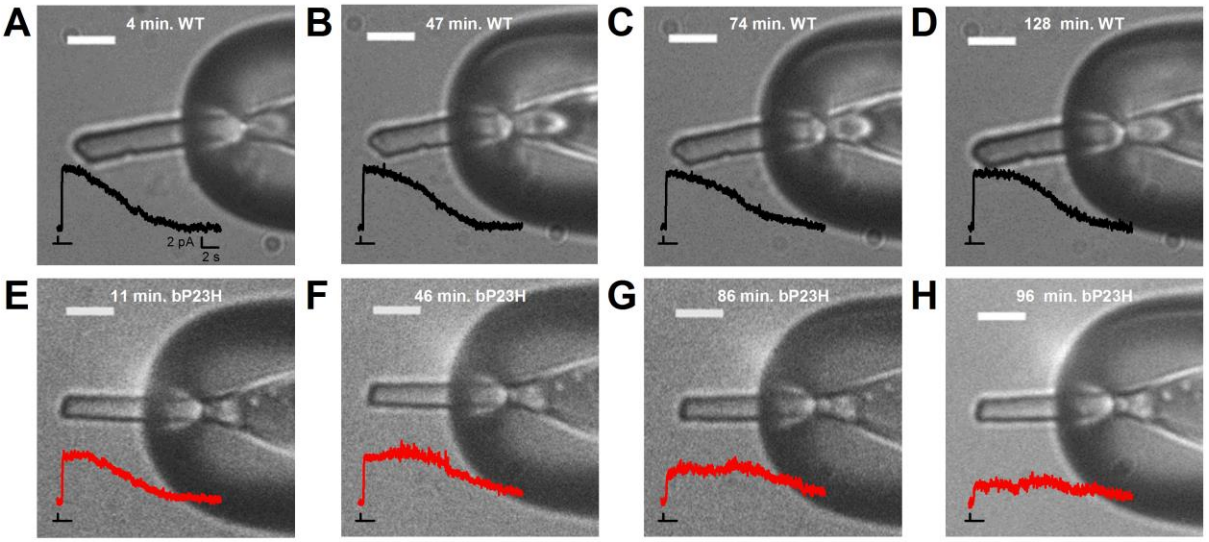

Figure 6

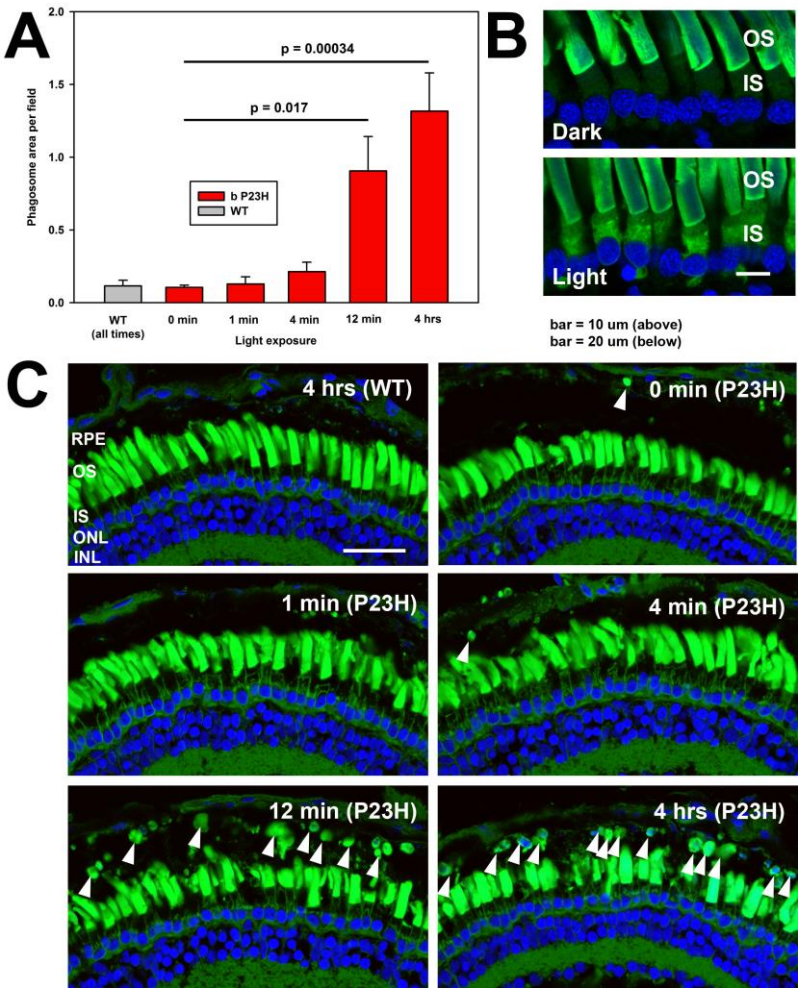

Figure 7

TABLE 1

VARIOUS PARAMETERS OF WT AND BP23H RODS

	rod length (µm)	OS lenght (µm)	diameter (µm)	I_{dark} (pA)	$I_{1/2}$ (Rh*)	$S_{f(n)}$ (1/Rh*)	T_{peak} (ms)	T_{integr} (ms)
WT	51.5 ± 1.3 (38)	44.8 ± 1.2 (38)	5.1 ± 0.1 (38)	7.4 ± 0.5 (7)	10 - 16 (7)	0.037 ± 0.0003 – 0.062 ± 0.0005 (7)	1135 ± 108 (7)	3429 ± 222 (7)
BP23H	39.7 ± 0.7 *** (70)	33.6 ± 0.6 *** (70)	4.7 ± 0.1 * (70)	5.3 ± 0.6 * (4)	16 - 27 ± 2 ** (4)	0.021 ± 0.0003 – 0.035 ± 0.0005 ** (4)	1009 ± 150 (NS)(4)	2623 ± 323 * (4)
WT CYCLIC LIGHT	40.2 ± 1.2 (3)	34 ± 1.2 (3)	4.2 ± 0.4 (3)	6.2 ± 0.5 (3)	//	//	908 ± 117 (3)	3590 ± 137 (3)
BP23H CYCLIC LIGHT	31.4 ± 4.7 (2)	25.3± 5.1 (2)	4.2 ± 0.4 (2)	3 ± 0.5 (2)	//	//	797 ± 86 (2)	1580 ± 78 (2)

5. References

1. Lamb, T. D., Collin, S. P. & Pugh, E. N. Evolution of the vertebrate eye: Opsins, photoreceptors, retina and eye cup. *Nat. Rev. Neurosci.* **8,** 960–976 (2007).

2. Yau, K. W. & Hardie, R. C. Phototransduction Motifs and Variations. *Cell* **139,** 246–264 (2009).

3. Fain, G. L., Hardie, R. & Laughlin, S. B. Phototransduction and the Evolution of Photoreceptors. *Curr. Biol.* **20,** R114–R124 (2010).

4. Hardie, R. C. A histamine-activated chloride channel involved in neurotransmission at a photoreceptor synapse. *Nature* **339,** 704–706 (1989).

5. Borst, A. Drosophila's View on Insect Vision. *Curr. Biol.* **19,** R36–R47 (2009).

6. Rao-Mirotznik, R., Harkins, A. B., Buchsbaum, G. & Sterling, P. Mammalian rod terminal: Architecture of a binary synapse. *Neuron* **14,** 561–569 (1995).

7. Pugh T.D., E. N. L. Phototransduction in vertebrate rods and cones: molecular mechansims of amplficaition, recovery and light adaptation. *Handb. Biol. Phys.* **3,** 183–255 (2000).

8. Baylor, D. How photons start vision. *Proc Natl Acad Sci U S A* **93,** 560–565 (1996).

9. Mazzolini, M. *et al.* The phototransduction machinery in the rod outer segment has a strong efficacy gradient. *Proc. Natl. Acad. Sci.* **112,** E2715–E2724 (2015).

10. Seeliger, M. W. *et al.* Modulation of rod photoreceptor output by HCN1 channels is essential for regular mesopic cone vision. *Nat. Commun.* **2,** (2011).

11. Liu, X. D. & Kourennyi, D. E. Effects of tetraethylammonium on Kx channels and simulated light response in rod photoreceptorss. *Ann. Biomed. Eng.* **32,** 1428–1442 (2004).

12. Palczewski, K. & Saari, J. C. Activation and inactivation steps in the visual transduction pathway. *Curr. Opin. Neurobiol.* **7,** 500–504 (1997).

13. Luigi, C. & Edward, F. M. Inactivation of Horizontal Cells in Turtle Retina by Glutamate and Aspartate. *Science (80-.).* **178,** (1972).

14. Palczewski, K. *et al.* Crystal Structure of Rhodopsin : A G Protein – Coupled Receptor. *Science* **289,** 739–745 (2000).

15. Okawa, H., Sampath, A. P., Laughlin, S. B. & Fain, G. L. ATP Consumption by Mammalian Rod Photoreceptors in Darkness and in Light. *Curr. Biol.* **18,** 1917–1921 (2008).

16. CERVETTO, L. Influence of Sodium, Potassium and Chloride Ions on the Intracellular Responses of Turtle Photoreceptors. *Nature* **241,** 401 (1973).

17. Baylor, D., Lamb, T. & Yau, K. The membran current of single rod outer segments. *J. Physiol* **288,** 589–611 (1979).

18. Torre, V., Ashmore, J. F., Lamb, T. D. & Menini, A. Transduction and Adaptation in Sensory Receptor Cells. *J. Neurosci.* **15,** (1995).

19. Cevetto, L. & Piccolino, M. Synaptic Transmission between Photoreceptors and Horizontal Cells in the Turtle Retina. *Science (80-.).* **183,** 417–419 (1974).

20. Koutalos, Y. & Yau, K. W. Regulation of sensitivity in vertebrate rod photoreceptors by calcium. *Trends Neurosci.* (1996). doi:10.1016/0166-2236(96)89624-X

21. Hsu, Y.-T. & Molday, R. S. Modulation of the cGMP-gated channel of rod photoreceptor cells by calmodulin. *Nature* **361,** 76 (1993).

22. Govardovskii, V. I., Calvert, P. D. & Arshavsky, V. Y. Photoreceptor Light Adaptation: Untangling Desensitization and Sensitization. *J. Gen. Physiol.* **116,** 791–794 (2000).

23. Pugh, E. N., Nikonov, S. & Lamb, T. D. Molecular mechanisms of vertebrate photoreceptor light

adaptation. *Current Opinion in Neurobiology* **9,** 410–418 (1999).

24. Baylor, B. Y. D. A., Lamb, T. D. & Yau, K. Response of retinal rods to single photons. *J. Physiol.* 613–634 (1979).

25. Korenbrot, J. I. Speed, sensitivity, and stability of the light response in rod and cone photoreceptors: Facts and models. *Prog. Retin. Eye Res.* **31,** 442–466 (2012).

26. Baylor, D. A., Nunn, B. & Schnapf, J. The photocurrent, noise, and spectral sensitivities of rods of the monkey Macaca fascicularis. *J. Physiol.* **357,** 575–607 (1984).

27. Baylor, D. A., Hodgkin, A. L. & Lamb, T. D. The electrical response of turtle cones to flashes and steps of light. *J. Physiol.* 685–727 (1974). doi:10.1113/jphysiol.1974.sp010733

28. Schnapf, J. L., Kraft, T. W. & Baylor, D. A. Spectral sensitivity of human cone photoreceptors. *Nature* **325,** 439–441 (1987).

29. Forti, S., Menini, A., Rispoli, G. & Torre, V. Kinetics of phototransduction in retinal rods of the newt triturus cristatus. *J. Physiol.* 265–295 (1989).

30. Matthews, H. R., Murphy, R. L. W., Fain, G. L. & Lamb, T. D. Photoreceptor light adaptation is mediated by cytoplasmic calcium concentration. *Nature* (1988). doi:10.1038/334067a0

31. Nakatani, K. & Yau, K. W. Calcium and light adaptation in retinal rods and cones. *Nature* (1988). doi:10.1038/334069a0

32. Hodgkin, A. L., Nunn, B. J. & Street, D. Control of light sensitive current in salamander rods. *J. Physiol.* 439–471 (1988). doi:10.1113/jphysiol.1988.sp017258

33. Koutalos, Y., Nakatani, K., Tamura, T. & Yau, K. W. Characterization of guanylate cyclase activity in single retinal rod outer segments. *J Gen Physiol* (1995).

34. Baylor, D. A. & Hodgkin, A. L. Changes in time scale and sensitivity in turtle photoreceptors. *J. Physiol.* 729–758 (1974). doi:10.1113/jphysiol.1974.sp010732

35. Fain, G. L. *et al.* Cytoplasmic calcium as the messenger for light adaptation in salamander rods. *J. Physiol.* 215–243 (1989). doi:10.1113/jphysiol.1989.sp017757

36. Torre, V., Matthews, H. R. & Lamb, T. D. Role of calcium in regulating the cyclic GMP cascade of phototransduction in retinal rods. *Proc. Natl. Acad. Sci. U. S. A.* **83,** 7109–7113 (1986).

37. Nikonov, S., Engheta, N. & Pugh, E. N. Kinetics of recovery of the dark-adapted salamander rod photoresponse. *J. Gen. Physiol.* **111,** 7–37 (1998).

38. Lagnado, L. & Baylor, D. A. Calcium controls light-triggered formation of catalytically active rhodopsin. *Nature* (1994). doi:10.1038/367273a0

39. Gray-Keller, M. P. & Detwiler, P. B. Ca2+dependence of dark- and light-adapted flash responses in rod photoreceptors. *Neuron* **17,** 323–331 (1996).

40. Xu, J. *et al.* Prolonged photoresponses in transgenic mouse rods lacking arrestin. *Nature* **389,** 505–509 (1997).

41. Chen, C. K. *et al.* Abnormal photoresponses and light-induced apoptosis in rods lacking rhodopsin kinase. *Proc. Natl. Acad. Sci. U. S. A.* **96,** 3718–22 (1999).

42. Matthews, H. R. Static and dynamic actions of cytoplasmic Ca2+in the adaptation of responses to saturating flashes in salamander rods. *J. Physiol.* **490,** 1–15 (1996).

43. Lyubarsky, a, Nikonov, S. & Pugh Jr., E. N. The kinetics of inactivation of the rod phototransduction cascade with constant Ca2+i. *J. Gen. Physiol.* **107,** 19–34 (1996).

44. Verbakel, S. K. *et al.* Non-syndromic retinitis pigmentosa. *Prog. Retin. Eye Res.* (2018).

45. Parmeggiani, F. *et al.* Retinitis Pigmentosa: Genes and Disease Mechanisms. *Curr. Genomics* **12,** 238–249 (2011).

46. Mendes, H. F., Van Der Spuy, J., Chapple, J. P. & Cheetham, M. E. Mechanisms of cell death in rhodopsin retinitis pigmentosa: Implications for therapy. *Trends Mol. Med.* **11,** 177–185 (2005).

47. Sullivan, L. S. *et al.* Prevalence of disease-causing mutations in families with autosomal dominant retinitis pigmentosa: A screen of known genes in 200 families. *Investig. Ophthalmol. Vis. Sci.* **47,** 3052–3064 (2006).

48. Athanasiou, D. *et al.* The molecular and cellular basis of rhodopsin retinitis pigmentosa reveals potential strategies for therapy. *Prog. Retin. Eye Res.* **62,** 1–23 (2018).

49. Kaushal, S. & Khorana, H. G. Structure and function in rhodopsin. 7. Point mutations associated with autosomal dominant retinitis pigmentosa. *Biochemistry* **33,** 6121–8 (1994).

50. Sung, C. H., Schneider, B. G., Agarwal, N., Papermaster, D. S. & Nathans, J. Functional heterogeneity of mutant rhodopsins responsible for autosomal dominant retinitis pigmentosa. *Proc. Natl. Acad. Sci.* **88,** 8840–8844 (1991).

51. Krebs, M. P. *et al.* Molecular Mechanisms of Rhodopsin Retinitis Pigmentosa and the Efficacy of Pharmacological Rescue. *J. Mol. Biol.* **395,** 1063–1078 (2010).

52. Chen, Y. *et al.* Inherent instability of the retinitis pigmentosa P23H mutant opsin. *J. Biol. Chem.* **289,** 9288–9303 (2014).

53. Noorwez, S. M. *et al.* Retinoids Assist the Cellular Folding of the Autosomal Dominant Retinitis Pigmentosa Opsin Mutant P23H. *J. Biol. Chem.* **279,** 16278–16284 (2004).

54. Tam, B. M. & Moritz, O. L. Characterization of rhodopsin P23H-induced retinal degeneration in a Xenopus laevis model of retinitis pigmentosa. *Investig. Ophthalmol. Vis. Sci.* **47,** 3234–3241 (2006).

55. Sakami, S., Kolesnikov, A. V., Kefalov, V. J. & Palczewski, K. P23H opsin knock-in mice reveal a novel step in retinal rod disc morphogenesis. *Hum. Mol. Genet.* **23,** 1723–1741 (2014).

56. Haeri, M. & Knox, B. E. Rhodopsin mutant P23H destabilizes rod photoreceptor disk membranes. *PLoS One* **7,** (2012).

57. Price, B. A. *et al.* Mislocalization and degradation of human P23H-rhodopsin-GFP in a knockin mouse model of retinitis pigmentosa. *Investig. Ophthalmol. Vis. Sci.* **52,** 9728–9736 (2011).

58. Tam, B. M. & Moritz, O. L. The Role of Rhodopsin Glycosylation in Protein Folding, Trafficking, and Light-Sensitive Retinal Degeneration. *J. Neurosci.* **29,** 15145–15154 (2009).

59. Chiang, W. C. *et al.* Robust Endoplasmic Reticulum-Associated Degradation of Rhodopsin Precedes Retinal Degeneration. *Mol. Neurobiol.* **52,** 679–695 (2015).

60. Illing, M. E., Rajan, R. S., Bence, N. F. & Kopito, R. R. A rhodopsin mutant linked to autosomal dominant retinitis pigmentosa is prone to aggregate and interacts with the ubiquitin proteasome system. *J. Biol. Chem.* **277,** 34150–34160 (2002).

61. Tam, B. M. & Moritz, O. L. Dark Rearing Rescues P23H Rhodopsin-Induced Retinal Degeneration in a Transgenic Xenopus laevis Model of Retinitis Pigmentosa: A Chromophore-Dependent Mechanism Characterized by Production of N-Terminally Truncated Mutant Rhodopsin. *J. Neurosci.* **27,** 9043–9053 (2007).

62. McKibbin, C. *et al.* Opsin Stability and Folding: The Role of Cys185 and Abnormal Disulfide Bond Formation in the Intradiscal Domain. *J. Mol. Biol.* **374,** 1309–1318 (2007).

63. Bogéa, T. H., Wen, R. H. & Moritz, O. L. Light induces ultrastructural changes in rod outer and inner segments, including autophagy, in a transgenic Xenopus laevis P23H rhodopsin model of retinitis pigmentosa. *Investig. Ophthalmol. Vis. Sci.* **56,** 7947–7955 (2015).

64. Lee, D. C. *et al.* Dysmorphic Photoreceptors in a P23H Mutant Rhodopsin Model of Retinitis Pigmentosa Are Metabolically Active and Capable of Regenerating to Reverse Retinal Degeneration. *J. Neurosci.* **32,** 2121–2128 (2012).

65. Kemp, C. M., Jacobson, S. G., Roman, A. J., Sung, C. H. & Nathans, J. Abnormal rod dark adaptation in

autosomal dominant retinitis pigmentosa with proline-23-histidine rhodopsin mutation. *Am. J. Ophthalmol.* (1992). doi:10.1016/S0002-9394(14)71529-6

66. Ramon, E. *et al.* Differential light-induced responses in sectorial inherited retinal degeneration. *J. Biol. Chem.* **289,** 35918–35928 (2014).

67. Moore, A. *et al.* Abnormal Dark-Adaptation Kinetics in Autosomal Dominant Sector Retinitis-Pigmentosa Due To Rod Opsin Mutation. *Br. J. Ophthalmol.* 465–469 (1992).

68. Goto, Y. *et al.* Rod phototransduction in transgenic mice expressing a mutant opsin gene. *J. Opt. Soc. Am. A* **13,** 577–585 (1996).

69. Panda, S. Circadian physiology of metabolism. *Science (80-.).* **354,** 1008–1015 (2016).

70. Section, S. Science-2010-Bass-Circadian Integration of Metabolism and Energetics. 1–7 (2010). doi:10.1126/science.1195027

71. McMahon, D. G., Iuvone, P. M. & Tosini, G. Circadian organization of the mammalian retina: From gene regulation to physiology and diseases. *Prog. Retin. Eye Res.* **39,** 58–76 (2014).

72. David-Gray, Z. K., Janssen, J. W. H., Degrip, W. J., Nevo, E. & Foster, R. G. Light detection in a 'blind' mammal. *Nat. Neurosci.* **1,** 655–656 (1998).

73. Freedman, M. S. *et al.* Regulation of Mammalian Circadian Behavior by Non-rod,\rNon-cone, Ocular Photoreceptors. *Science (80-.).* **284,** 502–504 (1999).

74. Lee, H. S., Nelms, J. L., Nguyen, M., Silver, R. & Lehman, M. N. The eye is necessary for a circadian rhythm in the suprachiasmatic nucleus. *Nat. Neurosci.* **6,** 111–112 (2003).

75. Cahill, G. M. & Besharse, J. C. Retinal melatonin is metabolized within the eye of xenopus laevis. *Proc. Natl. Acad. Sci. U. S. A.* **86,** 1098–102 (1989).

76. Besharse, J. C. & Iuvone, P. M. Circadian clock in Xenopus eye controlling retinal serotonin N-Acetyltransferase. *Nature* (1983). doi:10.1038/305133a0

77. Cahill, G. M. & Besharse, J. C. Resetting the circadian clock in cultured Xenopus eyecups: regulation of retinal melatonin rhythms by light and D dopamine receptors. *J. Neurosci.* **11,** 2959–2971 (1991).

78. Cahill, G. M. & Besharse, J. C. Circadian clock functions localized in xenopus retinal photoreceptors. *Neuron* **10,** 573–577 (1993).

79. Berson, D. M., Dunn, F. A. & Takao, M. Photoransduction by retinal ganglion cells that set the circadian clock. *Science (80-.).* **295,** 1070–1073 (2002).

80. Panda, S. *et al.* Melanopsin Opn4 Requirement for Normal Light-Induced Circadian Phase Shifting. *Science (80-.).* **298,** 2213 LP-2216 (2002).

81. Panda, S. *et al.* Melanopsin Is Required for Non – Image-Forming Photic. *Schizophr. Bull.* **301,** 525–527 (2003).

82. Hattar, S. *et al.* Melanopsin and rod—cone photoreceptive systems account for all major accessory visual functions in mice. *Nature* **424,** 76–81 (2003).

83. Scott Basinger, R. H. and M. M. Photoreceptor Shedding Is Initiated by Light in the Frog Retina. *Science (80-.).* **194,** 1074–1076 (1976).

84. LaVail, M. M. Rod Outer Segment Disk Shedding in Rat Retina : Relationship to Cyclic Lighting. *Science (80-.).* **194,** 1071–1074 (1976).

85. Joseph C. Besharse, J. G. H. & Rayborn, M. E. Turnover of rod photoreceptor outer segments. *J. Cell Biol.* **75,** 507–527 (1977).

86. Schremser, J. L. & Williams, T. P. Rod outer segment (ROS) renewal as a mechanism for adaptation to a new intensity environment. I. Rhodopsin levels and ROS length. *Exp. Eye Res.* **61,** 17–24 (1995).

87. Bobu, C. & Hicks, D. Regulation of retinal photoreceptor phagocytosis in a diurnal mammal by circadian

clocks and ambient lighting. *Investig. Ophthalmol. Vis. Sci.* **50,** 3495–3502 (2009).

88. Codega, P. *et al.* Prolonged illumination up-regulates arrestin and two guanylate cyclase activating proteins: A novel mechanism for light adaptation. *J. Physiol.* **587,** 2457–2472 (2009).

89. Tikidji-Hamburyan, A. *et al.* Rods progressively escape saturation to drive visual responses in daylight conditions. *Nat. Commun.* **8,** (2017).

90. Jackson, C. R. *et al.* Retinal Dopamine Mediates Multiple Dimensions of Light-Adapted Vision. *J. Neurosci.* **32,** 9359–9368 (2012).

91. Xue, Y., Shen, S. Q., Corbo, J. C. & Kefalov, V. J. Circadian and light-driven regulation of rod dark adaptation. *Sci. Rep.* **5,** 1–10 (2015).

92. Ribelayga, C., Cao, Y. & Mangel, S. C. The Circadian Clock in the Retina Controls Rod-Cone Coupling. *Neuron* **59,** 790–801 (2008).

93. Jin, N. G. & Ribelayga, C. P. Direct Evidence for Daily Plasticity of Electrical Coupling between Rod Photoreceptors in the Mammalian Retina. *J. Neurosci.* **36,** 178–184 (2016).

94. Besharse, J. C. & McMahon, D. G. The Retina and Other Light-sensitive Ocular Clocks. *J. Biol. Rhythms* **31,** 223–243 (2016).

95. Witkovsky, P. *et al.* Cellular location and circadian rhythm of expression of the biological clock gene Period 1 in the mouse retina. *J. Neurosci.* **23,** 7670–7676 (2003).

96. Storch, K. F. *et al.* Intrinsic Circadian Clock of the Mammalian Retina: Importance for Retinal Processing of Visual Information. *Cell* **130,** 730–741 (2007).

97. Li, P. *et al.* CLOCK is required for maintaining the circadian rhythms of opsin mRNA expression in photoreceptor cells. *J. Biol. Chem.* **283,** 31673–31678 (2008).

98. Schlichting, M. *et al.* Cryptochrome Interacts With Actin and Enhances Eye-Mediated Light Sensitivity of the Circadian Clock in Drosophila melanogaster. *Front. Mol. Neurosci.* **11,** 1–13 (2018).

99. Korenbrot, J. I. & Fernald, R. D. Circadian rhythm and light regulate opsin mRNA in rod photoreceptors. *Nature* **337,** 454–457 (1989).

100. Rakshit, T. *et al.* Adaptations in rod outer segment disc membranes in response to environmental lighting conditions. *Biochim. Biophys. Acta - Mol. Cell Res.* **1864,** 1691–1702 (2017).

101. Zhao, Q. *et al.* Structure and mechanogating mechanism of the Piezo1 channel. *Nature* **554,** 487–492 (2018).

102. Saotome, K. *et al.* Structure of the mechanically activated ion channel Piezo1. *Nature* **554,** 481–486 (2018).

103. Iwata, R., Kiyonari, H. & Imai, T. Mechanosensory-Based Phase Coding of Odor Identity in the Olfactory Bulb. *Neuron* **96,** 1139–1152.e7 (2017).

104. Franze, R. C. H. and K. Photomechanical Responses in Drosophila Photoreceptors. *Science (80-.).* 260–264 (2012).

105. Gilliam, J. C. & Wensel, T. G. TRP channel gene expression in the mouse retina. *Vision Res.* **51,** 2440–2452 (2011).

106. Thomas Voets, Karel Talavera, G. O. & B. N. & Drosophila. Sensing with TRP channels. *Nat. Chem. Biol.* **1,** 85–93 (2005).

107. Haeri, M., Knox, B. E. & Ahmadi, A. Modeling the flexural rigidity of rod photoreceptors. *Biophys. J.* **104,** 300–312 (2013).

108. Lamb, T. D., McNaughton, P. A. & Yau, K. W. Spatial spread of activation and background desensitization in toad rod outer segments. *J. Physiol.* **319,** 463–496 (1981).

109. Hillmann, D. *et al.* In vivo optical imaging of physiological responses to photostimulation in human

photoreceptors. *PNAS* **113,** (2016).

110. Zhang, P. *et al.* In vivo optophysiology reveals that G-protein activation triggers osmotic swelling and increased light scattering of rod photoreceptors. *Proc. Natl. Acad. Sci.* **114,** E2937–E2946 (2017).

111. Falleroni, F., Torre, V. & Cojoc, D. Cell Mechanotransduction With Piconewton Forces Applied by Optical Tweezers. *Front. Cell. Neurosci.* **12,** 1–11 (2018).

112. Kwok, M. C. M., Holopainen, J. M., Molday, L. L., Foster, L. J. & Molday, R. S. Proteomics of Photoreceptor Outer Segments Identifies a Subset of SNARE and Rab Proteins Implicated in Membrane Vesicle Trafficking and Fusion. *Mol. Cell. Proteomics* **7,** 1053–1066 (2008).

113. Christensen, A. P. & Corey, D. P. TRP channels in mechanosensation: Direct or indirect activation? *Nat. Rev. Neurosci.* **8,** 510–521 (2007).

114. YOSHIZAWA, T. & WALD, G. Pre-lumirhodopsin and the bleaching of visual pigments. *Nature* **197,** 1279–86 (1963).

115. Baylor, D. A., Lamb, T. D. & Yau, K. W. Responses of retinal rods to single photons. *J. Physiol.* **288,** 613–34 (1979).

116. Kwok-Keung Fung, B. & Stryer, L. Photolyzed rhodopsin catalyzes the exchange of GTP for bound GDP in retinal rod outer segments. *Proc. Natl. Acad. Sci. U. S. A.* **77,** 2500–4 (1980).

117. Molday, R. S. & Moritz, O. L. Photoreceptors at a glance. *J. Cell Sci.* **128,** 4039–45 (2015).

118. Fotiadis, D. *et al.* The G protein-coupled receptor rhodopsin in the native membrane. *FEBS Lett.* **564,** 281–288 (2004).

119. Baehr, W., Devlin, M. J. & Applebury, M. L. Isolation and characterization of cGMP phosphodiesterase from bovine rod outer segments. *J. Biol. Chem.* **254,** 11669–77 (1979).

120. Dumke, C. L., Arshavsky, V. Y., Calvert, P. D., Bownds, M. D. & Pugh, E. N. Rod outer segment structure influences the apparent kinetic parameters of cyclic GMP phosphodiesterase. *J. Gen. Physiol.* **103,** 1071–98 (1994).

121. Leskov, I. B. *et al.* The gain of rod phototransduction: reconciliation of biochemical and electrophysiological measurements. *Neuron* **27,** 525–537 (2000).

122. Fesenko, E. E., Kolesnikov, S. S. & Lyubarsky, A. L. Induction by cyclic GMP of cationic conductance in plasma membrane of retinal rod outer segment. *Nature* **313,** 310–3

123. Kaupp, U. B. & Seifert, R. Cyclic Nucleotide-Gated Ion Channels. *Physiol. Rev.* **82,** 769–824 (2002).

124. Chapter 5 Phototransduction in vertebrate rods and cones: Molecular mechanisms of amplification, recovery and light adaptation. **3,** 183–255 (2000).

125. Forti, S., Menini, A., Rispoli, G. & Torre, V. Kinetics of phototransduction in retinal rods of the newt Triturus cristatus. *J. Physiol.* **419,** 265–95 (1989).

126. Hartong, D. T., Berson, E. L. & Dryja, T. P. Retinitis pigmentosa. *Lancet* (2006). doi:10.1016/S0140-6736(06)69740-7

127. Daiger, S. P., Sullivan, L. S. & Bowne, S. J. Genes and mutations causing retinitis pigmentosa. *Clin. Genet.* **84,** 132–41 (2013).

128. Sohocki, M. M. *et al.* Prevalence of mutations causing retinitis pigmentosa and other inherited retinopathies. *Hum Mutat* **17,** 42–51 (2001).

129. Lee, D. C. *et al.* Dysmorphic photoreceptors in a P23H mutant rhodopsin model of retinitis pigmentosa are metabolically active and capable of regenerating to reverse retinal degeneration. *J. Neurosci.* **32,** 2121–8 (2012).

130. Tam, B. M. & Moritz, O. L. Characterization of rhodopsin P23H-induced retinal degeneration in a Xenopus laevis model of retinitis pigmentosa. *Invest Ophthalmol Vis Sci* **47,** 3234–3241 (2006).

131. Sung, C. H. *et al.* Rhodopsin mutations in autosomal dominant retinitis pigmentosa. *Proc Natl Acad Sci U S A* **88,** 6481–6485 (1991).

132. Paskowitz, D. M., Lavail, M. M. & Duncan, J. L. Light and Inherited Retinal Degeneration. *Br J Ophthalmol* (2006).

133. Noorwez, S. M. *et al.* Retinoids assist the cellular folding of the autosomal dominant retinitis pigmentosa opsin mutant P23H. *J Biol Chem* **279,** 16278–16284 (2004).

134. Tam, B. M., Qazalbash, A., Lee, H. C. & Moritz, O. L. The dependence of retinal degeneration caused by the rhodopsin P23H mutation on light exposure and vitamin a deprivation. *Invest Ophthalmol Vis Sci* **51,** 1327–1334 (2010).

135. Sakami, S. *et al.* Probing mechanisms of photoreceptor degeneration in a new mouse model of the common form of autosomal dominant retinitis pigmentosa due to P23H opsin mutations. *J Biol Chem* **286,** 10551–10567 (2011).

136. Tam, B. M., Noorwez, S. M., Kaushal, S., Kono, M. & Moritz, O. L. Photoactivation-Induced Instability of Rhodopsin Mutants T4K and T17M in Rod Outer Segments Underlies Retinal Degeneration in X. laevis Transgenic Models of Retinitis Pigmentosa. *J. Neurosci.* **34,** 13336–48 (2014).

137. De Palo, G. *et al.* Common dynamical features of sensory adaptation in photoreceptors and olfactory sensory neurons. *Sci. Rep.* **3,** 1251 (2013).

138. Rieke, F. & Baylor, D. A. Origin of Reproducibility in the Responses of Retinal Rods to Single Photons. *Biophys. J.* **75,** 1836–1857 (1998).

139. Vent-Schmidt, R. Y. J. *et al.* Opposing Effects of Valproic Acid Treatment Mediated by Histone Deacetylase Inhibitor Activity in Four Transgenic *X. laevis* Models of Retinitis Pigmentosa. *J. Neurosci.* **37,** 1039–1054 (2017).

140. Schindelin, J., Rueden, C. T., Hiner, M. C. & Eliceiri, K. W. The ImageJ ecosystem: An open platform for biomedical image analysis. *Mol. Reprod. Dev.* **82,** 518–529 (2015).

141. Xiong, W.-H. & Yau, K.-W. Rod sensitivity during Xenopus development. *J. Gen. Physiol.* **120,** 817–27 (2002).

142. Solessio, E. *et al.* Developmental regulation of calcium-dependent feedback in Xenopus rods. *J Gen Physiol* **124,** 569–585 (2004).

143. Matthews, B. Y. H. R., Fain, G. L., Murphy, R. L. W. & Lamb, T. D. LIGHT ADAPTATION IN CONE PHOTORECEPTORS OF THE SALAMANDER: A ROLE FOR CYTOPLASMIC CALCIUM BY. 447–469 (1990).

144. Lobanova, E. S. *et al.* Mechanistic basis for the failure of cone transducin to translocate: why cones are never blinded by light. *J. Neurosci.* **30,** 6815–24 (2010).

145. Lobanova, E. S. *et al.* Transducin Translocation in Rods Is Triggered by Saturation of the GTPase-Activating Complex. *J. Neurosci.* **27,** 1151–1160 (2007).

146. Gunkel, M. *et al.* Higher-order architecture of rhodopsin in intact photoreceptors and its implication for phototransduction kinetics. *Structure* **23,** 628–38 (2015).

147. Liang, Y. *et al.* Organization of the G protein-coupled receptors rhodopsin and opsin in native membranes. *J. Biol. Chem.* **278,** 21655–62 (2003).

148. Fotiadis, D. *et al.* Atomic-force microscopy: Rhodopsin dimers in native disc membranes. *Nature* **421,** 127–128 (2003).

149. Liang, Y. *et al.* Rhodopsin signaling and organization in heterozygote rhodopsin knockout mice. *J. Biol. Chem.* **279,** 48189–96 (2004).

150. Govardovskii, V. I., Korenyak, D. A., Shukolyukov, S. A. & Zueva, L. V. Lateral diffusion of rhodopsin in photoreceptor membrane: a reappraisal. *Mol. Vis.* **15,** 1717–29 (2009).

151. Palczewski, K. *et al.* Crystal structure of rhodopsin: A G protein-coupled receptor. *Science (80-.).* **289,**

739–745 (2000).

152. Kraft, T. W. *et al.* Altered light responses of single rod photoreceptors in transgenic pigs expressing P347L or P347S rhodopsin. *Mol. Vis.* **11,** 1246–56 (2005).

153. Makino, C. L. *et al.* Rhodopsin expression level affects rod outer segment morphology and photoresponse kinetics. *PLoS One* **7,** e37832 (2012).

154. Moritz, O. L. & Tam, B. M. Recent insights into the mechanisms underlying light-dependent retinal degeneration from x. Laevis models of retinitis pigmentosa. *Adv Exp Med Biol* **664,** 509–515 (2010).

6. Manuscript in preparation

In addition to my experimental work on photoreceptors, together with Fabio Falleroni we have integrated an electrophysiological setup with an optical tweezers system. We have combined these two technique in order to stimulate neuronal cells with very small forces (**5-10 pN range**) and to understand if these kind of stimuli could trigger a detectable variation of the current passing through the cells membrane.

Integrating optical tweezers with patch-clamp electrophysiology.

Authors: Fabio Falleroni, Ulisse Bocchero, Yunzhen Li, Vincent Torre and Dan Cojoc

Abstract

Neuronal activity is not solely influenced by chemical and electrical factors. Mechanical stimulation can also modulate neuronal excitability and signaling. Here we have integrated the mechanical stimulation of the cell membrane using a pulsing optical tweezers with the patch-clamp technique, to measure the electrical signals generated in neuronal cells. The forces are applied by axially displacing a trapped bead with an electrical tunable lens (ETL) and measured in Z directions by back focal plane (BFP) interferometry on a quadrant photo diode (QPD). The electrical activity of the cell is monitored in cell voltage clamp by measuring the ionic currents. We demonstrate, both for primary hippocampal cells and NG108-15 cells, that stimulation with piconewton forces is enough to regulate the ion currents through the cell membrane.

Introduction

Mechanotransduction studies how cells sense physical forces and the cellular signal transduction in response to mechanical stimuli[1]. Cells perceive force through a variety of molecular sensors, of which the mechanosensitive ion channels are the most efficient and act the fastest[2]. Tension in the membrane alters the probability of channel opening and leads to an influx of ions[3]. Patch-clamp is a traditional technique to study the electrical activity of living neurons, with the goal to unravel the molecular and cellular processes that govern their signaling induced by different stimuli.

Patch-clamp versatility allows measuring currents through single ion channels or whole-cell recordings, with sub millisecond temporal resolution[4]. The whole-cell variation in combination with voltage clamp allows direct electrical control of the cell transmembrane potential[5].

Recently we have developed an oscillatory optical tweezers to apply piconewton forces perpendicularly to the cell membrane and demonstrated that also these small forces can trigger cellular calcium transients[6] by fluorescence imaging. Optical tweezers have been also proposed to pull tether membranes[7] or to stretch actin stress fibers[8]. Here we demonstrate the integration of the patch-clamp with a pulsed optical tweezers, showing that piconewton forces applied vertically on the cell membrane induce detectable ion currents.

The force is applied by a trapped bead in a pulsed-oscillatory optical trap. By using a focus tunable lens (FTL), the trap position can be precisely and fast moved vertically in a range of 12 um, while the 3D position of the bead is measured by back focal plane (BPF) interferometry using a quadrant photo detector (QPD)[9].

The ability to measure the applied force and the membrane indentation during the experiment and correlate these quantities with the ionic currents passing through the cell membrane, in our approach, might be essential in understanding the function of the mechanical sensors, especially regarding the MSCs. Here, we demonstrate the capability of the system in mouse neuroblastoma NG 108-15 cells and mouse hippocampal neurons.

Material and methods

Hippocampal cell culture

Hippocampal neurons were dissected from Wistar rat brain (P1-P2). After decapitation the meninge-free hippocampi were incubated with 5 mg/ml trypsin (Sigma) and 0.75 mg/ml DNase I (Sigma) for 5 minutes at room temperature for the enzymatic dissociation.

Then trypsin was neutralized by 1 mg/ml trypsin inhibitor (Sigma) and a mechanical dissociation was performed with a Pasteur pipette. The cell suspension was then centrifuged at 100 G for 5 min, and the pellet was re-suspended.

Finally, hippocampal neurons were plated on coverslip coated with 50 µg/ml poly-L-ornithine (Sigma). The hippocampal cultures were incubated (95% O2, 5% CO2 at 37 °C) for 4-6 days in Neurobasal medium (Sigma) containing 25 µm GlutaMAX (Thermo Fisher Scientific) and B27 supplement at 2% (Sigma).

Cell were used for experiment after 5-6 days in culture. All experimental procedure on animals were done in accordance with the European Communities Council Directive of November 2016 (86/609/EEC).

Ng108-15 cell culture

Mouse neuroblastoma/rat glioma hybrid (NG108-15) cells were obtained from Sigma-Aldrich. The cells were cultured as described in Falleroni 2018[6].

Mechanical cell stimulation and current recording experimental approach

To mechanically stimulate a silica bead was trapped and positioned above the cell of interest (label 1 in Figure 1A and left image in Figure 1B) by an infrared trapping laser (1064 nm, max 5W, cw, IPG Photonics, US).

Then we used a manual micromanipulator to move vertically the patch clamp pipette in contact with the cell membrane. After reaching a seal between the membrane and the electrode of more than 1 GΩ resistance, we applied a gentle suction to break the membrane patch in order to enter in whole-cell configuration. Whole-cell currents were recorded using borosilicate glass pipette (Blaubrand, intramark micropipette, Germany) with a resistance of 2-5 M Ω filled with intracellular solution containing (in mM): 10 NaCl, 140 KCl, 1 MgCl2, 5 EGTA and 10 HEPES.

To confirm the integrity of the whole-cell configuration, we kept the cell at an holding potential of -80 mV and induced voltage gated Na^+ and K^+ currents by depolarizing the cell with voltage

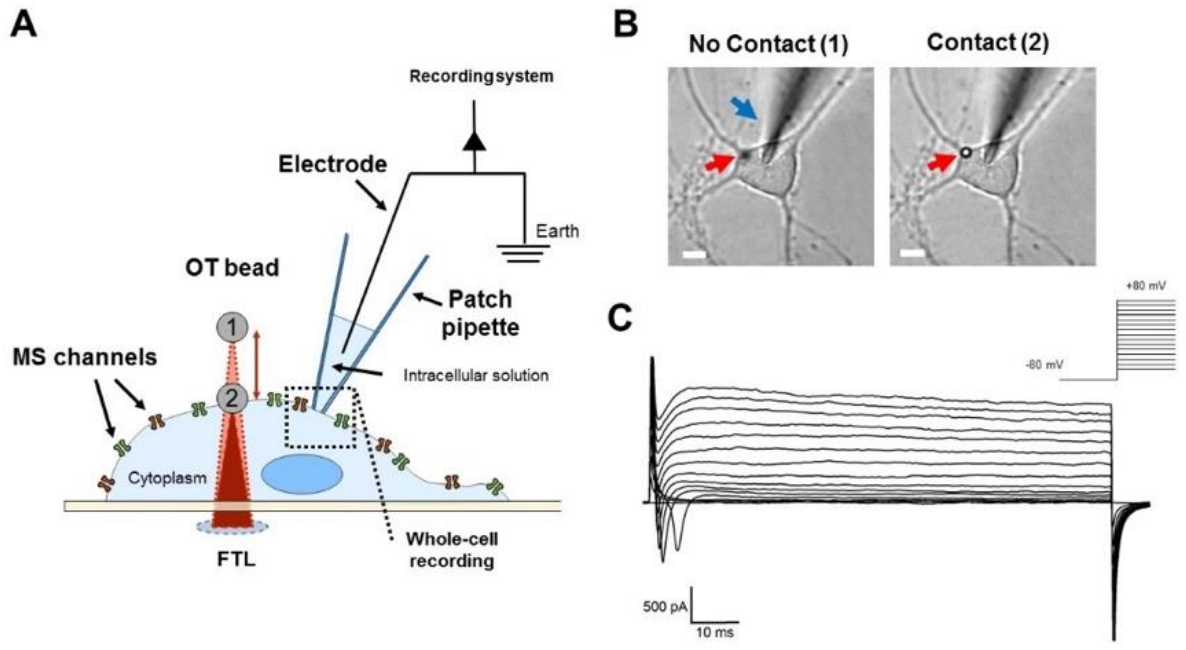

Figure 1. Schematic of the integrated patch-clamp current recording with the pulsed optical tweezers mechanical stimulation. (A) Scheme of the mechanical stimulation using an optically trapped (OT) bead positioned first above the cell (label 1) and then moved in contact to the cell membrane (label 2) by means of the Focused Tunable Lens (FTL) and schematic of the patch-clamp approach. **(B)** Image of an hippocampal neuron approached by the patch pipette (blue arrow) and the trapped bead (red arrows) above the cell (1) and in contact with the cell membrane (2). **(C)** Example of recorded Na^+ and K^+ currents in whole cell configuration.

steps from -80 mV to + 80 mV (10 mV increments). Figure 1C display an example of such recording. The negative portion of the current, at the beginning of the traces, is an inward Na^+ current, while the positive part immediately after evidenced an outward K^+ currents.

Then, we proceeded with the simultaneous cell mechanical stimulation with forces in the range of 5-20 pN and the characterization of the responses in the whole-cell configuration.

The mechanical stimulation is achieved as described in our previous article [6].

For all experiments, the cells were bathed in an extracellular ringer solution containing in mM: 140 NaCl, 2.8 KCl, 1 $MgCl_2$, 2 $CaCl_2$ and 10 HEPES and maintained at an holding potential of -80 mV.

The combined patch-clamp -- optical tweezers setup

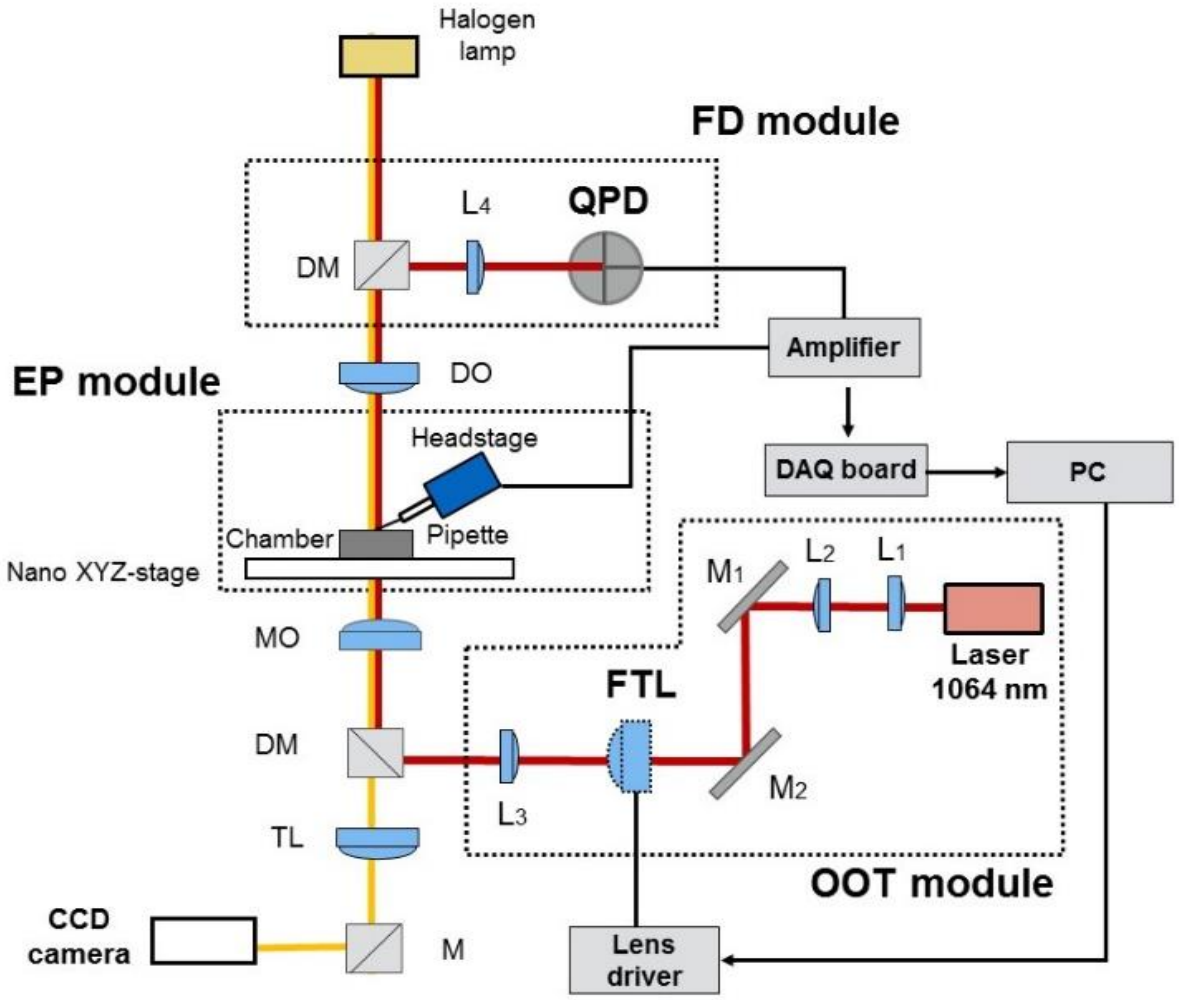

Figure 2. Integrated patch clamp – optical tweezers cell stimulation and force detection setup. The cell is imaged in brightfield on the CCD camera (yellow optical path).
OOT: Oscillatory Optical Tweezers; **FTL**: Focus Tunable Lens. **FD**: Force Detection; **QPD**: Quadrant Photo Diode. **EP**: Electrophysiology Patch-clamp.
L_1, **L_2**, **L_3**, **L_4**: convergent Lenses; **DM**: Dichroic Mirrors; **MO**: Microscope Objective lens; **DO**: detection objective lens; **TL**: Tube Lens; **M_1**, **M_2**: mirrors

The integrated patch-clamp with pulsed/oscillatory optical tweezers setup is shown in Figure 2. The system was built on an inverted microscope (IX81, Olympus), to which tree custom modules were adapted: Oscillatory optical trap (OOT), Force detection module (FD) and the Electrophysiology module (EP) (see Figure 2). The sample chamber is imaged in brightfield by the microscope lens MO (60X, NA 1.4 oil immersion, Olympus) and through the tube lens, TL on the CCD camera (Orca D2, Hamamatsu). The pulsed/oscillatory optical tweezers (OOT) was designed and built as described in our recent paper[6]. Briefly, the trapping laser is an ytterbium continuous wave fiber laser operating at 1064 nm (IPG Laser GmbH). The laser beam is directed toward a custom collimator (L1, L2 f1=f2= 100 mm) to fit the size of the FTL (fFTL= 55-90 mm) and a third convergent lens (L3, f3=150 mm) is used to size the diameter

of the beam such that it overfills the entrance pupil of the microscope lens and ensure efficient trapping.

The position of the trap above the coverslip of the sample chamber is determined by the focal lengths of the four lenses (f1, f2, fFTL and f3) used for collimation, the focal length of the microscope lens, fMO and the relative distances between these components. We designed the configuration to obtain a trap shift of 12 um up from the initial position (2-3 um above the coverslip), linearly with a variation of the fFTL from 55 to 90 mm.

Details on the design and calibration (trap shift vs driver current FTL) of the system are given in[6]. The driver current and hence the focal length of the FTL are computer controlled by a custom LabView code. With the laser operating at 250 mW, the average power at the sample plane is 25 mW, allowing an axial trap stiffness K_{ot} ~ 0.03 pN/nm. The trap stiffness can be strengthened up to K_{ot} ~ 0.06 pN/nm increasing the laser power by a factor of two (500 mW).

The wavelength of the laser and the output power were chosen to minimize heating and photodamage of the sample. In our previous article[6] we demonstrated the absence of damaging effects of the 1064 nm infrared laser on calcium dynamics in the NG108-15. Measurement of the force of interaction between the bead and the cell membrane and the indentation of the cell membrane are enabled by the force detection (FD) module, using the principle of BFP interferometry.

The laser light scattered by the bead and sample is captured by detection objective lens (Olympus, 10X NA 0.3) and the interference pattern formed in the BFP is projected by the convergent lens L4 (f4= 40 mm) onto the QPD, (PDQ80A, Thorlabs). The electric signals coming from the QPD are amplified and then digitized by an analog-to-digital data acquisition (DAQ card, PCI-4462, National Instrument). The FD module allows to measure axial forces in the range: [0 - 20] pN.

The Electrophysiology setup (EP module) was composed by a patch clamp head stage (PH, CV 201, Axon Instruments) that was mounted onto a manual micromanipulator. Then the signal from the EP module were amplified (Axopatch 200, Axon instruments Inc.) and converted to differential outputs digitized at 10 kHz through a Digidata converter card (Digidata 1440, Molecular Device).

Experimental results and discussion

The mechanical stimulation was performed applying a sinusoidal waveform to FTL to produce an axial indentation on the cell membrane. In all experiments we applied a sinusoidal signal with amplitude A= 2 µm and frequency f= 1 Hz. Preliminary experiments on hippocampal neurons and Ng108-15 cells revealed that the application of mechanical stress in the range of 5-20 pN induced detectable currents.

Testing the protocol on primary neurons, such hippocampal neurons, was fundamental in order to understand if also these cells, obtained from the central nervous system of a mouse, were mechanosensitive. These hippocampal neurons displayed mechano-responses based on the increase of intracellular Ca^{2+} right after the stimulation, as evidenced in our previous work in which we used Fluo-4 AM calcium dye. Figure 3 display an example of a hippocampal neuron during the application of a mechanical stimulus of about 14 pN. In this case, we detected a

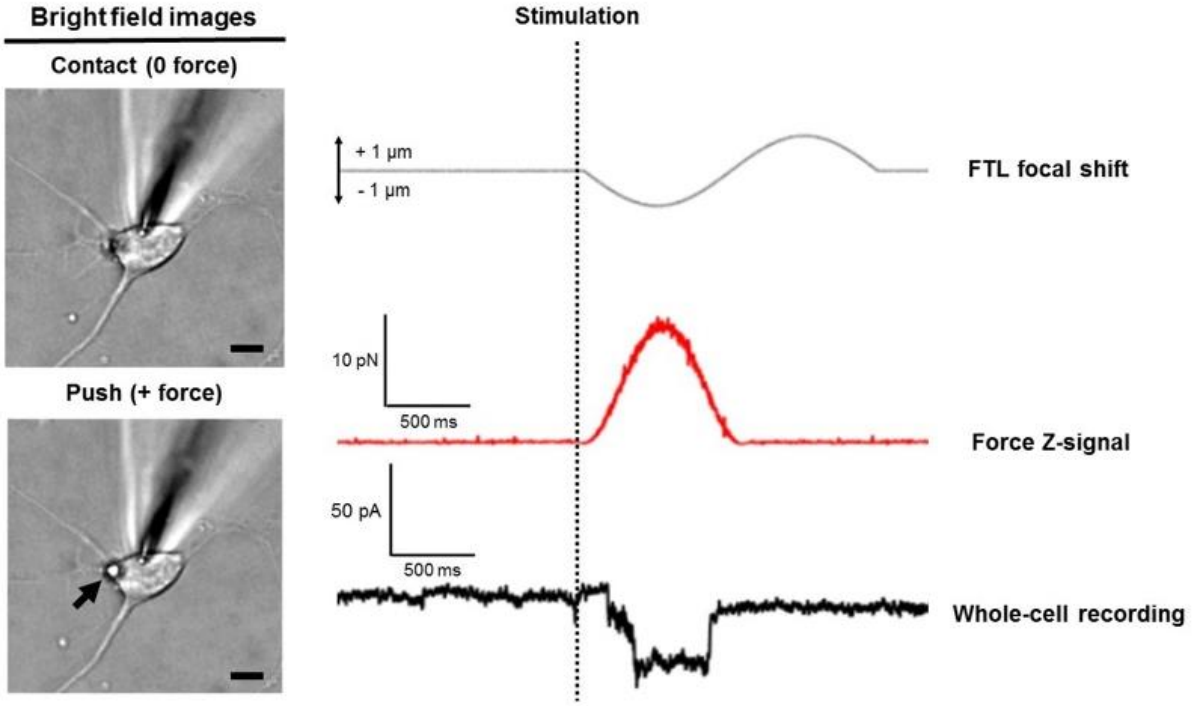

Figure 3. Force and current recordings during the application of a mechanical stimulus to an hippocampal neuron. The two bright field images display the position of the bead. The first one is in the contact position **(0 force)** during which no force was applied to the cell. The second one shows a gentle push **(+ force)** during which a force of approximately 14 pN was applied to the cell membrane. The amplitude of the recorded current was 65 pA. **FTL focal shift** gray trace indicates the variation of the focal length; **Force Z-signal** red trace indicates the strength applied through the bead to the cell membrane; **Whole-cell recording** black trace indicates the current variation due to the mechanical stimulus. Scale bar 10 µm.

current subsequent to the stimulus with an amplitude of approximately 65 pA. In this case the onset of the current corresponds to the beginning of the mechanical stimulus. Using the same protocol, we tested the possible effect on NG108-15 cells, as displayed in Figure 4 . Here the mechanical stimulation induces a current with a mean amplitude of ~27 pA. In this experiment,

the peak of force (force z-signal in red) of the mechanical stimulus corresponds to the onset of the current.

The variability of the delay between the beginning of the mechanical stimulation (contact bead-cell) and the current is probably do to the nature of the stimulus, which in our case is a very gentle pressure, approximately 0.020 mmHg, applied to the cell membrane [6]. Indeed, the

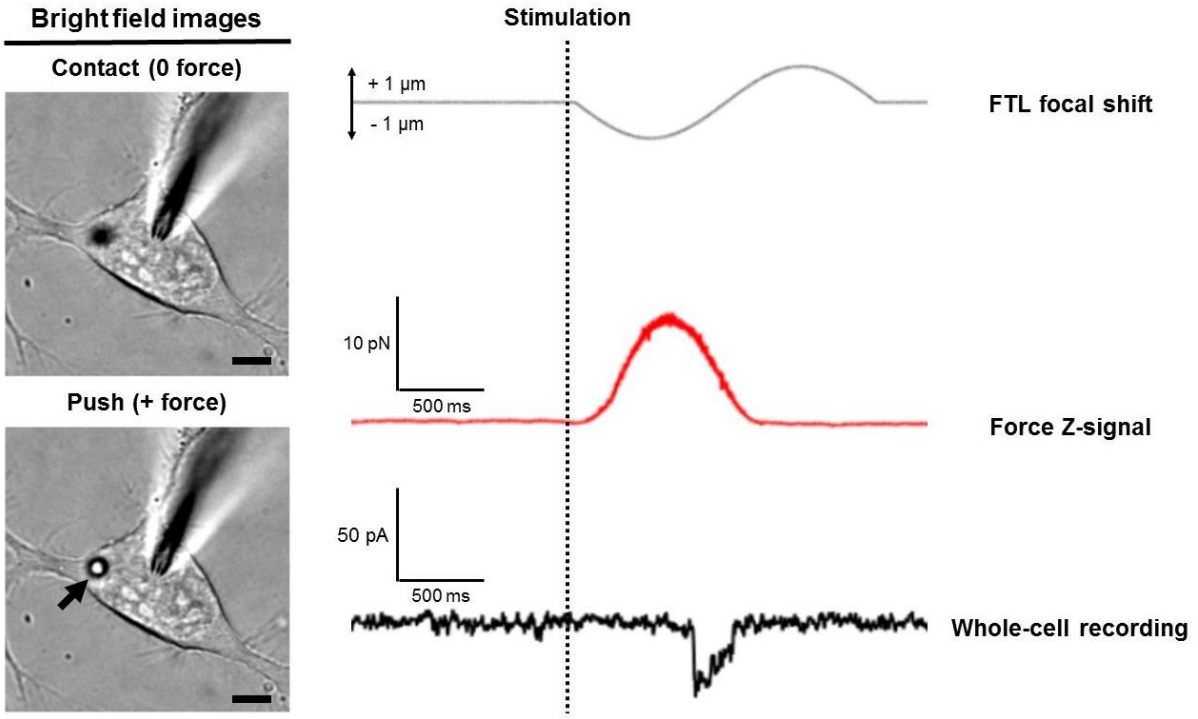

Figure 4. Force and current recordings during the application of a mechanical stimulus to a NG108-15 cell. As in **Figure 3**, the two bright field images display the position of the bead. The force applied in this case was approximately of 12 pN. The amplitude of the recorded current was 38 pA. **FTL focal shift** gray trace indicates the variation of the focal length; **Force Z-signal** red trace indicates the strength applied through the bead to the cell membrane; **Whole-cell recording** black trace indicates the current variation due to the mechanical stimulus. Scale bar 10 µm.

opening of very few channels may be more stochastic with these range of forces, if compared to the responses obtained with higher forces stimuli applied with different setups[11,12]. Therefore, we need to perform more experiments in order to have a clearer view of the dependence between our type of stimuli and the elicited currents.

Conclusion

We presented a new method to apply weak forces in the 5-20 pN range vertically to cell membrane, by using an FTL, while simultaneously monitoring the electrophysiological response. The FTL allow us to change the focus of the trapping plane axially. To our knowledge, this is the first application of focus (electrically) tunable lens (FTL) in optical trapping and manipulation. Its integration with patch-clamp electrophysiology opens new

opportunities to study mechanotransduction in neuronal cells. Previous applications of the FTL included laser material processing, high-speed microscopy and imaging for laparoscopic fluorescence-guided surgery [13,14,15]. As a proof of principle, the whole-cell mechano-response was studied on the NG108-15 cells and Hippocampal neurons. These preliminary experiments suggest that pN forces may induce detectable currents across the plasma membrane in whole cell patch-clamp configuration.

The future experiments will be performed in order to attempt a quantitatively characterization of the responses of the neuronal cells. Indeed, further investigations are needed to confirm and understand the nature of these currents, using specific ionic concentrations in the bath and in the pipet solution, as well as specific blockers for the mechanosensitive channels.

References

1) Marshall, Kara L., and Ellen A. Lumpkin. “The Molecular Basis of Mechanosensory Transduction.” *Sensing in Nature*, edited by Carlos López-Larrea, vol. 739, Springer US, 2012, pp. 142–55. *Crossref*, doi:10.1007/978-1-4614-1704-0_9.
2) Orr, A. Wayne, et al. “Mechanisms of Mechanotransduction.” *Developmental Cell*, vol. 10, no. 1, Jan. 2006, pp. 11–20. *Crossref*, doi:10.1016/j.devcel.2005.12.006.
3) Sukharev, Sergei, and Frederick Sachs. “Molecular Force Transduction by Ion Channels – Diversity and Unifying Principles.” *Journal of Cell Science*, vol. 125, no. 13, July 2012, pp. 3075–83. *Crossref*, doi:10.1242/jcs.092353.
4) Sakmann, B., and E. Neher. “Patch Clamp Techniques for Studying Ionic Channels in Excitable Membranes.” *Annual Review of Physiology*, vol. 46, no. 1, Oct. 1984, pp. 455–72. *Crossref*, doi:10.1146/annurev.ph.46.030184.002323.
5) Hamill, O. P., et al. “Improved Patch-Clamp Techniques for High-Resolution Current Recording from Cells and Cell-Free Membrane Patches.” *Pflugers Archiv: European Journal of Physiology*, vol. 391, no. 2, Aug. 1981, pp. 85–100.
6) Falleroni, Fabio, et al. “Cell Mechanotransduction With Piconewton Forces Applied by Optical Tweezers.” *Frontiers in Cellular Neuroscience*, vol. 12, May 2018. *Crossref*, doi:10.3389/fncel.2018.00130.
7) Brownell, William E., et al. “Cell Membrane Tethers Generate Mechanical Force in Response to Electrical Stimulation.” *Biophysical Journal*, vol. 99, no. 3, Aug. 2010, pp. 845–52. *PubMed*, doi:10.1016/j.bpj.2010.05.025.
8) K. Hayakawa, H. Tatsumi, and M. Sokabe, "Actin stress fibers transmit and focus force to activate mechanosensitive channels," J Cell Sci **121**, 496-503 (2008).
9) Neuman, Keir C., and Steven M. Block. “Optical Trapping.” *The Review of Scientific Instruments*, vol. 75, no. 9, Sept. 2004, pp. 2787–809. *PubMed*, doi:10.1063/1.1785844.
10) B. Coste, S. E. Murthy, J. Mathur, M. Schmidt, Y. Mechioukhi, P. Delmas, and A. Patapoutian, "Piezo1 ion channel pore properties are dictated by C-terminal region," Nat Commun **6**, 7223 (2015).
11) B. Coste, J. Mathur, M. Schmidt, T. J. Earley, S. Ranade, M. J. Petrus, A. E. Dubin, and A. Patapoutian, "Piezo1 and Piezo2 are essential components of distinct mechanically activated cation channels," Science **330**, 55-60 (2010).
12) Eberle, G., et al. “Simulation and Realization of a Focus Shifting Unit Using a Tunable Lens for 3D Laser Material Processing.” *Physics Procedia*, vol. 41, 2013, pp. 441–47. *Crossref*, doi:10.1016/j.phpro.2013.03.100.
13) Jiang, Jun, et al. “Fast 3-D Temporal Focusing Microscopy Using an Electrically Tunable Lens.” *Optics Express*, vol. 23, no. 19, Sept. 2015, p. 24362. *Crossref*, doi:10.1364/OE.23.024362.
14) Nakai, Yuichiro, et al. “High-Speed Microscopy with an Electrically Tunable Lens to Image the Dynamics of *in Vivo* Molecular Complexes.” *Review of Scientific Instruments*, vol. 86, no. 1, Jan. 2015, p. 013707. *Crossref*, doi:10.1063/1.4905330.
15) Volpi, Davide, et al. “Electrically Tunable Fluidic Lens Imaging System for Laparoscopic Fluorescence-Guided Surgery.” *Biomedical Optics Express*, vol. 8, no. 7, July 2017, pp. 3232–47. *PubMed*, doi:10.1364/BOE.8.003232.

Acknowledgments

I would like to thank Prof. Vincent Torre and Dr. Monica Mazzolini for all their advice, their guidance and their support during these four years; Prof. Orson Moritz and his group for the nice work done together; Dr. Dan Cojoc and Dr. Marco Lazzarino for their help and their advice.

I would like to thank also all the professors of the Neuroscience area that have given me very useful advice and support, as well for their nice lectures. In particular Prof. John G. Nicholls, Prof. Anna Menini, Prof. Laura Ballerini, Prof. Andrea Nistri and Prof. Davide Zoccolan.

I would like to thank Prof. Stefano Ruffo, Dr. Gabrile Rizzetto, all the members of the board of directors and all the students' representatives for the nice work done together during these years.

I would like to thank also all the Sissa staff for their help and assistance and the Sissa MediaLab for helping us becoming better science communicators.

All my gratitude goes to my family and friends, for their support and for helping me overcome all the bad moments, but also for the very nice and joyful time spent together.

Finally, a special thanks to my mother, my father and my sister.